GSBS Dissertations and Theses   Graduate School of Biomedical Sciences

2003-09-03

Poly(ADP)-Ribose Polymerase Activity in the Eukaryotic Mono-ADP-Ribosyl Transferase, ART2: a Dissertation

Alan R. Morrison
University of Massachusetts Medical School

Let us know how access to this document benefits you.

Repository Citation

A Dissertation Presented

By

Alan Ross Morrison

Submitted to the Faculty of the

University of Massachusetts Graduate School of Biomedical Sciences, Worcester

In partial fulfillment of the requirements for the degree of

DOCTOR OF PHILOSOPHY

September 3, 2003

PROGRAM IN BIOMEDICAL SCIENCES

COPYRIGHT PAGE

ii

Poly(ADP)-ribose Polymerase Activity in the Eukaryotic Mono-ADP-ribosyl Transferase,

ART2

A Dissertation Presented

By

Alan Ross Morrison

Approved as to style and content by:

Kendall Knight Ph.D., Chair of Committee

Joel Moss M.D./Ph.D., Member of Committee (extramural)

Rita Bortell Ph.D., Member of Committee

Robert Carraway Ph.D., Member of Committee

James Evans, PhD., Member of Committee

Aldo Rossini M.D., Dissertation Mentor

Anthony Carruthers Ph.D., Dean of the
Graduate School of Biomedical Sciences

M.D/Ph.D. Program in Biomedical Sciences

September 3, 2003

iii

Acknowledgements

> I shall be telling this with a sigh
> Somewhere ages and ages hence:
> Two roads diverged in the woods, and I--
> I took the one less traveled by,
> And that has made all the difference.
> -Robert Frost

My personal journey could not have been accomplished without some very important people in my life. I would like to acknowledge my parents, Gail and Glen Morrison, for their outstanding love and guidance. They were my first, best mentors in life, and I could never have arrived at this point without them. I would also like to acknowledge my brother, Gary, who has been an unwaivering rock that I could lean on from time to time. My wife, Nicole, and our daughter, Alexandra, are the loves of my life. They keep me fresh and grounded. Nicole has taught me patience and commitment, and her love and support has carried me through many challenges, both personal and professional.

Aldo Rossini has been an amazing mentor and guide through this PhD experience. He is a fantastic judge of character and situations and has never failed to recognize areas where I could improve; I know that I am a much better professional and physician-scientist for that. Dr. Rossini's commitment to translational diabetes research is world-reknown as evidencend by his recent Banting Award accolades. A tremendous part of that commitment is the training of the next generation of physician-scientists, and I am honored to be counted among those pupils to whom he has given so much time and energy.

iv

Rita Bortell, with her vast and broad knowledge, has provided an invaluable resource to my education, and her collaborative spirit and guidance made the research experience so enjoyable. Dale Greiner and John Mordes have been outstanding guides through the dissertation process and have taken much time out of their busy schedules to sit with me and discuss data. I would also like to acknowledge the other members of the Rossini and Moss Laboratories for their support and friendship. The Rossini laboratory has been like a second home to me, and the faculty, post-docs, students, technicians and support staff, have always been kind, generous, and eager to share scientific ideas. Special thanks to Eric Merrithew from the Lambright lab for his advice and guidance about crystallography data, as well as his aid in designing the structural figures.

A special acknowledgement to Joel Moss is due for his unwaivering commmmitment to my education. He has taken countless hours of his time teaching me how to design better experiments and going over experimental data. His refusal to "lower the bar" has brought me to higher levels of science, and I know I will be more successful because of it. This little discovery of PARP activity would never have come about, if I did not heed his lessons in understanding data and challenging assumptions.

Finally, I would like to thank the other members of the thesis committee for taking time out of their busy schedules to read my dissertation and to sit for my defense. Dr. Knight, as chair, has really helped to guide me with the timing and writing of this whole process. Dr. Evans, with his fantastic mass spectrometry core facility, has been a tremendous help of late with generating the last bits of data needed to complete this work. Dr.

Carraway, whom I've known and respected since medical school classes, has always been willing to engage in enthusiastic scientific discussions about recent data or what went on at the latest conferences.

Abstract

The glycophosphatidylinositol(GPI)-linked membrane protein ART2 is an antigenic determinant for T lymphocytes that regulate the expression of diabetes in the BB/W rat model. Though little is understood of the physiologic role of ART2 on T lymphocytes, ART2 is a member of the mono-ADP-ribosyl transferase subgroup of the ADP-ribosyl transferase (ART) protein family. The ART protein family, which traditionally has been divided into mono-ADP-ribosyl transferases (mono-ARTs), poly(ADP)-ribose polymerases (PARPs), and ADP-ribosyl cyclases, influences various aspects of cellular physiology including: apoptosis, DNA damage repair, chromatin remodeling, telomere replication, cellular transport, immune regulation, neuronal function, and bacterial virulence. A structural alignment of ART2.2 with chicken PARP indicated the potential for ART2.2 to catalyze ADP-ribose polymers in an activity thought to be specific to the PARP subgroup and important for their regulation of nuclear processes. Kinetic studies determined that the auto-ADP-ribosyl transferase activity of ART2.2 is multitmeric and heterogeneous in nature. Hydroxylamine-cleaved ADP-ribose moieties from the ART2.2 multimers ran as polymers on a modified sequencing gel, and digestion of the polymers with snake-venom phosphodiesterase produced AMP and the poly(ADP)ribose-specific product, PR-AMP, which was resolved by analytical HPLC and structurally confirmed by ESI-MS. The ratio of AMP to PR-AMP was higher than that of PARP raising the possibility that the ART2.2 polymers had a different branching structure than those of PARP. This alternative branching was confirmed by the presence of ribose phosphate polymers

in the snake venom phophodiesterase treated samples. The site of the auto-poly(ADP)-ribose modification was determined to be R185, a residue previously proposed to influence the level of auto-ADP ribosylation of ART2.2 by mutational analysis. These data provide the first demonstration of a hybrid between mono-ARTs and PARPs and are the earliest indication that PARP-like enzymes can exist outside the nucleus and on the cell surface.

Table of Contents

List of Figures

xiv

Chapter 1 What is Diabetes?

Chapter Introduction

Since the evolution of glucose metabolism, there has existed the potential for errors. Diabetes, simply put, is the result of one such error caused by an inability to signal for the uptake of glucose from the blood into cells. The resulting phenomenon is hyperglycemia (high blood glucose), from which stems a myriad of secondary problems that have come to be associated with the disease, diabetes. There are many ways to get to that disregulation of glucose uptake, and thus there are many forms of diabetes. The following dissertation will center on insulin dependent diabetes mellitus (IDDM), which is commonly known as Type 1 diabetes. Though, as the abstract states, ART2 is the focus of this research, understanding IDDM and how to prevent it are the heart of this project. How then are diabetes and ART2 connected? To better understand the connection and where it is going, it becomes important to look at the evolution of the question, 'what is diabetes?' Chapter 1 will take a brief look at the evolution of that question from ancient times to today. It becomes a more complicated question over time, and has expanded in many directions. In many ways, it seems as though the Heisenberg Uncertainty Principle applies because as scientists learn more about what diabetes is, it becomes harder to answer what is diabetes. Nevertheless, some very practical answers have developed from the process allowing physicians to influence patient care and allowing physician-scientists to ask more sophisticated questions.

Diabetes History

Egypt, circa 1550 BCE

In 1872 an Egyptologist named Georg Ebers discovered a large medical compendium in an almost perfect state of preservation (1). Analysis of this compendium, which came to be known as Eber's papyrus (Fig 1), revealed that it dated back to 1550 BCE and even contained passages with language and text that go back as far as 3400 BCE. Found in the Eber's papyrus upon translation were some of the earliest descriptions of medical diseases known to man along with antidotes that were both mythical and magical. Topics covered a wide range of disciplines including: the anatomy and pathology of the circulatory system; morbid conditions of the alimentary and urinary tract; obstetrics and gynecology; diseases of skin, teeth, ears, eyes; and even a study of cosmetics. Sections on "remedies" were extremely diverse ranging from things like keeping rats out of the granary to things like getting rid of sweaty feet. Of interest to this dissertation, Eber's papyrus contained what many believe to be the earliest known written descriptions of diabetes. The description was found under disease of the "cardia" (stomach or mouth) (2). Symptoms include weight loss, excessive urine, thirst, and periods of unconsciousness. The remedies were often various mythological reagents boiled with beer, strained and taken by the patient. In one section, a diabetic-like childhood illness of the "accumulation of urine" called for "an old book cooked in oil and rubbed all over the abdomen (3)."

Figure 1

A

B

Figure 1. **A. Imhotep, the Egyptian God of Medicine.** This is a copy of a rendering of Imhotep, also known as Thoth (or Athothis), a mortal who lived around the time of 3400 BCE. Thoth is known as a mortal who gathered such a great sum of healing knowledge and rendered such an extraordinary service to mankind that he was acclaimed a god by a grateful people and raised to the Egyptian Pantheon as the God of Healing Arts (3). Thoth passed into the Greek mythos as the god Hermes. **B. A "Page" from the Papyrus Ebers.** The Papyrus Ebers, containing some of the most ancient descriptions of diseases that still plague mankind today, is one of the oldest intact documents of the practice of medicine and can be found in a preserved state in the University Library of Leipzig. The Papyrus is merely one long scroll; twelve inches in diameter and 61.125 feet in length. Throughout its length, however, it was divided into "pages" like the one copied above. Each page was of equal size and averaging twenty lines.

Greece and Rome, circa 200 CE

Little else is known to be written of diabetes until about 1700 years after the writings of Eber's papyrus, when a famous Greek physician, Aretaeus of Cappedocia, actually coined the term "diabetes" for a series of patients with whom he had worked (1). The word, diabetes, is Ionian greek and literally means, "to siphon or to pass through." Aretaeus writes of diabetes:

> the patient never stops making water, but the flow is incessant, as if from the opening of aqueducts. The nature of the disease is chronic... but the patient is short-lived... for the melting is rapid, the death speedy. Moreover, life is disgusting and painful; thirst, unquenchable; excessive drinking, which, however, is disproportionate to the large quantity of urine, for more urine is passed and one cannot stop them (the patients) either from drinking or making water.

Around the same time Roman physicians were using the terms, diarrhea urinosa and dipsakos (excessive thirst) to describe similar illnesses. In many ways, the descriptions of the Roman and Greek physicians did not differ much with their Egyptian predecessors. Diabetes was an illness where the patient could not hold fluids: there was excessive thirst that could not replenish the fluids lost due to the tremendous volumes of urine (2). The patients appeared to waste away into phases of unconsciousness at first and then finally to death.

India, circa 600 CE

Two Indian physicians, Susruta and Charuka, made two interesting observations circa 600 CE when characterizing this disease of excessive thirst and excessive urine (1). The observations should really be noted for being hundreds of years before their time. In

fact, it probably was not until the seventeenth century that physicians began to truly appreciate the significance of these observations. The first observation was that the urine of diabetic patients was of a different consistency than that of the normal population. In fact, it was described as "sweet tasting like honey, sticky, and attractive to ants." The second observation made was that the disease seemed to come in two contrasting forms: the first presenting in 'older, fatter' people and the second in much 'younger, thinner' people. This second observation appears to be the earliest recognition of diabetes types 2 and 1, respectively.

England, circa 1620 CE

About 1000 years after Susrata and Charuka, while British colonies were being established in America, physicians in Europe continued to be perplexed by the illness of diabetes. One such physician, Thomas Willis, had written a statement that in some sense still holds true today. He wrote, "as to what belongs the cure, it seems a most hard thing in this disease to draw propositions for curing, for that its cause lies so deeply hid, and hath its origin so deep and remote." Many physicians at the time were operating under a false assumption made by Paracelsus a century earlier (2). Paracelsus, noted as one of the first physicians to receive special training in chemistry, concerned himself with diabetes, and after boiling down the urine of diabetic patients, he found a sizable amount of white crystals he interpreted to be salt. The result was a theory that linked diabetes solely with the kidneys, and that theory predominated the better part of a few centuries of medicine. Willis, like Susruta and Charuka, made reference to the sweet taste of diabetic urine, but

it was not until a century later that Matthew Dobson of Liverpool would identify the sweet white crystalline substance in urine as sugar (1). Dobson went on to discover that the sugar came from serum. This was the first evidence of what could be thought of as a systemic illness rather than a urinary/kidney disease. Around the same time, Michel-Eugene Chevrul, a French chemist, made similar independent finds (2). Further evidence of a systemic illness came from Richard Mead, another contemporary of the time period, who was the first to observe that the livers of diabetics were "fatty" compared to normal persons.

Germany, 1869 CE

In the late nineteenth century, a 21 year-old doctoral student in Berlin, Paul Langerhans, would discover the islets which now bear his name embedded in the pancreas (1). Langerhans refrained from postulating any function for his islets but instead focused on describing them with great accuracy. However, by the turn of the twentieth century, Edouard Laguesse and Jean de Meyer realized that the islets were endocrine tissue and reasoned that this tissue was the source of insulin (from the Latin insula for island), a largely hypothetical sugar/glucose-lowering hormone.

Canada, 1921 CE

A well-known fact at the turn of the twentieth century was that the diagnosis of diabetes was a death sentence for any patient, but by October 31, 1920, that fact began to radically change (4). At the time, a dissatisfied, practicing physician, named Frederick Grant Banting, was busy preparing a lecture on carbohydrate metabolism for the physiol-

ogy department of London's Western University. After working on the lecture, Banting read a copy of the article, "The Relation of the Islets of Langerhans to Diabetes with Special Reference to Cases of Pancreatic Lithiasis," by Moses Barron in the November issue of *Surgery, Gynecology, and Obstetrics*. Baron was relaying the observation that though acinar cells atrophied upon pancreatic duct obstruction, the islets survived intact. The data further supported the rising hypothesis that although the pancreas appeared to be involved in diabetes, the health of the islets was the important factor in the etiology of diabetes. While mulling over his life in bed that night, the combination of the lecture preparation and the article struck Banting with the idea that an experimental ligation of the pancreatic duct and subsequent atrophy of the acinar cells might allow for purification of the islet secretions. Those secretions according to his hypothesis should relieve glycosurea in pancreatectomized animals. He soon introduced his idea to J.J.R. Macleod in Toronto, and though Banting had little research experience, Macleod was impressed enough with Banting's idea that he allowed Banting to work on the experiment over the summer of 1922. Charles Best, a medical student at the time, was assigned by Macleod to work with Banting on the project. Though it was a difficult and hot summer in the physiology laboratories, Banting and Best succeeded at getting their pancreatic extracts to alleviate the blood glucose levels of pancreatectomized dogs (Fig 2). The experiments won them the Nobel Prize for Physiology and Medicine in 1923 and evolved into the most successful treatment for diabetes to date.

Figure 2

48

dog 408   Aug. 7th

4.00 A.M. Blood sugar — .21
the extract of aug 1st +
the remainder of Aug 5th extract
mixed — and somewhat diluted
⑤ making 25 cc in all injected
no urine obtained.
Blood Sugar .15
5.00, A.M. dog suddenly
became lifeless & appeared
to be dying. 30 cc Ringers
sol injected intraperitoneally
6.00 A.M. — 50 cc ringers
sol intravenously — slightly
improved. Bowels moved
twice during last ½ hour
saliva dribbled from mouth.
7.00 A.M. — dog slightly improved
8.00 A.M. Blood Sugar — .11
dog still more improved +
is now able to stand up

Figure 2. Banting Journal Entry. This is a photocopy of the famous "page 48" from the laboratory journal of Fredrick Grant Banting in the summer of 1921. The actual journal sits in the library of the University of Toronto. This page depicts the first experimental success that Banting and Best had at reviving a dying diabetic dog with their pancreatic extracts. As the page states, at "5:00 am the dog suddenly became lifeless and appeared to be dying with saliva dribbling from its mouth." After a couple injections of their extract containing insulin, the page states that within a few hours the blood sugar dropped and the dog was able to stand up. This page marks the beginning of a virtual overnight success as insulin treatment rapidly became the mainstay for patients around the world with diabetes.

Diabetes Today

Spectrum

Today the term diabetes reflects a broad spectrum of heterogeneous disorders with two etiologic poles; absolute insulin deficiency and relative insulin deficiency (Fig 3). Examples of absolute insulin deficiency include primary (idiopathic) disorders such as IDDM (insulin-dependent diabetes mellitus or type 1) as well as secondary disorders like pancreatectomy and chronic pancreatitis (5). Primary disorders such as NIDDM (non-insulin-dependent diabetes mellitus or type 2) fall under the auspices of a relative insulin deficiency. The primary symptom of all forms of diabetes, irrespective of where they lie along the two etiologic poles, is hyperglycemia (high blood glucose). It is estimated that diabetes causes about 144,000 deaths each year, making it the seventh leading cause of death in the United States. The focus of this dissertation is IDDM; also known as type 1, juvenile-onset, and ketosis-prone.

IDDM

IDDM is a variant of the forms of absolute insulin deficiency that accounts for about 10-20% of all cases of idiopathic diabetes in the United States, with the other 80-90% of idiopathic diabetes being primarily caused by the relative insulin deficiency, NIDDM. Clinically, IDDM patients often present before the age of 20 and fall in the category of the "young, thin" patients described by Sasruta and Charuka, nearly 1500 years ago. The prevalence of cases in the United States is 2-3 per thousand, a number that varies from country to country. IDDM is largely viewed as having its etiology from

Figure 3

DIABETES SPECTRUM

HYPERGLYCEMIA

RELATIVE INSULIN DEFICIENCY

ABSOLUTE INSULIN DEFICIENCY
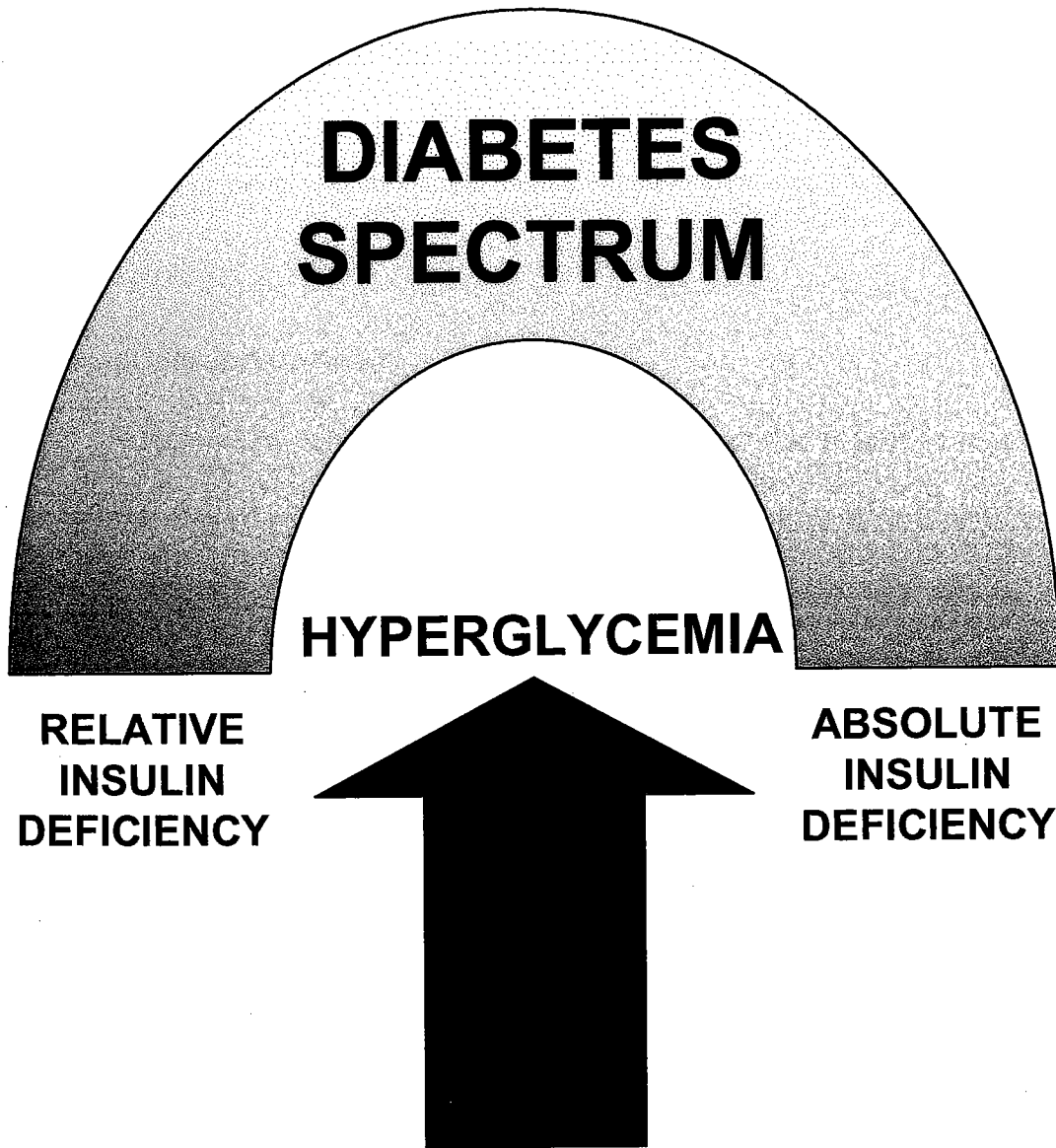
Figure 3. **Diabetes Spectrum.** Diabetes is thought to be a large spectrum of disorders with two primary etiological poles; absolute insulin deficiency and relative insulin deficiency. At the center of the spectrum regardless of etiology, there is a single common resulting symptom of all diabetogenic phenomena; hyperglycemia (high blood glucose).

both genetic and environmental factors which give rise to an autoimmune phenomenon that targets the insulin-secreting β-cells of the pancreas for destruction (6).

Genetics

Early evidence for the influence of genetics on diabetes comes from susceptibility studies of families. The concordance rate of monozygotic twins tends to average 50%, suggesting some level of genetic influence (7-9). In the same studies, dizygotic twins have the same rates as non-twin siblings. The concordance rate for first order (parent to offspring) inheritance averages 5-10%.

In more recent studies, a genome-wide search identified at least 4 genetic markers for diabetes expression in the human (10). In addition, a number of susceptibility loci in mice and rats have been identified and mapped to various chromosomal regions. Prevalence of the susceptibility genes varies with ethnicity and may explain why diabetes is common in Scandinavia and Sardinia, but uncommon in China (11). One susceptibility locus is found on human chromosome 6, in the genes encoding for the major histocompatability region, HLA-D (10;12). The HLA-D region contains three subregions: DP, DQ, and DR; the regions are highly polymorphic with numerous alleles. The *HLA-DQ3.2*(DQB1*0302) gene is most common in whites and is present in 70% of patients, giving individuals with this gene an eight-fold increase over those without for risk of developing IDDM (13). DR3 has also been linked to increased risk for IDDM and there appears to be synergism between DQ3.2 and DR3, resulting in a 20-fold increased risk for

diabetes. One of the major characteristics of the different susceptibility genes is that they code for an amino acid other than aspartate at position 57 on the beta chain of the HLA molecule (14). Conversely, there exists protective alleles (DQB1*0602, 0303, 0301, and 0403), most of which have an aspartate at position 57 and appear to decrease the risk of diabetes (14).

Other alleles not linked to the HLA region have also been found in the human as well as the two major animal models for IDDM, the NOD (non-obese diabetic) mouse and the BB rat. Although considered extremely important, the MHC genes are not sufficient for the development of diabetes, suggesting that there is some level of polygenic inheritance (10) In the human, there are three such genes that map to chromosomes 11 (IDDM2) (15), 15 (IDDM3) (10), and 2 (IDDM 13) (10;16). It has been demonstrated that the IDDM2 locus appears to regulate insulin transcription (15). The IDDM13 locus appears to affect insulin-like growth factor binding protein 2, but how a mutation in this gene affects susceptibility is unclear at present (16).

Environment

The same studies that provide rationale for a genetic component to IDDM 1 also provide the argument for environmental influences. After all, monozygotic twin concordance is not 100%, suggesting influences outside the realm of the genome. If one looks worldwide, the prevalence of IDDM varies from country to country. Finnish children have a 60 to 70 fold increased risk for IDDM than Korean children (5). Though one might argue that this is genetic, regional susceptibility studies involving Japanese, Israeli,

and Canadian emigrants have revealed that over time the emigrants assume risk ratios that more closely mimic those of the destination country. Regional susceptibility is not the only argument for environmental influences of diabetes. In the clinical setting, one often finds viral associations with overt IDDM onset. Mumps, measles, rubella, infectious mononucleosis, and Cocksackie B virus had all been correlated to early onset of diabetes (17).

Other data that support the role of the environment on IDDM expression comes from studies concerning diet (18). Studies of infants weaned from breast milk to cow's milk earlier in life reveal an increased incidence of IDDM. These patients contain anti-bodies to BSA (bovine serum albumin). It is thought that a 17 amino acid region of BSA stimulates the immune system to form antibodies against an islet β-cell protein called p69 through the process of molecular mimicry (19). Other studies have indicated another form of molecular mimicry between the F2C protein of Cocksakie B4 virus and GAD (glutamic acid decarboxylase, an enzyme found in the islets) that appears to influence diabetes expression (20;21).

Autoimmunity

The combination of a genetic predisposition and an environmental insult is thought to lead to the development of an autoimmune process that ultimately culminates in the selective destruction of the pancreatic β-cells, the very cells that secrete insulin. Evidence for this comes from both human and animal studies where, early in the diabetic process, during a period called the "honeymoon" phase, there is vast mononuclear infil-

tration of the islet cell mass of the pancreas. This insulitis (inflammation of the islet) eventually resolves with a selective loss of the β-cells (Fig 4) and culminates in the fully diabetic state, because without β-cells generating insulin, there is an absolute insulin deficiency that results in an inability to regulate blood glucose levels. The patients and animal models often develop antibodies specific to the islet β-cell, and in humans, there have been associations of IDDM with other autoimmune disorders like Graves' disease, Addison's disease, thyroiditis, and pernicious anemia (5;22). The BB rat, an animal model of IDDM, also demonstrates an association of diabetes with thyroiditis (23). Further evidence of an autoimmune phenomenon comes from patient studies, demonstrating that the presentation of diabetes can be delayed or prevented by immuno-suppression (24;25).

In the clinic, many patients present with an elevated presence in the bloodstream of antibodies specific to the Islet cells (6;26). Proteins like GAD (glutamic acid decarboxylase), insulin, carboxypeptide H, glima 38, p40 tyrosine phosphatase, and insulinoma-associated protein 2 (IA-2, tyrosine phosphatase) have all been targets of these autoantibodies. Islet cell cytoplasmic antibodies have also been demonstrated. In the NOD (non-obese diabetic) mouse, another animal model for IDDM, a T cell response targeting GAD appears to precede overt diabetes (27). Further, autoantibodies to GAD are found in about 70% of patients with IDDM at the time of diagnosis (28). There is reactivity to GAD epitopes early in the honeymoon phase, and tolerance to GAD in the NOD mouse appears to prevent other autoantigens and insulitis from occurring (29). The

Figure 4
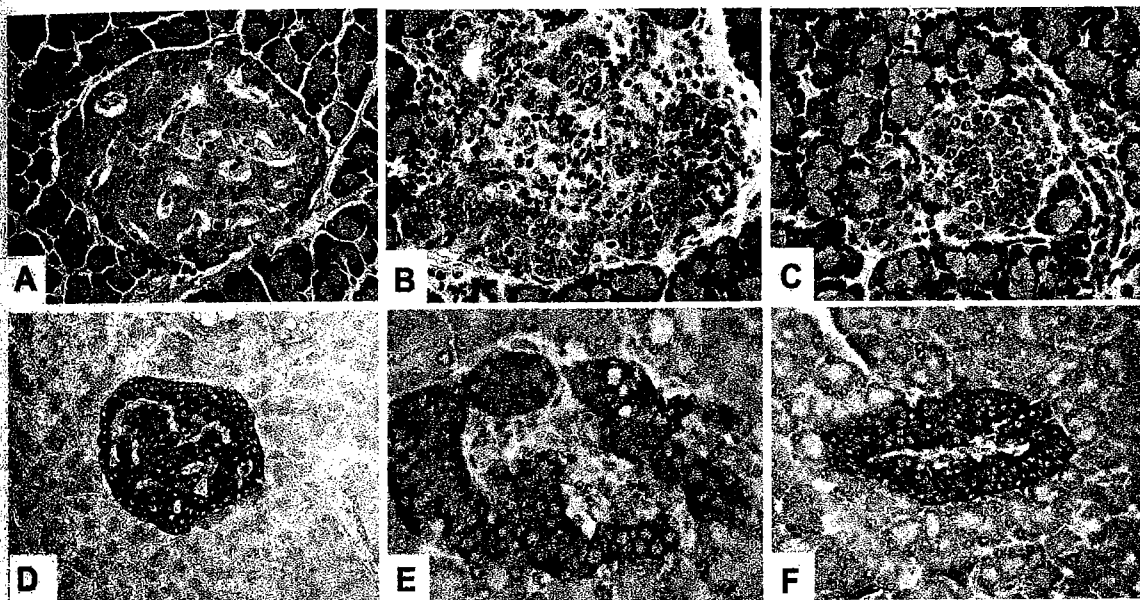
Figure 4. **Histological progression of spontanseous autoimmune diabetes mellitus in the BB/W rat. A.** Normal islet, H & E stain, x250. **B.** Insulitis progresses with an intense destructive mononuclear infiltration into the islet interior, H & E, x250. **C.** "End stage" islets exhibit a reduced cellular mass when insulitis subsides, H & E, x250. **D.** With two-color immunohistochemistry, islet glucagon, somatostatin and pancreatic poly-peptide cells comprise the peripheral islet mantle (blue) of a normal islet and the pre-dominant insulin-positive cells are seen in the islet interior (brown), peroxidase immuno-histochemistry, x160. **E.** Cytotoxic inflammatory cells are specifically targeted against the insulin producing β-cells within the islet interior and mantle glucagon, somatostatin and pancreatic polypeptide-producing cells (brown) remain intact, peroxidase immuno-histochemistry, x250. **F.** At the conclusion of autoimmune insulitis, non-imflammed "end-stage" islets remain and are devoid of insulin-positive cells and are comprised of exclusively glucagon, somatostatin, and pancreatic polypeptide-producing cells (brown), peroxidase immunohistochemistry, x250. Images were courtesy of Mike Appel of the University of Massachusetts Medical Center Diabetes Division.

NOTE: Panel D – blue cells are identified using an antibody slurry of primary antibodies having a final dilution as follows: glucagon (1:2000 prepared by M. Appel); somatostatin (1:1000, a gift from J. Einsink); and pancreatic polypeptide (1:1000, DAKO). Insulin primary antibody (1:1000, produced by M. Appel) identified brown cells. In panels E and F, brown cells are identified by the antibody slurry and insulin cells are absent.

significance of GAD is still debated, however, since cloned T cells that do not respond to GAD can still transfer diabetes to other mice.

Antibodies targeting insulin also appear early in overt diabetes. It has been estimated that >80 percent of T cells infiltrating islets in four week old NOD mice recognize the same epitope on the insulin B chain (30). There are similar responses in the peripheral lymphocytes from patients with recent-onset IDDM (31). Furthermore, administration of insulin or B chain during the prediabetic phase can prevent or delay diabetes in susceptible mice (32;33). Though little is understood as to how insulin would become a target for the immune system, it has been shown that alternate forms of insulin can lead to misfolding and the blockage of transport of proinsulin from the endoplasmic reticulum to the Golgi apparatus, resulting in an absolute insulin deficiency in the Akita diabetic mouse (34). One might hypothesize that under the right conditions, altered presentation of insulin to the immune system could account for the initiation of the diabetic autoimmunity. However like GAD, the significance of insulin in the initiation of autoimmunity is still widely debated.

Several drugs, some immunosuppressive, have been shown to prolong the "honeymoon phase," effectively delaying the onset of IDDM. Azathioprine, an immunosuppressive drug, which inhibits T cell responses to antigen in combination with glucocorticoids demonstrated such effects (35). Cyclosporine also had similar effects in patients, sending some patients into a remission period of up to three years (36). Nicotinamide was found in the NOD and steptozotocin toxicity mouse models of diabetes to protect the

β−cells from undergoing cell death (37;38). It is thought that nicotinamide, an inhibitor of PARP, acts to protect β−cells by preventing energy depletion (see Okamoto Model, Chapter 3) (39). In clinical trials with nicotinamide, endogenous insulin production measured by C peptide in the sera, was prolonged though patients did not show signs of remission (40).

Chapter Conclusions

The understanding of the etiology of diabetes has evolved tremendously over the last 3000 years from the early basic observations of poly-urea and poly-phagia. The observation of sweet-tasting urine has evolved to excess sugar in urine and then to excess glucose in the blood, leading to the understanding that diabetes is a systemic illness. The observations that there are two general types of diabetes occurring in either young and thin patients or old and obese has evolved into a theory that diabetes is a complex disorder with multiple etiologies but with two main poles, absolute or relative insulin deficiency. For IDDM, there is a general recognition that both genetics and the environment play an important role in the initiation of overt diabetes. The role of GAD and insulin and other islet cell antigens in the initiation of autoimmunity is currently under active investigation. Though there have been answers to some basic questions, there are still even more questions to the etiology of diabetes. To answer those questions, scientists turn to animal models. Chapter 2 will introduce a few models and lead into some of the major hypotheses that drive this work.

Chapter 2 Rat models of IDDM, and in particular the BB rat

Introduction

For the past eighty years, insulin has been the mainstay of treatment for patients with IDDM, but there are many caveats that come with insulin. There are patients that have aversions to needles; a diabetic injects insulin an average of 30,000 times over the course of his/her life. There are "brittle" patients who have difficulty controlling their blood glucose levels regardless of how rigidly they monitor their blood glucose levels. Even with the best care, there are several secondary illnesses related to chronically elevated blood glucose that these patients have to worry about: neuropathies, angiopathies, and heart and kidney diseases. The overarching hypothesis is that a fuller understanding of the etiology of diabetes might allow physicians to recognize predisposed individuals and allow treatment that prevents the onset of diabetes. For those who already have the disease, transplantation of islets without immuno-suppression or recurrence of the auto-immunity is the goal.

The study of human diseases can often be quite limited and difficult due to various ethical and practical considerations that limit access to human tissue for experimental work. In the case of diabetes, practical considerations include inaccessibility of the diseased organ, the difficulty in identifying predisposed individuals (currently due to costly and imprecise technologies), the complexity of having multiple genes involved, and the difficulty of isolating and identifying the environmental influences. To resolve these issues, the development of animal models for various illnesses has become a widespread

practice (41). Over the past few decades several animal models for IDDM have been developed: the BB rat, the NOD mouse, the Komeda rat, and the congenic LEW rat (LEW.1AR1/Ztm-*iddm*). Chapter 2 will serve to briefly introduce the various rat models. The focus of the chapter will be the BB rat from which are derived the major hypotheses of this dissertation.

Komeda rat

The Komeda rat is an animal model of IDDM that was developed in the late 1990's (42). It is a diabetes-prone substrain of the Long-Evans Tokushima lean rat. The Komeda is characterized by autoimmune destruction of the pancreatic β-cells that results in overt diabetes. Unlike other diabetic models such as the BB rat, there is no significant T cell lymphopenia associated with this phenomenon. The cumulative frequency of diabetes is 80% at 220 days of age, though moderate to severe mononuclear lymphocyte infiltration of the pancreatic islets occurs in most animals. Genome-wide scans for diabetes susceptibility revealed the MHC (major histocompatability complex) on chromosome 20, which functions in a mostly recessive manner, and *Iddm/kdp1* on chromosome 11, which functions in a completely recessive manner (43). The locus was placed in a 9.3 then 4.6 then 3.0 cM region between *D11M16Mit14* and *D11M16Mit46*.

Recently, the *Iddm/kdp1* susceptibility locus was identified, using positional cloning of the region (44). The result was a nonsense mutation in *Cblb*, a member of the Cbl/Sli family of ubiquitin-protein ligases. Cbl-b has been shown to regulate the dependence of T-cell activation on CD28 co-stimulation in mice (45). *Cbl-b* knock-out mice do

not require CD28 engagement for interleukin-2 (IL-2) production. Lymphocytes of the Komeda rat infiltrate into the pancreatic islets, the thyroid, and the kidneys, indicating autoimmunity involving multiple tissues (44). This is similar to the *Cbl-b* knockout mice, which develop an autoimmune encephalitis that appears to mimic multiple sclerosis (45). The theory is that these animals experience enhanced T cell activation. Because of these findings, Cbl-b has been termed a negative regulator of autoimmunity as well as one of the major non-MHC susceptibility loci for diabetes in the rat.

Congenic LEW rat

The Congenic LEW (LEW.1AR1/Ztm-*iddm*) rat was first described in 2001 (46). It arose through a spontaneous mutation in congenic Lewis rat strain with the defined MHC haplotypes ($RT1.A^aB/D^uC^u$). The incidence of diabetes was 20% by 60 days of life. Unlike the BB rat, the proportion of T cells in the periphery expressing the ART2.1 differentiation antigen was normal. There is severe mononuclear infiltration of the islets with selective β-cell loss. By electron microscopic structural analysis, the β-cells have an apoptotic phenotype. GAD, islet cell cytoplasmic, and IA-2 antibodies were not detected in the LEW. Concavalin A-stimulated T cells could adoptively transfer diabetes with an increased incidence of 64%.

BB rat

The focus of this thesis has developed from studies of the BB rat, the oldest known rat model of IDDM, which began as a spontaneously diabetic rat colony from BioBreeding Laboratories in Ottawa, Canada, in 1974 (47). From this colony, several

secondary breeding colonies were produced and selective breeding has established colonies with >90% frequency of spontaneous diabetes (48). The BB rats mimic the presentation and pathology of the human IDDM disease. Spontaneous insulitis occurs, followed by selective β-cell destruction that results in an absolute insulin deficiency and hyperglycemia (49). Unless treated with exogenous insulin, hyperglycemic rats progress to fatal ketoacidosis. Also similar to the human is the association of diabetes with other autoimmune phenomena. In particular, the BB rat often develops a thyroiditis that occurs at different frequencies depending on the subcolony (48). Like the Congenic LEW and other autoimmune predisposed rat models, the BB rat has pancreatic insulitis, and severe β-cell destruction appears to correlate with the class II $RT1^u$ MHC (48). Unlike the LEW, in the BB rat there is a severe lymphopenia associated with spontaneous diabetes.

BB rats contain a variety of autoantibodies which are present in some substrains but not others. GAD antibodies for the most part are reportedly absent in most lines of the BB, but may be present in the BB/OK strain. IA-2 antibody is either absent or present at low levels in BB rats. IAAs (insulin auto-antibodies) also appear to be present in some strains of the BB rat and not others. As in the human, the extent to which humoral immunity may play a role in the pathogenesis of the disease in unclear at present.

Diabetes Prone

The diabetes-prone BB rat (BBDP) is a strain derived from the original BB rats, which through selective breeding has a cumulative frequency of diabetes >90%. A majority of the animals turn diabetic between the ages of 55 and 120 days. Like the human

IDDM, 100% of diabetic rats have insulitis during the early stages of overt diabetes. Of the rats that are non-diabetic, approximately 50% have insulitis. Treatment of DP rats with cyclophosphamide has been shown to inhibit diabetes expression (50).

The BBDP strain is also noted for its marked peripheral lymphopenia. This lymphopenia is due to a frameshift mutation in the *lyp/iddm 1* gene, recently identified as Ian4 (51), which appears to be a survival factor for T cells that mature through the thymus (52). Ian4 is a member of a unique set of G proteins and is expressed in the mitochondria (53). It is thought to stabilize mitochondrial membrane potential of naïve T cells because BBDP T cells have decreased mitochondrial membrane potential and appear to undergo apoptosis. Treatment with cyclosporin A can rescue these T cells from apoptosis. The lymphopenia affects particular subsets of the lymphocyte populations and in particular, ART2-expressing cells (48). The remaining lymphocyte fractions appear to contain an autoimmune-effector population that can adoptively transfer diabetes to nude recipients.

Diabetes Resistant

The diabetes-resistant (DR) subline of the BB rat was established from inbreeding DP rat forebears that were normoglycemic, nonlymphopenic, and immunocompentent (48). Unlike the DP, the DR does not contain the nonsense mutation for Ian4 (*lyp/iddm1*). When housed in a viral antibody free (VAF) vivarium, 0 % of the rats become diabetic. One interesting feature of the DR rat is its propensity to become diabetic in response to environmental perturbation. A viral infection such as KRV, a combination treatment of the ART2-deleting antibody, DS4, with an immune stimulus such as polyI:C,

low-dose irradiation, and cyclophosphamide (counter to its effects in the DP) are typical examples of the environmental queue. The DR appears to harbor a population of auto-immune effector cells that are normally regulated by subpopulations of ART2$^+$ T lym-phocytes. Like other autoimmune models and the human, DR rats are susceptible to other autoimmune states and in particular, collagen-induced arthritis and thyroiditis.

The BBDR rat is thought to model human diabetes more accurately than its DP predecessor because of the non-lymphopenic state and the need for environmental queues as well as the genetic components (49). As with humans the inheritance of the disease is associated with a permissive MHC, designated *iddm2* for the rat. This is the RT1u allele mentioned earlier. An additional susceptibility locus has been determined by backcrosses to normal WF rats and selection for inducible diabetes using the low-dose poly I:C and ART2-deleting antibody, DS4 (54). The locus was mapped to chromosome 4 and termed *iddm4*. As it stands, *iddm4* is centered on a small segment of chromosome 4 bound by the proximal marker *D4Rat135* and the distal marker *D4Got51*, an interval of <2.8 cM. The allele has 79% sensitivity and 80% specificity in prediction of diabetes in rats that segregate for this locus. That suggests that *iddm4* is a major non-MHC determinant of susceptibility for IDDM.

The Balance Hypothesis

The etiology of autoimmunity with respect to IDDM has been depicted as analo-gous to a teeter-totter through a working hypothesis derived from the BB rat (Fig 5) (48).

Figure 5

DP-BB Rat
Iddm1/Ian4, iddm2, iddm4

DR-BB Rat
iddm2, iddm4

β cell

ART2⁺ Cell Transfusion

ART2

β cell

ART2⁺ Cell Depletion And Immune Stimulation
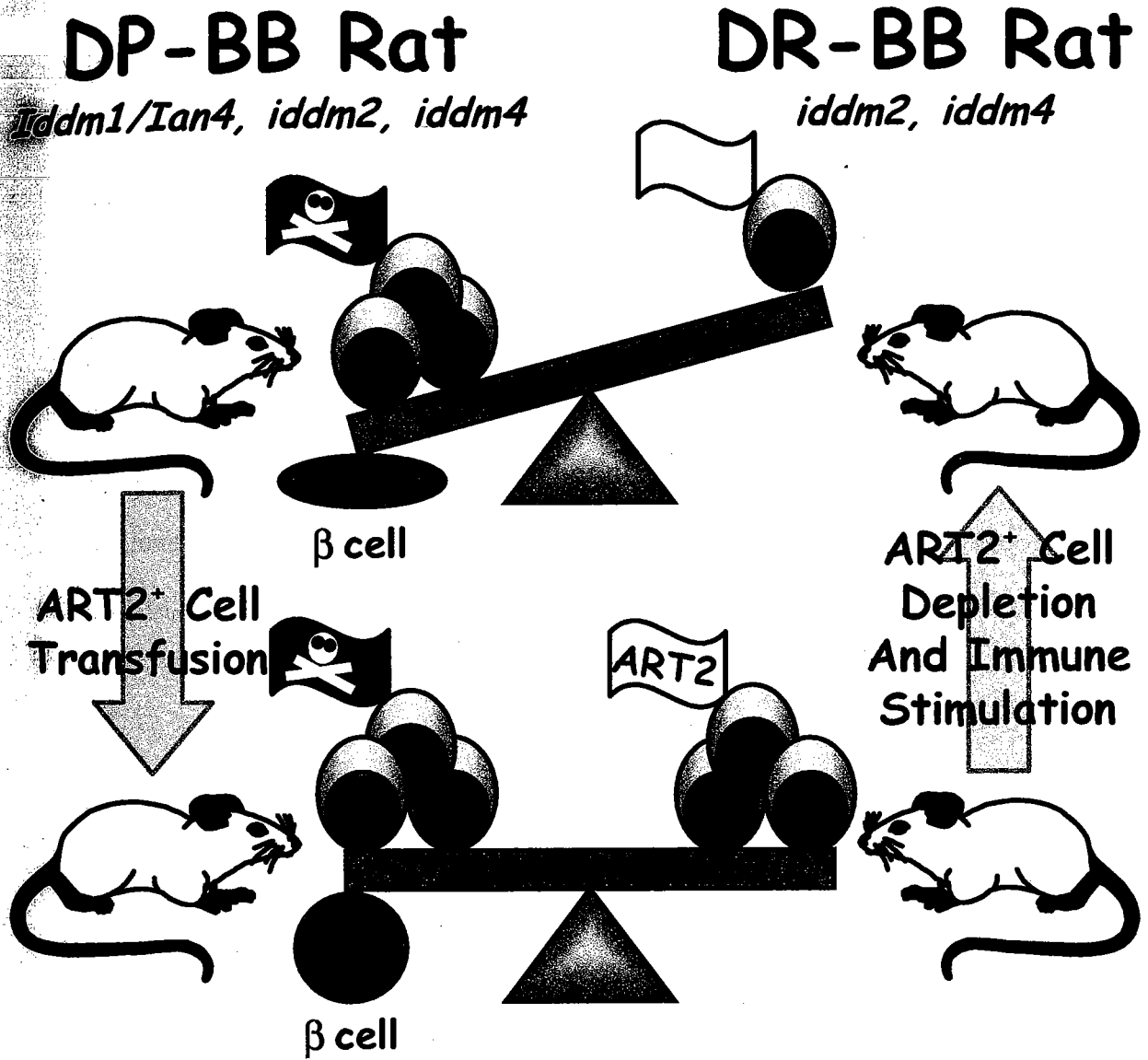
Figure 5. **The Balance Hypothesis of Autoimmunity as it pertains to IDDM in the BB/W Rat Model.** Depicted are the diabetes prone (DP-BB) and the diabetes resistant (DR-BB) rats, together with the situations known to alter the balance between autoreactive (A) and ART2$^+$ "regulatory" (R) cells. Also indicated are the genetic susceptibility loci associated with DP-BB and the DR-BB strains. The DP-BB rat is in a state of disequilibrium between its autoreactive cells and "regulatory" cells because of the lymphopenia caused by *iddm1/ian4*. The end result is that the autoreactive cells selectively squelch the β-cells of the pancreatic islets. Balance can be restored by transfusion of histocompatible ART2$^+$ T cells. The DR-BB rat is in a natural state of equilibrium, but that equilibrium can be perturbed by a depletion of ART$^+$ cells in conjunction with a strong immune stimulus such as poly I:C. Infection with a virus such as KRV (Kilham rat virus) can also disrupt the balance leading to overt diabetes expression.

The hypothesis states that expression of diabetes is dependent on a balance between autoreactive effector cells and "regulatory" suppressor-like cells that keep these autoreactive cells in check. With the DPBB, the ability to adoptively transfer splenic populations to non-diabetic animals causing overt diabetes, suggests the presence of some autoreactive lymphocytic population. The ability to prevent disease in the DPBB rat by transferring ART2$^+$ T cells to deficient animals suggests some sort of regulatory population amongst the ART2$^+$ cells. The DRBB provides a secondary example that further supports the "Balance Hypothesis". Because there is no lymphopenia in the DRBB, the balance between autoimmune effector populations and regulatory populations is favorable. By perturbing that balance with a depleting antibody for ART2$^+$ cells and an immune stimulus such as poly I:C, one can generate a state that results in overt disease. Cyclophosphamide and low dose irradiation can also precipitate diabetes in the DRBB as can viral infection with KRV (Kilham rat virus). Adoptive transfer experiments have shown that the DRBB harbor autoreactive populations, similar to the DP, that are capable of attacking the pancreatic β-cells.

ART2

Because ART2 has remained a major marker that differentiates between autoimmune effector cells and regulatory cells, the physiologic role of ART2 becomes an important question for immunologists. What is ART2? ART2 is a glycosylphosphatidylinositol (GPI) – linked protein found on the surface of various populations of T lymphocytes, NK cells, and intra-epithelial gut lymphocytes (IELs) (55). As previously noted, ART2 is

an antigenic determinant of "regulatory" T cell populations that prevents diabetes expression in the BB rat. ART2 comes in two forms: cell associated (GPI-linked) and soluble. In the rat, ART2 is encoded at a single locus on chromosome 1; two alleles, ART2.1 and ART2.2 have been identified. ART2.1 and ART2.2 are 95% identical differing by ten amino acids. Within that ten amino acids, ART2.1 contains a glycosylation consensus site; ART2.1 has been demonstrated to be glycosylated on lymphocytes (56). In the mouse, ART2 is found as two genes from a duplication event; Art2a and Art2b (57). The human ART2 locus contains a pseudogene with three stop codons and is not expressed (58). Though this fact has caused some controversy over the relevance of studying ART2, there are at least four other known ARTs that are expressed in the human and two of them have already been demonstrated to be expressed by the immune system, ART1 and ART4 (59).

ART2 is a member of the mono-ADP-ribosyl transferase family of proteins including the bacterial toxins, cholera toxin and pertussis toxin (60). This protein family exerts its effects by catalyzing the ADP-ribosylation of proteins in a post-translational modification that, analogous to phosphorylation, can modulate target function. The result of this ADP-ribsoylation is either activation or inactivation of the target molecule. ART activity in the BB rat appears to alter T cell immune function and may modulate directly diabetes expression (61). In the mouse, ART2 levels are known to correlate inversely with autoimmunity in at least two models (62;63). There is also evidence in normal mice that an ART2-like molecule is important in regulation of T cell cytotoxicity (64).

ART2 Hypothesis

The long-term hypothesis of this dissertation is that as a member of the ADP-ribosyl transferase super-family of proteins, ART2 modulates immune function via the enzymatic activities that are intrinsic to that super-family. Furthermore, ART2 immuno-modulation may play a role in regulating the autoimmune effector cells that can, when unrestrained, initiate processes that lead to overt diabetes in the BB rat model.

Chapter Conclusions

Intrinsic to development of a plan for diabetes prevention is a better understanding of the underlying etiologies that lead to overt disease. In the human, as described in Chapter 1, a combination of genetics and the environment appear to lead to an autoim-mune state that selectively attacks and destroys the pancreatic β-cells, the very cells that are responsible for insulin secretion. Several animal models have been developed over the years to better understand the varying genetic, environmental, and immune states that can lead to overt diabetes. The focus of this work has been the BB rat from which the Balance Hypothesis was derived. Important to the hypothesis is the antigenic determinant ART2, which remains the only marker that distinguishes between autoimmune effector cells and "regulatory" cells over the 30 years since the discovery of the BB rat. This leads to the question, 'what is ART2?' ART2 is a GPI-linked T cell surface protein that is part of a family of enzymes called ARTs. Often an intrinsic enzymatic activity can provide insight into the physiologic role of a protein. Before exploring ART2 further, the next

chapter will serve to introduce the ART superfamily and provide the background needed

to take a closer look at the ART2 molecule.

Chapter 3 ADP-Ribosyltransferase Super-family

Chapter Introduction

The purpose of this chapter is to introduce the ADP-ribosyltransferase (ART) super-family and its various subgroups and develop an understanding of how their enzymatic functions can influence physiologic conditions. What has previously been established about ARTs, their catalytic activities as well as their relationships to ART2 will be introduced. The chapter will take a two-pronged approach; first, an introduction to the biology of these molecules and second, a closer inspection of the structural biochemistry behind the catalytic activities. Since the pool of ARTs that have been modeled by x-ray crystallography is steadily growing, patterns should emerge that provide insights into the activities of the entire super-family.

Prokaryotic ADP-Ribosyltransferases

Cholera toxin

Early studies of the mono-ARTs center on the bacterial toxins involved in the pathogenesis of cholera, diphtheria, and pertussis. The toxins play a major role in virulence of colonizing bacteria and are often responsible for the pathogenesis of disease. Cholera, a disease with the principal symptom of severe, dehydrating diarrhea, is endemic to the developing countries of Asia and Africa. It was among a group of emerging infectious diseases of the 1990's particularly in South and Central America where the Vibrio cholera O1 serotype reached epidemic levels (65;66). A second and new major serotype

O139 spread from India throughout Asia and the Middle East at almost epidemic levels in 1992 (67;68). There are also several other "non-O1" strains that are responsible for the sporadic cases of gastroenteritis that can occur. Cholera is caused by ingestion of food or water contaminated by the bacteria, *Vibrio cholerae*. In fact, municipal water supplies were determined to be the source of a majority of cases in the Peruvian epidemics of the 1990's (69). The seminal observation that water was one of the major routes for cholera transmission was made by John Snow during the cholera epidemic of London in 1854 (70). In 1883, Robert Koch was the first to demonstrate that cholera is produced by an organism that he designated the "comma-shaped" bacteria (71).

Following colonization of the intestinal tract, *V. cholerae* go on to produce their major virulence factor, cholera toxin (CT). CT is an oligomeric protein consisting of one catalytic A subunit and five B subunits (72) (Fig 6). The B subunit of the toxin binds to ganglioside GM1 on the surface of epithelial cells (73). Upon GM1 binding, CT is then endocytosed and follows retrograde transport from the endosomes to the Golgi and ER before translocation to the cytosol (74). The A subunit is then activated by reduction into fragments A1, the enzymatically active ART, and A2, the anchor to the B subunit (72). A1 passes into the cytosol and ADP-ribosylates an arginine residue in the α-subunit of the heterotrimeric GTP-binding protein, Gs, which is the stimulatory subunit of the adenylyl cyclase complex (75). This leads to constitutive activation of the adenylyl cyclase complex, resulting in increased and sustained production of the second messenger, cAMP. Because of the effects of cAMP on various cellular systems, there is increased chloride secretion. This results in decreased sodium absorption, and because of the subsequent

Figure 6

GUT LUMEN

DIARRHEA

Cl⁻ Cl⁻
Cl⁻ Cl⁻
Cl⁻ Cl⁻
Cl⁻ Cl⁻ Cl⁻

CT

ADPR

GSα Of
Adenylyl
Cyclase

cAMP
elevation

ENTEROCYTES

IL-6, IL-10
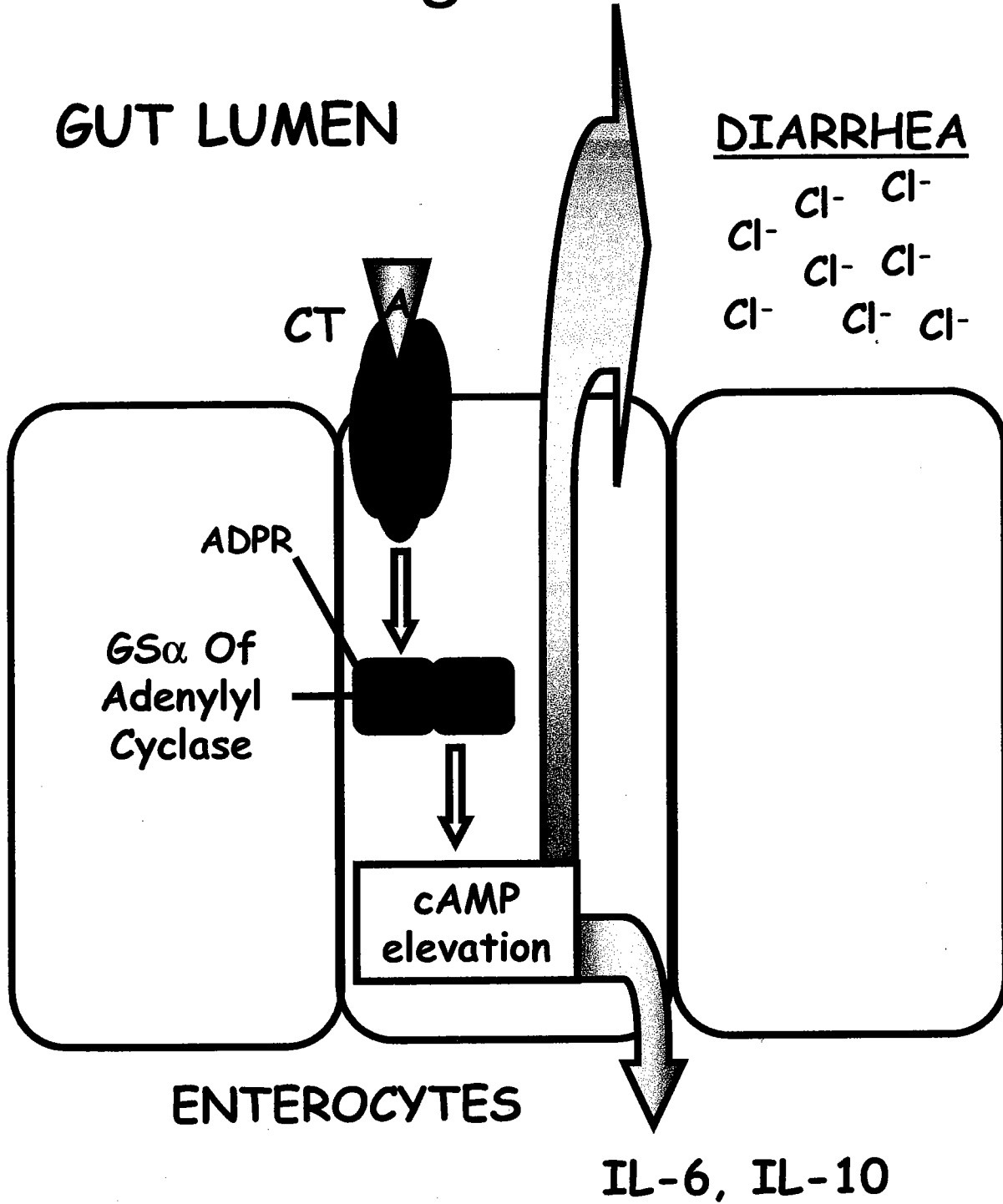
Figure 6. **Illustration of Cholera Toxin (CT) Biology.** Cholera toxin is secreted by the bacteria *Vibrio cholerae* upon colonization of the intestinal tract. CT is an oligomeric protein consisting of one catalytic **A** subunit and five **B** subunits. The B subunits bind to GM1 ganglioside on the surface of epithelial cells and promote the internalization of the A subunit. Upon translocation to the cytosol, the A subunit proceds to make use of intracellular stores of NAD to catalyze the ADP-ribosylation of the $G_s\alpha$-subunit of the adenylyl cyclase complex. This results in constitutive activation of the adenylyl cyclase complex and elevation of cytosolic levels of cyclic AMP (cAMP), a potent second messenger which influences various processes such as the transcription of cytokines and the regulation of Cl⁻ ion pumps. Disruption of Cl⁻ pumps results in massive fluid and electrolyte losses that culminate in a severe, dehydrating diarrhea, the hallmark symptom of cholera.

osmotic effects, massive fluid losses that translate to the severe, dehydrating diarrhea and electrolyte loss that are the hallmark of the disease.

Secondary effects of elevated cAMP include changes in the transcription and translation of the immunoregulatory cytokines, IL-6 and IL10, which are secreted from the epithelial cells. CT may also lead to increased prostaglandin production which has been suggested to be even more relevant to the gastrointestinal fluid and electrolyte losses. This stems from data showing decreased fluid and electrolyte loss in animals that are treated with inhibitors to prostaglandin synthesis (76). Other correlative data have demonstrated that patients with cholera have increased prostaglandin E2 concentrations in their intestinal samples (77).

Pertussis

Pertussis Toxin (PT) is the main virulence factor of several toxins secreted by the bacterium, *Bordetella pertussis*, which causes the disease commonly known as whooping cough (78). Vaccination against this toxin can actually confer considerable protection against infection by *B. pertussis* (79). Like CT, PT is an A-B toxin. The S1 subunit (A) contains the catalytic domain for ADP-ribosyltransferase activity (78). The B oligomer is composed of subunits S2, S3, S4 (x2), and S5, and is responsible for binding to the cells. Pertussis toxin catalyzes the transfer of ADP-ribose from NAD to cysteine residues of the α-subunit of heterotrimeric, inhibitory G-proteins. The α-subunit of G_i, an inhibitory protein, becomes uncoupled from its receptor, resulting in constitutive activation of ade-nylyl cyclase, thus accomplishing an effect similar to cholera toxin though through a

different target. PT also ADP-ribosylates cysteine 347 of transducin, an abundant retinal heterotrimeric GTP-binding protein that couples the rod outer segment light receptor, rhodopsin, to a cGMP phosphodiesterase involved in retinal signal transduction (80).

Diphtheria

Diphtheria is an acute respiratory disease caused by *Corynebacterium diphtheria*, a pleiomorphic gram-positive bacillus. Toxigenic strains cause a pseudomembranous pharyngitis with myocarditis, neuritis and, nephritis developing as secondary complications. The principal cause of virulence in toxigenic strains is diphtheria toxin (DT), which was actually the first toxin found to produce its effect through ADP-ribosylation (81). DT is a 58 kDa protein secreted by strains of C. diphtheria that are infected by a phage that carries the DT gene (82). DT consists of three domains; R, T, and C. The R and T domains assist with binding and delivery of the catalytic C domain to the cytosol of the host cell. The N-terminal C domain of 22 kDa, is proteolytically cleaved and reduced (Fig 7) to become the active toxin during delivery (83;84). The active fragment catalyzes the transfer of the ADP-ribosyl moiety to the diphthamide (85) of the eukaryotic protein, elongation factor 2 (eEF-2), inactivating eEF-2 in a way that results in inhibition of protein synthesis (81). Diphthamide is a unique, posttranslationally modified histidine residue found only in EF-2. By shutting down protein synthesis, DT effectively kills the target cell. Dilution studies have revealed that the catalytic activity of diphtheria toxin is so efficient at inactivating eEF-2 that it only takes a single molecule of fragment A of DT to kill an entire cell (86).

Figure 7

1. Proteolytic Nicking
2. Sulfhydryl Reduction
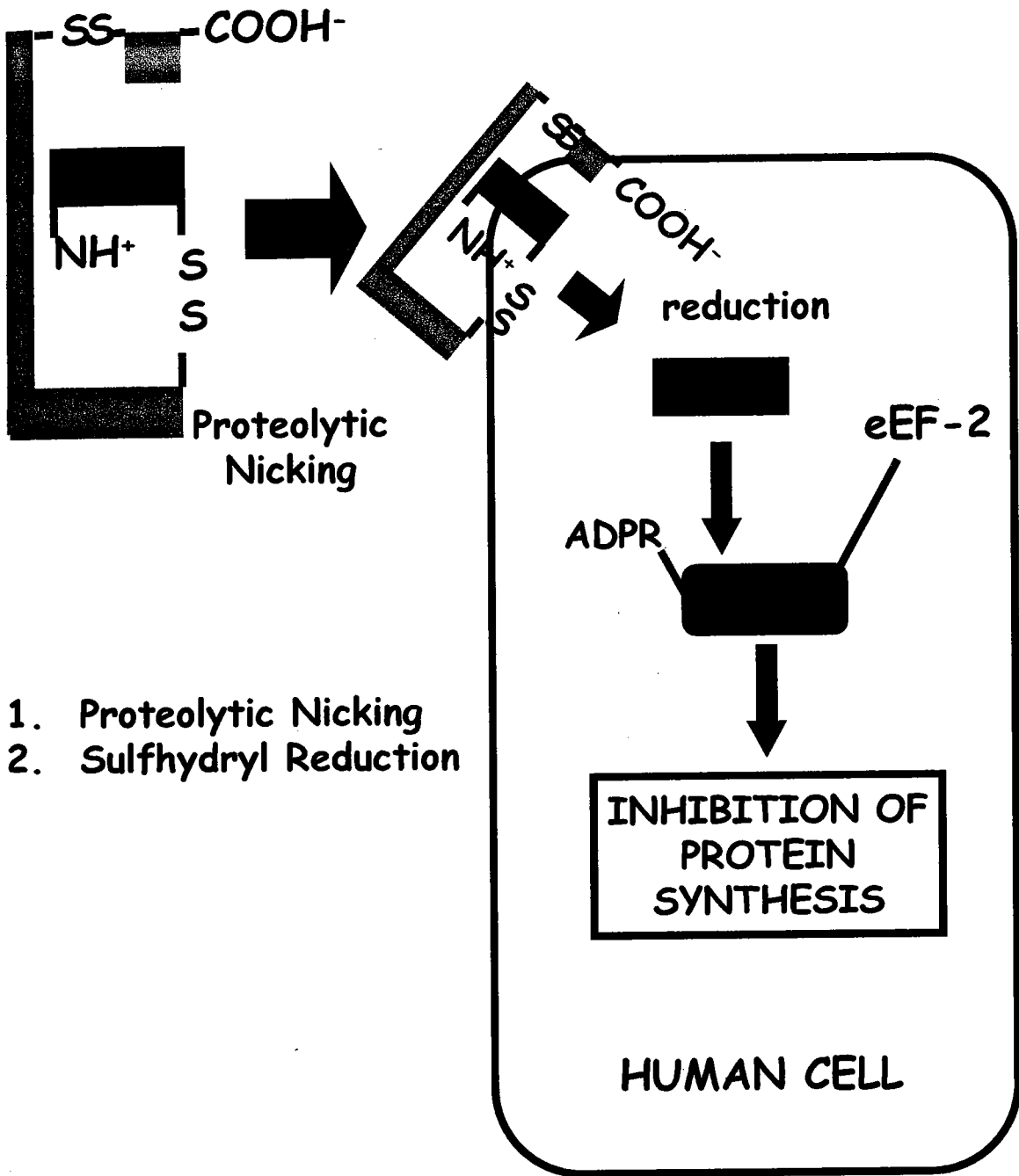
Figure 7. **Diphtheria Toxin Biology.** Diphtheria toxin (DT) is secreted by the bacterium, *Corynebacterium diphtheriae*, and is composed of three domains. The N-terminal C domain is responsible for catalytic activity. The C domain is activated by a process of proteolytic nicking and sulfhydryl reduction as it enters the cytosol. In the cytosol, DT makes use of the cellular NAD stores to ADP-ribosylate eukaryotic elongation factor 2 (eEF-2) at diphthamide, the posttranslationally modified histidine found only in elongation factor 2. This ADP-ribosylation inactivates eEF-2 and shuts down all cellular protein synthesis, ultimately resulting in cell death.

Pseudomonas

Pseudomonas aeruginosa is a gram negative, nonfermenting bacillus that is relatively common in the environment and can contaminate sources of water and distilled water (87). In the past, it has been demonstrated to be the cause of infections from hot tubs and contact lens solutions (88;89). *P. aeruginosa* is of particular significance because of its potential as a pathogen in hospitals. It is often found in immunocompromised hosts (90), burn patients, and cystic fibrosis patients (91). Of concern some strains are resistant to multiple antibiotics (92).

The virulence of *P. aeurigonosa* has been demonstrated to be associated with a number of substances including toxins, proteases, hemolysins, lipases, adhesions, agglutinins, pili, enterotoxins, and various other enzymes (93). Of interest to this present work are two ADP-ribosyltransferase toxins, exotoxin A (ETA) and exoenzyme S (ExoS). ETA, one of the more toxic factors secreted by *P. aeruginosa*, behaves in a similar fashion to DT by ADP-ribosylation of diphthamide on eEF-2 and subsequent inhibition of protein synthesis followed by cell death (94). ExoS, on the other hand, appears to ADP-ribosylate arginine residues on members of the Ras GTP-binding protein family (95). In contrast to ETA, ExoS is inserted into the cell by a type III secretory apparatus requiring contact between the bacterium and cell during infection. In cultures, ExoS ADP-ribosylates Ras during the course of infection and disrupts Ras-mediated signal transduction (96;97). ExoS appears to ADP-ribosylate Ras at two arginine locations, R41 and R128 (97;98). ADP-ribosylation at these sites, in particular R41, appears to disrupt gua-

nine nucleotide exchange factor (Cdc25) stimulated nucleotide exchange rates, thus affecting signal transduction (99).

C3

Clostridium botulinum C3 exoenzyme represents a group of toxins that selectively modifies the low molecular mass GTP-binding proteins, RhoA, B, and C (100;101). The C3 group, which include toxins secreted from *C. botulinum* and *C. limosum* as well as *Bacillus cereus*, and epidermal differentiation inhibitor (EDIN) from *Staphylococcus aureus* tend to be about 25 kDa in molecular mass and are very basic with pIs>9 (102). Unlike the toxins previously mentioned, the C3 group ADP-ribosylate asparagine residues, in particular N41 of rho (103). ADP-ribosylation of rho proteins inactivates them causing a disruption of the actin cytoskeleton, resulting in depolymerization of the actin (102). Inactivation of rho also leads to a number of down-stream effects aside from the disregulation of the actin cytoskeleton. There is disruption of several signal transduction processes including those involving phosphoinositide-3-kinase, phosphatidylinositol-4-phosphate-5-kinase, phospholipase D, smooth muscle contraction, endocytosis, and transcriptional activation (including inhibition of IL-2 transcription following ligation of the T cell receptor) (104;105).

Eukaryotic ADP-Ribosyltransferases

Mammalian ARTs, in particular ART1 and ART2

Early biological studies of the mono-ARTs, which centered around the principal virulence factors of cholera, pertussis, and diphtheria, revealed that these toxins influ-

enced cellular physiology by modifying various target proteins, in particular, G proteins. As recently as 10 years ago, the first mammalian mono-ART was identified and was associated with rabbit skeletal muscle (106). The transferase was a GPI-anchored cell surface protein, termed ART1, and determined to have NAD-dependent, arginine-specific ADP-ribosyl transferase activity (59;106). Though the biological relevance of this activity was not clear at the time, it became evident that ART1 could play an important role in signaling. In C2C12 mouse myoblasts, GPI-linked ART1 activity increased on differentiation to myotubes (107). Incubation of intact C2C12 cells with exogenous NAD resulted in the ADP-ribosylation of the laminin-binding protein, integrin $\alpha7$, suggesting a regulatory role for ADP-ribosylation in cell adhesion and myogenesis (59).

Not long after the cloning of ART1 came the recognition that there was a larger pool of mammalian mono-ARTs. ART1 enzymes had significant sequence identity to the ART2 (known as RT6 at the time) family of rodent T cell alloantigens, and ART2 expressed in mammalian cell lines demonstrated GPI-anchored NAD glycohydrolase activity but not an arginine-specific transferase activity like ART1 or CT (108). To date, five mammalian mono-ADP-ribosyl transferases (ART1-5) have been cloned and their expression has been demonstrated in cardiac and skeletal muscle, lymphocytes, brain, and testis (59).

Aside from the correlative relationship that established ART2 as an antigenic determinant for T cells that may regulate the expression of diabetes in the BB/W rat, little is understood of the physiologic role of ART2. Several lines of evidence began to appear

that suggest ART2 or the other ARTs (ART1 and 4) expressed in lymphocytes may have a role in modulating T cell function. Enzymatic studies demonstrated that ART2 functions primarily as an NAD glycohydrolase with auto-ADP-ribosyl transferase activity (109), and *in vitro* cellular assays established that NAD and related compounds resulting from the glycohydrolase activity of ART2 appear to inhibit proliferation of rat T cells (61). Further studies demonstrated that exogenous NAD appears to induce T cell apoptosis in naive mouse T cells which express Art2 but not ART1 (110), and in addition, Art2 double-knockout mice were resistant to NAD-induced apoptosis and NAD-mediated suppression of proliferation (111).

Work on T cell lymphomas demonstrated that the signaling kinase p56^{lck} served as a substrate for ART1 and concominant to the ADP-ribosylation of p56^{lck}, T cell receptor activation signalling was suppressed (112). Many other mouse T cell surface proteins like LFA-1, CD8, CD27, CD43, CD44, and CD45, also appeared to be ADP-ribosylated by incubation with exogenous NAD (113). ADP-ribosylation of cell surface proteins of cytotoxic T cells correlated with a reduction in cytolytic activity and decrease proliferation (114). The mono-ART(s) that influence CTL activity appeared to be GPI-linked because activation of those cells by antiCD3, PMA, or IL-2 appeared to clip the GPI-linkage and release the ART into the media (115). Similar shedding studies indicated that the shedding of ARTs upon activation may be mediated by a TNF-α-converting enzyme (TACE) or another closely related metalloprotease (116).

Recent studies have demonstrated that innate antimicrobial proteins, called defensins, are also targets for ADP-ribosylation by ART1-like molecules (117). Functional assays revealed that defensin-1 specifically lost its antimicrobial and cytotoxic activities upon ADP-ribosylation by ART1 but was still able to stimulate chemotaxis of T cells and IL-8 production. The study went on to demonstrate that ADP-ribosylation of defensins could be detected in humans and that a higher level of ADP-ribosylated defensins could be found in bronchoalveolar lavage fluids from smokers compared to non-smokers.

What has arisen from these studies is the idea that monoARTs may, in part, play a physiologic role in modulating T cell function by ADP-ribosylating cell surface proteins and inhibiting activation induced signaling of lymphocytes. Coversely, when the immune system is activated, the ART is then clipped and released into the serum where it can no longer influence the activated lymphocyte. How then is the NAD available? Serum levels of NAD are estimated to be as low as 10-40nM (118). Intracellular stores of NAD vary from 200μM-1mM depending on the level of metabolic activity in the cell. There are three theoretical scenarios that can answer this (Fig 8). The first scenario is that the cell makes use of Connexin43 hemichannels which can serve as flux pores for NAD and whose flow may be regulated by Ca2+ levels and pH (118). Connexins have already been implicated in providing NAD for the monoART-related CD38-like glycohydrolases, which will be discussed in the ADP-ribosyl cyclase section of this chapter (119;120). The second scenerio is that in areas of inflammation where these lymphocytes would

Figure 8

A

0 mM $[Ca^{2+}]$
High pH

Basal

5 mM $[Ca^{2+}]$
Low pH

extracellular

Cx43

cytosol

Cx43

Cx43

NAD

NAD

NAD

B

tissue

Inflammation
Cell Lysis
↑[NAD]

lymphocytes

C

GPI-anchored
ARTs

NAD

endocytosis
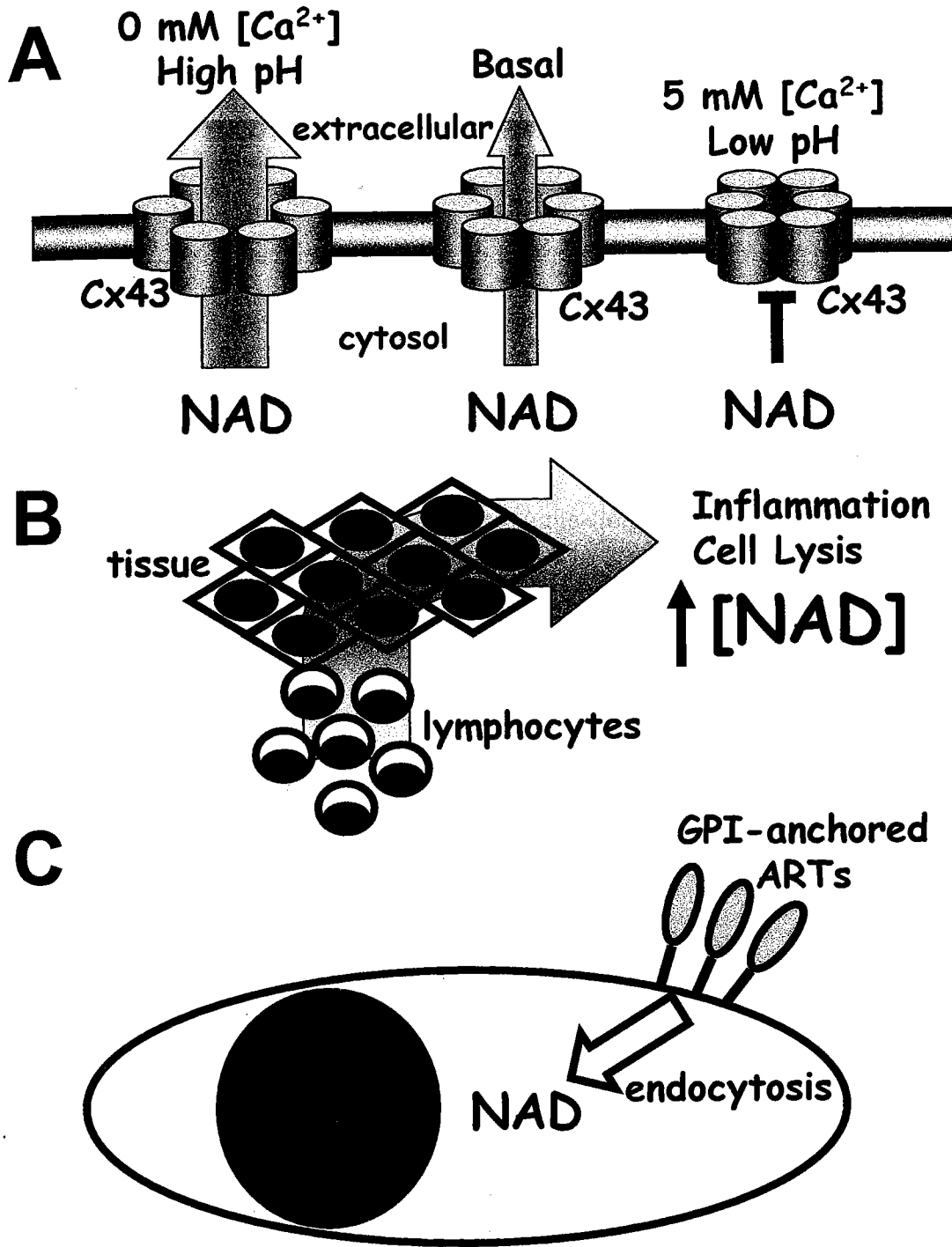
Figure 8. **Theoretical Mechanisms of NAD Availability.** **A.** Connexin 43
hemichannels. NAD can diffuse down its concentration gradient through the aid of Con-
nexin 43 hemichannels which are influenced by various conditions of pH and Ca^{2+}. The
NAD can then act in an autocrine or paracrine fashion to serve as a substrate for extracel-
lular ARTs. **B.** Inflammation. Under conditions of inflammation and lysis, intracellular
stores of NAD can be released in high concentrations into the microenvironment and be
available as a substrate for ARTs. **C.** Endocytosis. Because of their GPI-anchor and its
association with lipid rafts, it is possible that cell surface ARTs may be cycled to and
from endosomal vesicles. Under the right conditions, the ARTs, like their toxin cousins,
may undergo retrograde transduction through the Golgi and ER ultimately arriving in the
cytosol where they can make use of the intracellular stores of NAD.

travel, there is enough cell death and lysis to elevate the microenvironment levels of NAD to concentrations that are comparable to the cell, thus activating the ARTs (111). A final possible scenario is that under the right conditions, the ART may be internalized in a manner like the toxins that may allow retrograde transport and release into the cytosol where the ART can then make use of intracellular NAD stores.

PARPs

The PARPs are a growing subgroup of the ART super-family of proteins and are involved in regulation of a number of processes in the nucleus. Foremost, PARPs are shown to be among the earliest responders to DNA damage by synthesizing large polymers of ADP-ribose upon binding to nicks in DNA. PARP-1 activation can mediate caspase-independent cell death in ischemia-reperfusion injury after cerebral ischemia or myocardial infarction by the translocation of apoptosis-inducing factor (AIF) from the mitochondria to the nucleus (121). Tankyrase, a 142 kD protein with a catalytic PARP module, has been identified and localized to telomeres where it is thought to influence telomere function by poly(ADP)-ribosylation of TRF-1 (telomeric repeat binding factor-1), a negative regulator of telomere length maintenance (122). Lastly, *Drosophila* PARP has been shown to influence chromatin puffing in response to environmental stress as a mechanism for facilitating the transcription of certain heat-shock proteins (123).

PARP has also been implicated in the development of diabetes through the Okamoto Model developed some twenty years ago (39). The hypothesis of the Okamoto

model first based on the alloxan and streptozotocin models of diabetes proposed that, in response to alloxan or streptozotocin, free radicals would be generated that would cause DNA strand breaks upregulating the activity of PARP (124). Though the mechanism is not completely understood, PARP appears to activate the DNA repair machinery of the nucleus in response to these breaks by consuming NAD as a substrate in the process and leading to a depletion of energy stores and ultimately β-cell death. This NAD depletion and β-cell death could be dose-dependently blocked by the radical scavengers superoxide dismutase and catalase and PARP inhibitors such as nicotinamide (125;126). Further support for the Okamoto Model came from laboratories that developed PARP-knockout mice (127-129). The PARP-knockout mice were resistant to streptozotocin-induced diabetes.

ADP-Ribosyl cyclase

ADP-ribosyl cyclase was first discovered in sea urchin (*Aplysia californica*) egg extracts as catalytic activity that converted NAD to a Ca^{2+}-releasing metabolite (130;131). This metabolite turned out to be the molecule, cyclic ADP-ribose (cADPR), and its Ca^{2+}-mobilizing properties were discovered to be distinct from inositol 1,4,5 triphosphate (132). Since then accumulating evidence indicates that cADPR plays an important role as a Ca^{2+} messenger regulating a number of cellular functions in plants and animals. Cloning of the *Aplysia* ADP-ribosyl cyclase revealed an enzyme with close sequence identity to CD38, a lymphocyte antigenic marker for which no activity was previously known (133). CD38 and a couple of closely related enzymes had primarily NAD glycohydrolase

activity, with a small amount of ADP-ribosyl cyclase activity (132). CD38-like NAD glycohydrolases generate free ADPR through a short-lived intermediate of cADPR, giving CD38 a multifunctional role as both ADP-ribosyl cyclase and a cADP-ribosyl hydrolase (134;135).

Cyclic ADP-ribose is a potent and universal calcium mobilizer, and in mammals, cADPR is involved in a number of Ca^{2+}-dependent functions including proliferation, contraction, and secretion. Because CD38 is an ectoezyme anchored to the cell by a transmembrane region, NAD must be trafficked outside the cell to generate the cADPR signal and then the cADPR must be trafficked back into the cell to elicit the Ca^{2+}-induced signaling (118). Recent works have demonstrated that the protein Connexin43 (Cx43), a gap junction protein, can form hexameric hemichannels that allow efflux of NAD down its concentration gradient where it can serve as a substrate for CD38 (119). Once CD38 catalyzes the cADPR, oligomeric CD38 coupled to the cADPR allows translocation of the cADPR across the cell membrane and into the cytosol. In 3T3 fibroblasts, this Cx43-CD38 cross-talk has been demonstrated to have paracrine effects at increasing intracellular calcium and enhancing proliferation of 3T3 fibroblasts (120). In the βcell, the Okamoto group has demonstrated that cADPR generated by CD38 appears to play a role in the ATP-dependent glucose signaling of insulin secretion (136).

SIR2

The Sir2 (silent information regulator 2) family of histone/protein deacetylases deserve brief mention as potential distant cousins to the ART superfamily. The Sir2 fam-

ily of enzymes is a unique class of deacetylases that are highly conserved from prokaryotes to humans (137). In yeast, Sir2 is required for silencing at the mating-type loci, telomeres, and ribosomal DNA. Sir2 has also been implicated in life-span extension within yeast (138) and *Caenorhabditis elegans* (139). Sir2 is an NAD- dependent enzyme and though there has been some suggestion in the literature that Sir2 has a low level of ADP-ribosyl transferase activity (140;141), the main catalytic function of Sir2 appears to be as a deacetylase with the formation of an ADP-ribosylated acetyl group (1-O-acetyl-ADP-ribose) as the product (142).

Enzymatic reactions

Now that the biology of some of the ART family members has been established, it is important to expand on the catalytic activities that appear to be responsible for the physiologic roles of these molecules (Fig 9). ARTs catalyze the transfer of the ADP-ribose (ADPR) subunit of NAD to substrates in a covalent modification analogous to phosphorylation. There are four major classes of substrate for the ADP-ribosylation reaction; amino acid, the ADP-ribose molecule, NAD, and water. The SIR2-like enzymes, which are considered to be distantly related to the ARTs, catalyze the transfer of ADPR to acetylated lysines. For a breakdown of the different ARTs and their respective activities and target substrates, see Figure 10.

Figure 9

ADP-ribosylated R   Nicotinamide
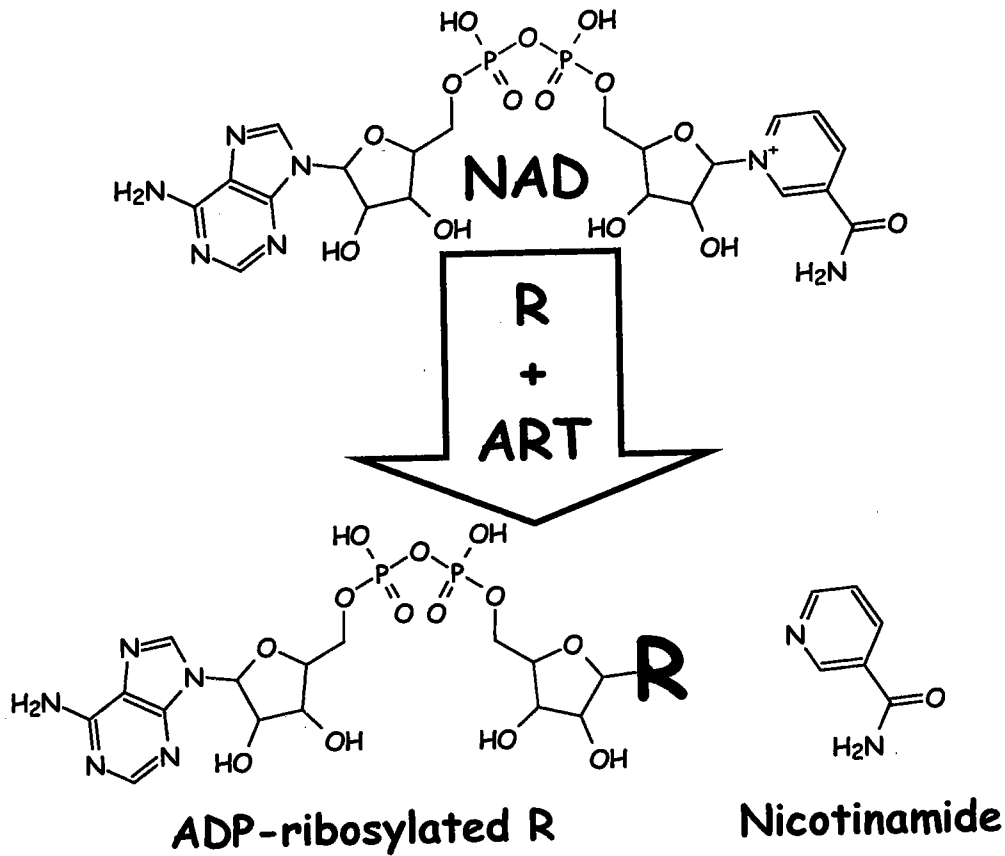
R: acceptor
1. Exogenous Amino Acid (ADP-ribosyltransferase)
2. ART Amino Acid (auto-ADP-ribosyltransferase)
3. ADPR (poly(ADP-ribose) polymerase)
4. NAD (ADP-ribosyl cyclase)
5. Water (NAD glycohydrolase)
6. Acetylated Lysine (Deacetylase)

Figure 9. **ADP-ribosylation Scheme.** All ARTs utilize NAD in a reaction that catalyzes the cleavage on the glycosidic bond between nicotinamide and ADP-ribose and transfers the ribose to some reactive substrate (R). R can be one of a number of amino acids, ADP-ribose, water, and in the case of the SIR2 family of deacetylases, R can be acetylated lysine.

Figure 10

ART	AMINO ACID TRANSFERASE/AUTO	RESIDUE	ADPR POLY/CYCLIC	H$_2$O NADase
DT	Y/N	*H*	N/N	Y
ETA	Y/Y	*H*	N/N	Y
PARP	Y/Y	K,E	Y/N	Y
ART2.2	N/Y	R	N/N	Y
ART1	Y/Y	R	N/N	Y
CT	Y/Y	R	N/N	Y
PT	Y/N	C	N/N	Y
VIP	Y/Y	R	N/N	Y
C3	Y/N	N	N/N	Y
ADPRcyclase	N/N		**D/Y	Y
SIR2	*Y/N		N	N

Notes:

H: diphthamide (post-translationally modified histidine)

*Y: low level of transferase activity detected

**D: low levels of dimerization activity demonstrated

Figure 10. **ADP-ribosylation Table.** There are various components to the catalytic activities of the ART family of proteins: amino acid tranferase, exogenous and auto; poly(ADP-ribose polymerase; ADP-ribosyl cyclase; and NAD glycohydrolase (NADase). Figure 10 summaries a series of ARTs and their respective activities. Note that most ARTs catalyze the NADase reaction; that only PARPs are known to catalyze the polymerase reaction; and that only cyclases appear to catalyze cyclic bond formation. DT, diphtheria toxin; ETA, *Pseudomonas aeruginosa* exotoxin A; PARP, chicken poly(ADP-ribose) polymerase; ART2.2, rat ART2.2 allele; ART1, rabbit ART1; CT, cholera toxin; PT, pertussis toxin; VIP, Bacillus cereus toxin; C3, Clotridial C3 exotoxin; ADPRcyclase, ADP-ribosyl cyclase; SIR2, silent information regulator 2 deacetylase.

Amino Acids as Substrates

Most ARTs catalyze the transfer of the ADP-ribose subunit from the NAD to some amino acid either on an exogenous protein or on the ART itself. When the transfer is to an exogenous protein the reaction is termed an ADP-ribosyltransferase reaction. When the modification takes place on the ART itself, it is termed auto-ADP-ribosyl transferase activity. Most monoARTs have mono-ADP-ribosyl transferase activity. ART2, however, has only auto-ADP-ribosyl transferase activity (143). PARP has both the mono-ADP-ribosyltransferase activity to initiate polymer formation and the auto-ADP-ribosyl transferase activity (144-146). There are no reports in the literature to date that demonstrate that the ADP-ribosyl cyclases have mono or auto-ADP-ribosyl transferase activity. The Sir2-like enzymes appear to have a low level of transferase activity by in vitro studies, although mono-ADP ribosylation does not appear to be their major function. Specific amino acid residues have been demonstrated to be ADP-ribosylated by the monoARTs depending on the enzyme, and they include arginine, dipthamide, cysteine and asparagine. PARPs tend to ADP-ribosylate at lysine and glutamate residues (147;148). Auto-ADP-ribosylation of PARP tends to take place in a 22 kDa internal fragment, designated as the automodification domain (149;150).

Auto-ADP-ribosylation often occurs at the same amino acid that the enzyme uses for exogenous ADP-ribosylation. ART2, for example, belongs to the arginine-specific class of ADP-ribosyl transferases by amino acid sequence similarity to molecules like ART1 and CT. It has been suggested by chemical stability studies of the ADP-

ribosylated amino acid bond that ART2 appears to modify arginine residues by auto-ADP-ribosyl transferase activity (109). Auto-ADP-ribosyltransferase activity appears to be an important regulator of ART function. In CT and PARP, auto-ADP-ribosyltransferase activity functions to shut-down further ADP-ribosylation of exogenous proteins in a negative-feedback loop. ART5, a monoART, was primarily thought to be a NAD glycohydrolase and an auto-ADP-ribosyltransferase, but recent studies have demonstrated that the auto-ADP-ribosylation of ART5 turns on a latent transferase activity for exogenous substrates (151). Further auto-ADP-ribosylation of ART5 then serves to shut down the exogenous activity. This suggests a very tight regulation of action for ART5 and its substrates *in vivo*.

Initial studies of ADP-ribosylation by CT of guanidino containing compounds (like arginine) by NMR revealed that there was a chiral switch from the β form of NAD used in the reaction to the α form of ADPR on the guanidine acceptor molecule. This kind of switch was indicative of an S_N2-like mechanism where the C1 carbon of the N-glycosidic bond between nitcotinamide and ribose would undergo a nucleophilic attack. Later, studies of the crystal structure of both CT and DT suggested a role for a key, highly conserved, catalytic-site glutamate residue in stabilizing an oxycarbonium intermediate, allowing nicotimamide to leave in an S_N1-like mechanism (152;153). Though S_N1-like mechanisms typically result in a chiral mix of α and β ADP-ribosyl-arginine bonds, the rationale for generating only α anomers is that there may be steric hindrance in the catalytic site that allows the nucleophile to attack only from one side. At this point, both

Figure 11
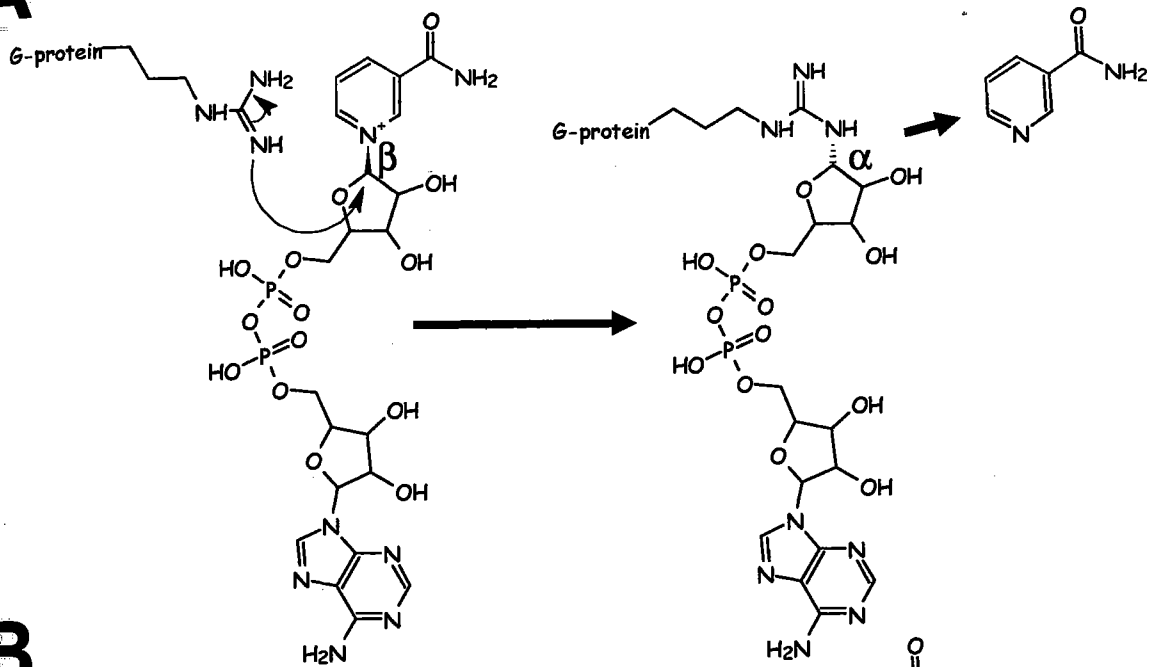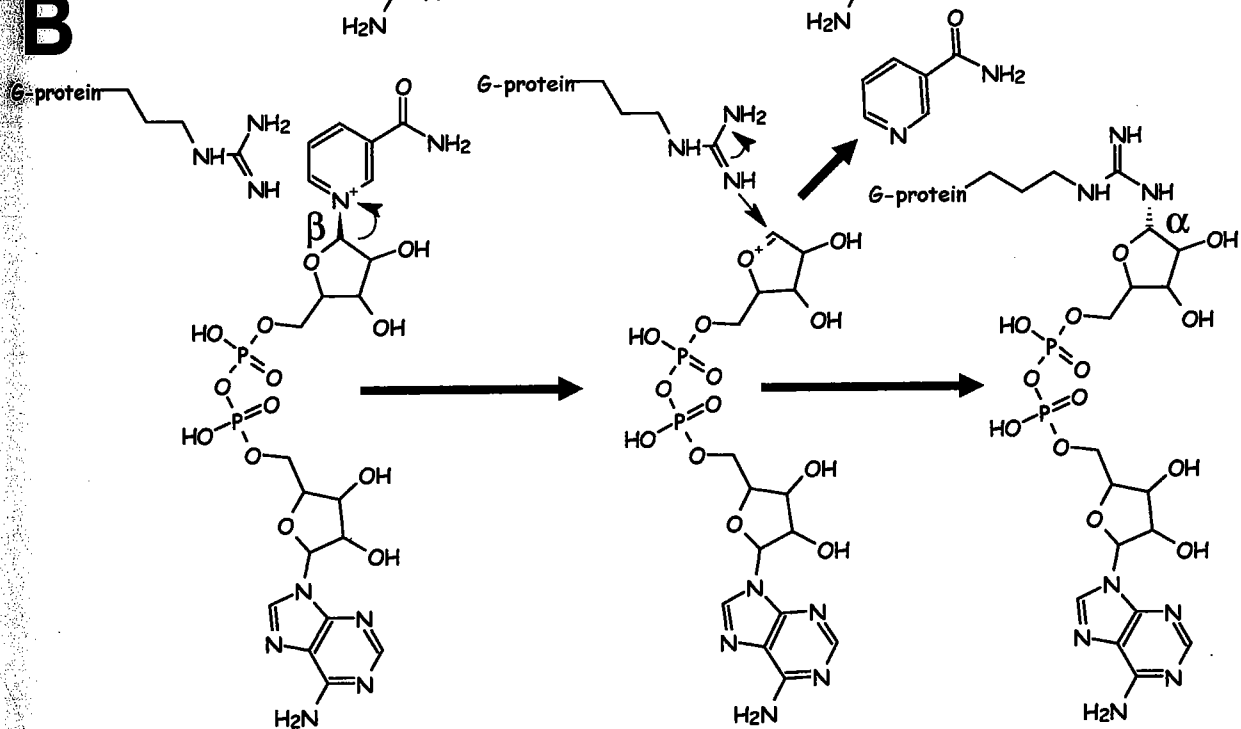
Figure 11. S_N2-like *vs.* S_N1-like **Reactions.** There are two hypothesized mechanisms for the catalysis an ART reaction; S_N2-like or S_N1-like. Regardless of the mechanism, nucleophilic substitution appears to be the theme. **A.** ARTs may carry out the ADP-ribosylation reaction by catalyzing a nucleophilic attack on the C1 carbon of nicotinamide mononucleotide. The result is a characteristic S_N2-like switch from the β anomer to the α anomer. **B.** ARTs may carry out the ADP-ribosylation reaction by catalyzing the formation of an oxycarbonium intermediate that would be subjected to a nucleophilic attack. Though this S_N1-like reaction could theoretically result in the formation of both α and β anomers, the hypothesis is that the enzyme sterically hinders the nucleophilic attack so that only α anomers are produced.

Figure 12
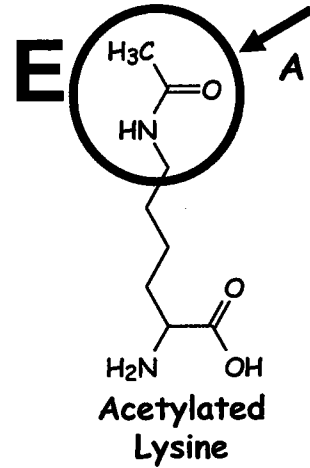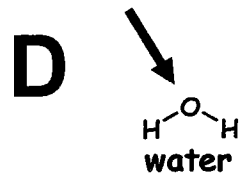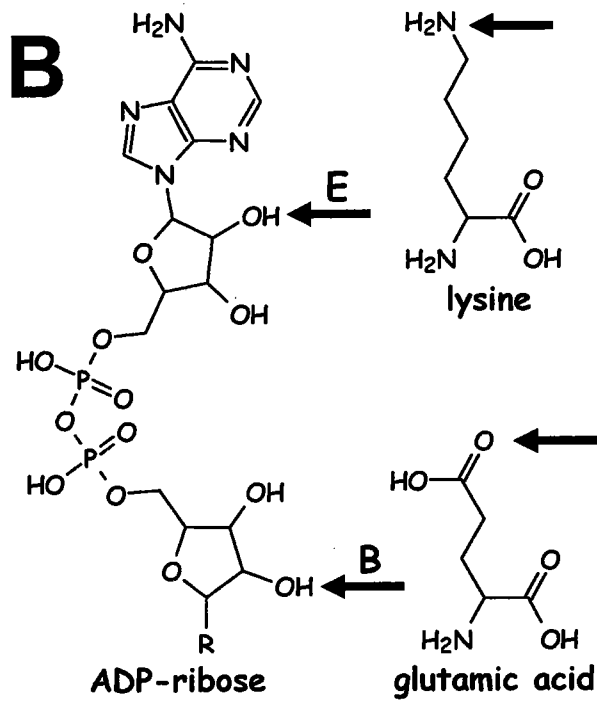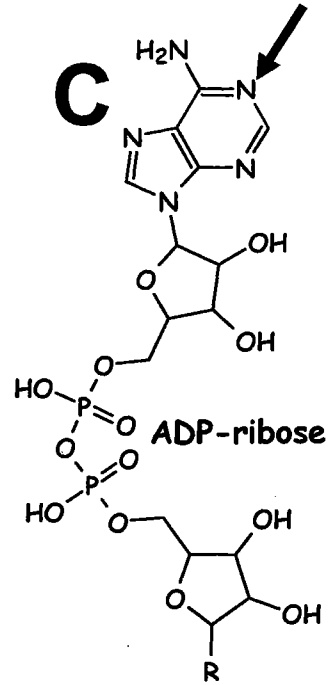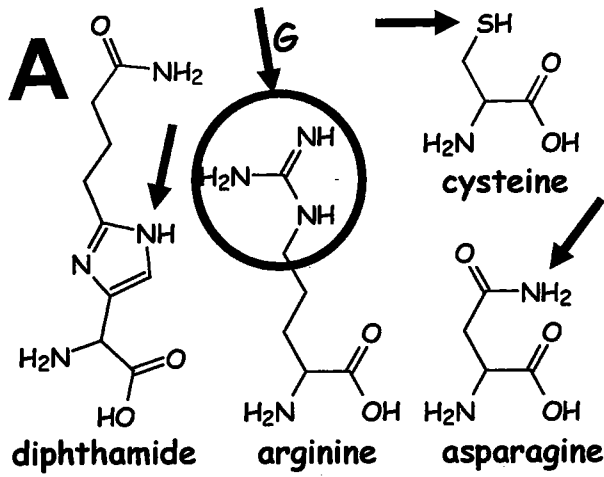
Figure 12. **Nucleophiles.** A summary of potential nuclephiles by ART subgroup. **A.** The mono-ADP-ribosyl transferases appear to prefer the amino acids arginine, dipthamide, cysteine, or asparagine as nucleophile-like substrates. **B.** The PARPs appear to prefer the amino acids lysine or glutamate as well as ADP-ribose, itself, for the initiation of polymer elongation at the 2'C hydroxyl moiety of adenosine. Branching reactions can also take plase at the 2'C hydroxyl moiety of nicotinamide mononucletide. **C.** ADP-ribosyl cyclases appear to prefer NAD, utilizing the N1 nitrogen of adenine rather than hydroxyl moieties. **D.** Most ARTs have some basal level of NAD glycohydrolase activity where water serves as the substrate. **E.** The Sir2 family of deacetylases appear to utilize acetatylated lysine as a nucleophile-like substrate.

Note that arrows denote the hypothesized attacking nucleophiles. G-arrow and circle signify entire guanidino group. For poly(ADP-ribose) polymerase activity, E-arrow signifies polymer elongation site, B-arrow signifies polymer branching site. A-arrow and circle signify acetyl group.

scenarios remain possible; see Figure 11 for a summary of the two theoretical reactions. Though Figure 11 illustrates the reactions with arginine; any other amino acid can be substituted. In fact, as discussed below not just the amino acids, but all substrates are thought to serve as nucleophiles. Figure 12 illustrates many of the known molecules thought to serve as nucleophiles, and any of these molecules could be substituted for arginine in the reactions shown in Figure 11.

ADP-ribose as a substrate

ADP-ribose itself can serve as an acceptor substrate for the ADP-ribosylation reactions with PARP. PARP catalyzes the transfer of ADP-ribose to amino acids as catalyzed by monoARTs but differs in that ADP-ribose can return to the catalytic region to serve as an acceptor for additional ADP-ribose moieties (154). In fact, PARP is so efficient at utilizing ADP-ribose side chain as a substrate that it can generate ADP-ribose polymers 100 or more in length (146). Also like the monoARTs, α anomeric products are formed suggesting a nucleophilic conversion from βNAD. In fact, NMR studies have demonstrated that polyADPR polymers appear to be connected by the same $\alpha(1-2)$ ribose-ribose linkages (155;156). Depending on whether the adenosine ribose or the ribose from the nicotinamide mononucleotide returns to the active site, PARP can generate linear or branching chains (154). Figure 13 illustrates the mechanism of elongation and branching for PARP. PARP is unique in its ability to catalyze mono-ADP-ribosylation, synthesize polymers from the monomer, and form polymer branch points. PARP catalyzes branch points at average intervals of 20 ADP-ribose units (145;156).

Figure 13

1. Elongation at C2 of Adenosine Ribose

2. Branching C2 of NMN Ribose
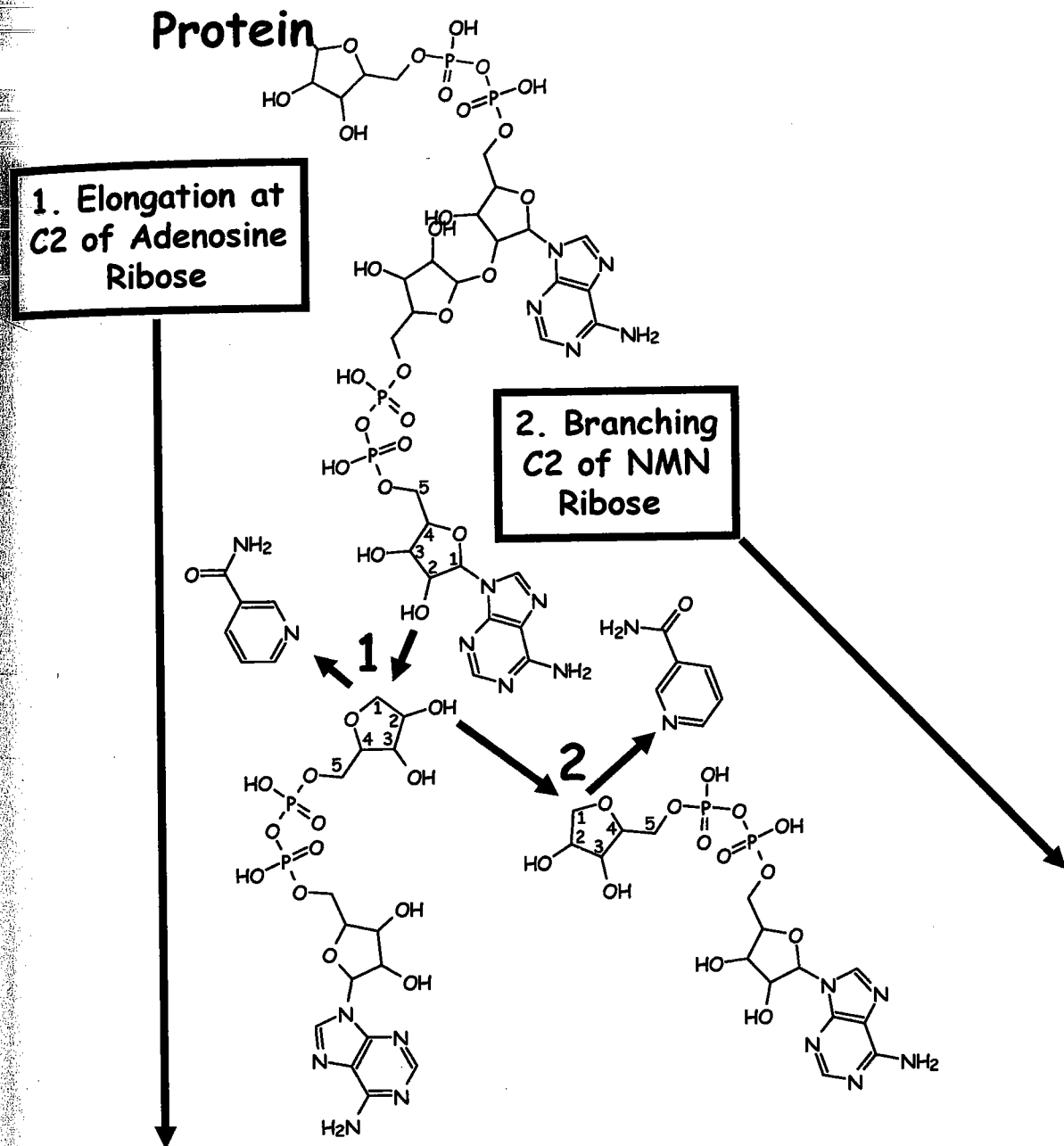
Figure 13. Elongation and Branching of poly(ADP-ribose) as catalyzed by PARP.

1. Elongation of the PARP polymer proceeds in a longitudinal fashion by catalyzing bond formation between C2 of the adenosine ribose on the acceptor chain and C1 of the nicotinamide mononucleotide (NMN) ribose from the donor NAD. **2.** Branching occurs between the C2 of the nicotinamide mononucleotide ribose on the polymer chain and the C1 of the nicotinamide mononucleotide ribose from the donor NAD.

NAD as a substrate

ADP-ribosyl cyclases appear to turn the ADP-ribose moiety of NAD over on itself forming a cyclic bond between N1 of the adenine ring and the C1 carbon of the ribose on the NMN moiety. Studies suggest this reaction also results from a nucleophilic-like substitution (132). Interestingly, ADPR cyclase can also form dimeric bonds between the adenine of free ADPR and the C1 carbon of the NMN ribose from the NAD that is being cleaved (157). It would appear that ADP-ribose from the NAD glycohydrolase activity of ADPR cyclase can return to the catalytic site to serve as an acceptor for the next ADPR in a similar fashion to the polymer elongation reaction PARP; however, dimers represent a small portion of the total product created by the enzyme and there is no evidence to date that oligomers of ADPR can occur.

Water

Most ARTs have some level of NAD glycohdrolase activity where water serves as the nucleophile in the transferase reaction. Studies have demonstrated that free ADP-ribose and its breakdown products can have marked effects on cellular metabolism by signaling via certain purinergic receptors (61). PARPs (145) and ADP-ribosyl cyclases (132) have also been demonstrated to have various degrees of NAD glycohydrolase activity.

Structural Studies

Despite the lack of overall identity of primary amino acid sequences, the ART super-family possess three regions of sequence similarity that appear to form the NAD-

Figure 14

REGION I   **REGION II**

```
DT       15  ENFSSYHGTK   24      50  WKGFYSTDNKYDAAGY   65
ETA     434  YVFVGYHGTF  443     466  WRGFYIAGDPALAYGY  481
PARP    856  NRQLLWHGSR  865     894  REGIYFADMVSKSANY  907
                        **                 *            *

ART2.2  120  DCHSVYRGTK  129     144  FTSSSLSKK  160
mART2   120  GCRSVYRGTN  129     144  FASSSLNRS  160
CT        1  NDDKLYRADS   10      59  YVSTSISLR   74
PT        3  PPATVYRYDS   12      50  FVSTSSSRR   63
VIP     343  ENITVYRWCG  352     384  YMSTSLSSE  397
C3      122  ENIMFLRGDD  131     172  YISTSLMVS  185
                        **                 *   *
```

REGION III

```
DT       143  GSSSVEYINNWE  154
ETA      548  EGGRLETILGWP  559
PARP     983  CLLYNEYIVYDV  994
                        *

ART2.2   185  RPDQEEVLIPGY  196
mART2    185  YTHEEEVLIPGY  196
CT       107  HPDEQEVSALGG  118
PT       124  ATYQSEYLAHRR  135
VIP      423  FASEKEILLDKD  433
C3       209  FAGQLEMLLPRH  220
ARTT R         φ--E-E
ARTT N         φ--Q-E
                        *
```

Figure 14. Sequence Similarity of Several ARTs. (Adapted from Okazaki and Moss (159)). Based on primary sequence alignment, mutational analysis and crystallography, there are three regions of sequence similarity shared by most mono-ARTs and PARP. Region I contains a critical arginine typically followed by glycine. Region II contains either a $YX_{10}Y$ or SXS motif. Region III contains the catalytic glutamate on a β-strand. DT, diphtheria toxin; ETA, *Pseudomonas aeruginosa* exotoxin A; PARP, chicken poly(ADP-ribose) polymerase; ART2.2, rat ART2.2 allele; mART2, mouse Art2a; CT, cholera toxin; PT, pertussis toxin; VIP, *Bacillus cereus* toxin; C3, Clotridial C3 exotoxin; ARTT R, ART Turn-Turn Motif for arginine specificity; ARTT ART Turn-Turn Motif for asparagine specificity.

binding cleft (Fig 14) (158). Region I typically contains a β-strand composed of a highly conserved doublet, consisting or either histidine or arginine typically followed by glycine or a small nonpolar amino acid, that appears to play a crucial role in binding NAD. Region II is a U-shaped (β-strand downward and α-helix upward) pocket that binds the NMN moiety for catalysis. Region II is largely nonpolar and hydrophobic, which is thought to aid in the packing of NMN, and it is marked by conserved $Y-X_{10}-Y$ (often called the "PARP-like" group) or SXS motifs. Region III is a β-strand that begins with a crucial glutamate residue (previously mentioned) that is present in all ARTs without exception thus far. Photoaffinity labeling, site-directed mutagenesis and crystallography have all confirmed the significance of the glutamate with respect to ART function.

Little is understood about the mechanisms that determine substrate specificity for the ART super-family (*ie.* amino acids, ADPR, water, acetylated-lysine). However, recent crystal structures, primary sequence alignments, and mutagenesis work have shed insight into how mono-ARTs target specific amino acids(160). Those studies identify a Pre-region III ARTT motif (ADP-ribosylating turn-turn motif) that may distinguish asparagine *vs.* arginine-specific ADP-ribosyltransferases. Turn 1 (T1) includes a conserved F/Y side chain and turn 2 (T2) contains a Q or E, two amino acids upstream of the highly conserved catalytic glutamate. The T2 glutamine appears to specify asparagine as a substrate whereas the T2 glutamate appears to specify arginine. Furthermore, mutational studies with ART2 have also indicated that the T2 glutamate confers arginine-specific transferase activity. ART2.1, which has NADase activity but not transferase activity for

an exogenous substrate, has a tyrosine at T1 and a glutamine at T2. There is no evidence to suggest that ART2.1 has asparagine-specific mono-ADP-ribosyltransferase activity, but mutational work has shown that conversion of the glutamine to glutamate does confer arginine-specific transferase activity on ART2.1 (161). The data are further supported by the fact that the mouse homologue of ART2.1, Art2, does contain a glutamate in the same position and has been shown to be arginine-specific transferase activity by *in vitro* studies. In the study, the glutamine in ART2.1 was mutated to Glu, Asp, or Ala, by site-directed mutagenesis (161). The Q207E mutant exhibited ADP-ribosyltransferase activity for exogenous arginine, while the Q207D mutant exhibited transferase activity, but at lower levels. The Q207A mutant did not exhibit any transferase activity. The NAD glycohydrolase activity was affected to a much lesser extent in all mutants. A reciprocal mutant with glutamate replaced by glutamine was carried out in mouse Art2a, and the mutant did not exhibit measurable levels of arginine-specific ADP-ribosyl transferase activity. These data are consistent with the hypothesis that a glutamate at the T2 position of the ARTT motif is important for the transfer reaction of ADP-ribose to arginine.

Crystallographic and mutational studies of chicken PARP have shed insight into how ADPR is targeted as a substrate for PARPs in the elongation reaction of poly(ADP)-ribose polymers (162). The crystal structure of PARP complexed with the inhibitor, carbonyl-NAD, revealed a superficial, secondary binding site adjacent to the primary NAD-binding site. This was interpreted as an "acceptor" or substrate binding site. Interestingly, most key amino acids for the acceptor site appeared to come from Regions II and III: the crucial glutamate from Region III, E988; Y896 and Y907 (conserved Ys of Re-

gion II); and K903 (Region II). K903 appears to be unique to the PARP subgroup of ARTs by primary sequence alignments. Because mutations of K903 completely abolished polymerization activity, K903 is thought to be important for that activity. Mutations of Y896 and Y907 appeared to affect binding more than polymerization. M890, pre-Region II, appeared to provide a hydrophobic pocket for the adenine of the acceptor site, and the mutation M890V reduced polymerization by a factor larger than 200.

Dissertation Hypothesis

Recently, the auto-ADP-ribosyltransferase activity of ART2.2 was demonstrated to be multimeric, and the level of modification appeared to be dependent upon an arginine, R185, in the T1 position of the ARTT motif (56). The observation that ART2.2 has a multimeric auto-ADP-ribosyl transferase activity was first made be Bonnie Dickinson in some unpublished data during a fellowship with Joel Moss's laboratory at NIH in the mid-nineties. The experiment was a simple one; when recombinant ART2.2 was incubated with various concentrations of NAD, multiple small band shifts indicating increasing mass occurred in a Western blot for ART2. If a ^{32}P-labeled form of NAD was used, autoradiography showed the same multimeric, band-shift pattern as by immunoblot, indicating auto-ADP-ribosylation. As mentioned previously, ART2.2 and ART2.1 are two known alleles in the rat that differ by ten amino acids; they also differ in that ART2.2 has the multimeric auto-ADP-ribosyl transferase activity but ART2.1 does not. The two alleles differ in position T1 of the ARTT motif described above; ART2.1 has a T1 tyrosine, consistent with many related ARTs, but ART2.2 has a T1 arginine. This led to the suspi-

cion that the T1 R may participate in the multimeric band shift patterns. The mutational studies have now demonstrated that loss of the T1 arginine obliterates any sign of auto-ADP-ribosylation, suggesting that it is crucial to the level of auto-modification (56). There are three possible scenarios to account for multimeric ADP-ribosylation (Fig 15).

First, there is auto-mono-ADP-ribosylation at multiple sites on the ART2 molecule, and that arginine185 is a crucial for allowing this to occur. Second, there may be intrinsic PARP activity in ART2 that allows polymers to form, perhaps on R185 itself. Lastly, there could be some combination of the two. It should be noted that there is precedent in the literature for mono-ADP-ribosylation at multiple sites with the toxins; however, there is no evidence in the literature at this time that a monoART can have poly(ADP-ribose) polymerase activity. Sequence alignments at this point would also support mono-ADP-ribosylation at multiple sites, since ART2 resembles the monoARTs more than the "PARP-like" ARTs.

The hypothesis of this dissertation is that ART2.2 has auto-poly(ADP-ribose) polymerase activity. There are four specific aims for this work. The first specific aim is to design a recombinant construct of ART2 that would allow high yields of relatively pure protein. The second aim is to design experiments that address whether or not the auto-modification of ART2 is in part a polymer. The third aim is to determine the structure of the polymer. The fourth aim is to identify the site of auto-poly(ADPribose) linkage.

Figure 15
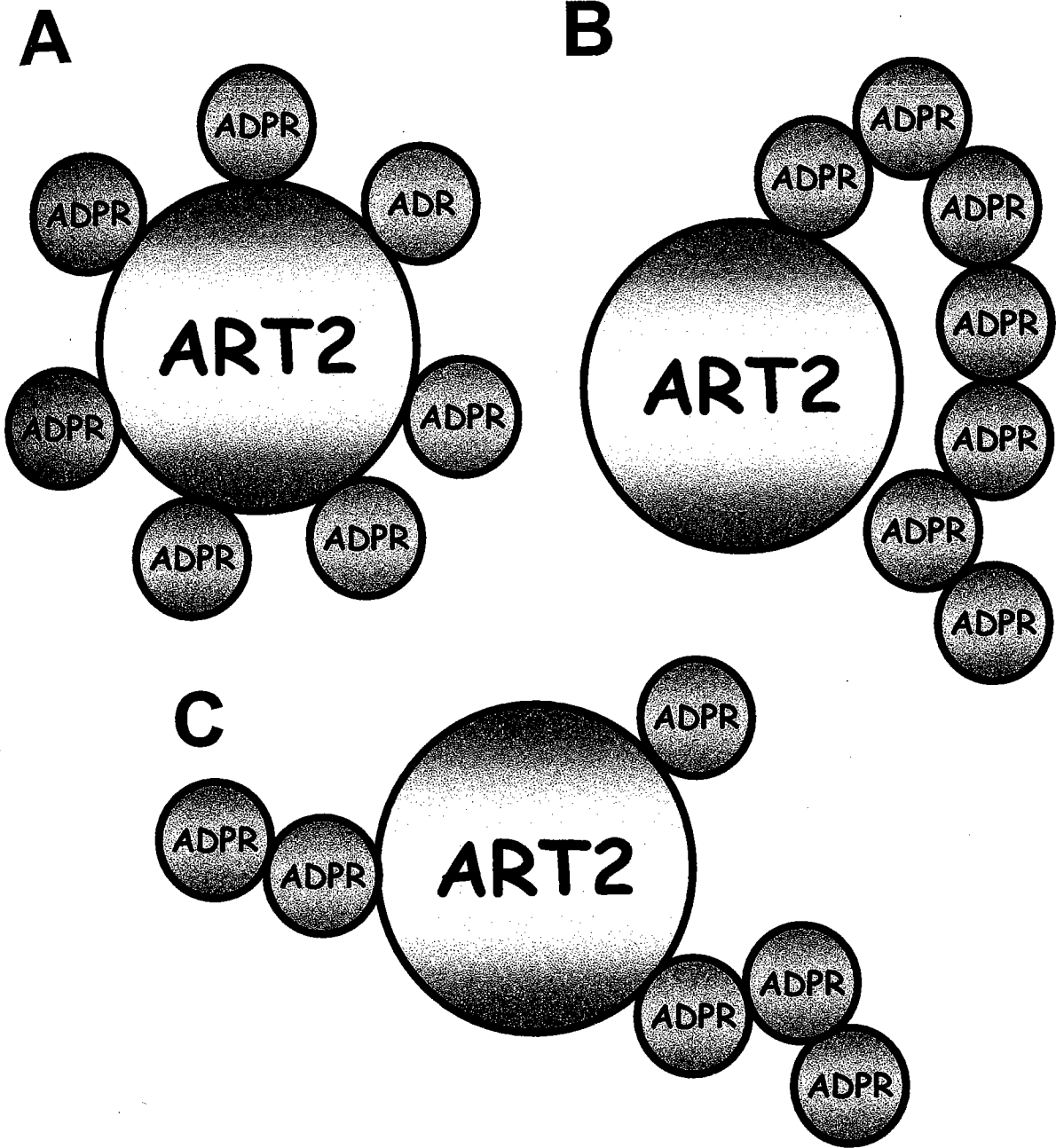
Figure 15. Models That Account for Multimeric Auto-ADP-ribosylation. **A.**
Mono-ADP-ribosylation at multiple sites. The polymer may be linear as depicted here, or
have various branch points that give it a tree-like or bush-like appearance. **B.** Poly-ADP-
ribosylation at a single site. **C.** Multiple sites of mono and short oligomers.

Chapter Conclusions

ARTs can be found to influence a wide range of biological systems. Aside from the toxins, several lines of evidence appear to link the mammalian monoARTs, ART1 and ART2, to modulation of the immune system. ARTs appear to carry out their biological roles as enzymes that catalyze the cleavage of the nicotinamide-ribose bond of NAD and the transfer of the ADP-ribose moiety to specific nucleophiles. Though water appears to be a universal nucleophile, each subgroup of ARTs tends to have their own specific nucleophile. The different proteins within the monoART group appear to prefer one of the amino acids, arginine, histidine, asparagine, or cysteine, as part of their acceptor proteins. PARPs tend to ADP-ribosylate the amino acids, lysine and glutamate, and, in addition, PARPs ADP-ribosylate the 2C-hydroxyls of the ribose moieties of ADPR, creating the long polymers that are specific to the PARP group. ADP-ribosyl cyclases use the N1 of the adenine ring as a nucleophile in the catalysis of the cyclic bond that generates cyclicADPR as a product. Lastly, the SIR2-like enzymes appear to utilize the acetyl moiety of acetylated lysine as a nucleophile in the deacetylation reaction specific to that subgroup. Though no hybrids between each of the subgroups appear to exist, several lines of data lead to the hypothesis that ART2 may have auto-poly(ADP-ribose) polymerase activity. This hypothesis sets the focus and specific aims for the dissertation research that follows.

Chapter 4 Materials and Methods

Chapter Introduction

The development, optimization, and/or utilization of several technologies from different fields, including molecular biology, cellular immunology, and biochemistry, were critical both to the development of the dissertation hypothesis and to the design of the experimental work. In many ways, the rate-limiting factor in all the work was the generation of a recombinant ART2 system that would allow a relatively high degree of purity and quantity. Subcloning of ART2 required several molecular techniques such as PCR sub-cloning, ligation, bacterial transformation, and plasmid purification. The recombinant construct was designed for affinity purification with a 6(His)-tag and a maltose binding protein fusion partner, both of which were readily removed from the ART core sequence by insertion of a Factor Xa protease recognition site. For purification of the recombinant protein, techniques like guanidine-hydrochloride resolubilization of inclusion bodies, Ni^{2+} affinity chromatography, ion exchange chromatography and amylose affinity chromatography were developed and optimized. The recombinant protein was characterized by sodium dodecyl sulfate polyacrylamide gel electrophoresis (SDS-PAGE), Western blots, and mass spectrometry. Enzymatic assays were performed to determine the levels of NAD glycohydrolase and auto-ADP-ribosyl transferase activity. Auto-ADP-ribosylation was followed both by band shift assay in western blots alongside autoradiography by ^{32}P-labeled NAD, and by mass spectrometry. Polymer isolation included hydroxylamine cleavage and purification, with boronate chromatography. Analysis of

reaction products required the development and optimization of anion exchange high performance liquid chromatography (HPLC) followed by electrospray ionization mass spectrometry (ESI-MS). Identification of the modified site utilized a combination of protein digestion and matrix-assisted laser desorption ionization time of flight (MALDI-TOF) mass spectrometry. Sequence information from modified peptides required peptide isolation and nanoscale HPLC-electrospray MS/MS.

Materials

Unless otherwise specified most chemical reagents including cell media, buffers, salts, and reaction substrates like βNAD, AMP, ADP, adenosine, adenine were obtained from Sigma. PCR primers were obtained from BioSynthesis, Inc; Gibco BRL; or CFAR. The pMAL-c2x vector was obtained from New England Biolabs (NEB). PCR and ligation were optimized from kits supplied by Roche. PCR production purification and plasmid purification followed protocols set by kits available from QIAGEN. Radio-labeled βNAD was obtained from either NEN (^{32}P) or Amersham (^{14}C). Scintillation fluid was obtained from Amersham. Scintillation counting was done on a Beckman Model LS5000TD scintillation counter. Spectrophotometry was carried out on a Pharmacia Ultraspec III UV/VIS spectrophotometer. Centrifugations were carried out on a Beckman model L-70 ultracentrifuge with rotor type SW41; a Sorvall Model RC-5B with rotor types SS-34 and GS3; and an Eppendorf model 5415C microcentrifuge. A BioRad BioLogic LP peristaltic chromatography apparatus was used for protein chromatography.

Methods

Unless otherwise specified, all data are presented as one representative of at least 3 independent experiments.

ART2.2 Construct

All DNA was quantified by spectrophotometric methods for absorption at 260 nm. Recombinant ART2.2 was subcloned from the pCR2.1 vector described previously (109) into the 6-His modified pMAL-c2x for expression. The PCR product (forward primer 5'-GTCAGCCGCGGATCCATGCTAGACACGGCTCCC-3'; reverse primer 5'-GGCGTGCCGTCGACTCACTTATTAGCTGTATAAGCAATTGTAGTTG-3') was ligated into a 6-His modified pMAL-c2x (see below) that was digested with BamHI and SalI. The PCR reaction was carried out in a 100 λ volume with 1X PCR Buffer (Roche), 0.5 μM of each primer, 100 ng template DNA (pCR2.1 containing ART2B), 0.2 mM 4dNTP, and 2.5 U Taq polymerase (Roche). The reaction cycle was carried out as 2 min at 94° C, 30 sec at 55° C, and 60 sec at 72° C; was followed by 30 cycles of 30 sec at 94 °C, 30 sec at 55° C, and 60 sec at 72° C; and was completed with a final extension of 7 min at 72° C. 10 μl of the reaction were run on a 2 % agarose gel in Tris·acetate·EDTA (TAE) buffer. The reaction product was purified using the Qiaquick PCR purification kit (QIAGEN). The purified product was digested with SalI and BamHI (NEB) by manufacturer's recommended protocols; the digested fragment was purified by the Qiaquick PCR purification kit, and the purified product was used in the ligation reaction.

To aid in purification of the protein product, the pMAL-c2x vector (NEB) was modified to express a 6-His tag at the N-terminus of maltose-binding protein by ligating the PCR product from the pMAL-c2x vector (forward primer 5'-GTCAGCCGCCATATGCATCATCATCATCATCATAAAATCGAAGAAGGTAAACTGG-3'; reverse primer 5'-GGCGTGCCGCTCAGCACGCCAACGAAC-3';GibcoBRL) into NdeI and BlpI digested pMAL-c2x.

The vector was sequenced in forward and reverse directions to confirm the presence of the 6-His modification and to confirm the sequence of the PCR product (Fig 16). Sequencing of the vector with insert was carried out by CFAR nucleic acids facility, a core facility at UMASS Medical School.

Purification of Recombinant rat ART2B

The BL21(DE3) strain was transformed with the vector and colonies were selected for by ampicillin (100μg/ml) resistance. Cultures were grown at 37° C to OD_{600} of 0.6-1.0, and expression was induced by 1mM IPTG for 60 minutes at 37° C. Cells were harvested and stored at -70° C until lysis and purification. Cell pellets were thawed from -70° C to 4° C in lysis buffer (50mM Tris·Cl; 500mM NaCl, pH 7.5). Cells were lysed by sonication (W-385 Ultrasonics Inc.) with the following settings: output control 9, 50% duty cycle, and 1 sec pulses. Lysates were spun at 32,000 x g, 40 minutes, 4° C. Because most of the ART2.2 expressed was in the form of inclusion bodies, the pellets were collected for guanidine resolubilization (25 mM Tris·Cl, pH 7.5; 6 M guanidine hydrochloride; 1 mM reduced glutathione). Resolubilization took place on a rotator at 4° C

Figure 16

```
AA   1     M   L   D   T   A   P   N   A   F   D   D   Q   Y   E   G     15
NUC  1     ATG CTA GAC ACG GCT CCC AAT GCA TTT GAT GAC CAG TAT GAG GGC   45

AA   16    C   V   N   K   M   E   E   K   A   P   L   L   L   Q   E     30
NUC  46    TGT GTC AAC AAA ATG GAG GAA AAG GCA CCC CTG CTT TTA CAG GAA   90

AA   31    D   F   N   M   N   A   K   L   K   V   A   W   E   E   A     45
NUC  91    GAC TTT AAT ATG AAT GCG AAA TTA AAA GTT GCG TGG GAA GAG GCA   135

AA   46    K   K   R   W   N   N   I   K   P   S   R   S   Y   P   K     60
NUC  136   AAG AAA CGA TGG AAC AAC ATA AAA CCT AGT AGG AGT TAT CCC AAA   180

AA   61    G   F   N   D   F   H   G   T   A   L   V   A   Y   T   G     75
NUC  181   GGT TTC AAT GAT TTC CAT GGA ACG GCT TTA GTT GCC TAC ACT GGG   225

AA   76    S   I   A   V   D   F   N   R   A   V   R   G   F   K   E     90
NUC  226   AGT ATC GCT GTA GAT TTT AAC AGA GCT GTT AGG GGA TTC AAG GAA   270

AA   91    N   P   G   Q   F   H   Y   K   A   F   H   Y   Y   L   T     105
NUC  271   AAT CCT GGT CAA TTC CAC TAC AAG GCC TTC CAT TAC TAC TTA ACA   315

AA   106   R   A   L   Q   L   L   S   N   G   D   C   H   S   V   Y     120
NUC  316   AGA GCT CTT CAG CTT TTG AGT AAC GGG GAT TGT CAT TCA GTC TAC   360

AA   121   R   G   T   K   T   R   F   H   Y   T   G   A   G   S   V     135
NUC  361   CGA GGC ACT AAG ACC AGG TTT CAC TAT ACT GGA GCT GGC TCC GTG   405

AA   136   R   F   G   Q   F   T   S   S   S   L   S   K   K   V   A     150
NUC  406   CGA TTC GGG CAG TTC ACG TCT TCA TCT TTA TCT AAG AAA GTA GCT   450

AA   151   Q   S   Q   E   F   F   S   D   H   G   T   L   F   I   I     165
NUC  451   CAA TCT CAA GAG TTT TTC AGT GAT CAT GGG ACG CTG TTC ATC ATC   495

AA   166   K   T   C   L   G   V   Y   I   K   E   F   S   F   R   P     180
NUC  496   AAA ACC TGC TTG GGG GTT TAT ATC AAA GAA TTC TCT TTC CGT CCT   540

AA   181   D   Q   E   E   V   L   I   P   G   Y   E   V   Y   Q   K     195
NUC  541   GAC CAA GAG GAG GTG TTA ATT CCA GGC TAT GAG GTA TAT CAG AAA   585

AA   196   V   R   T   Q   G   Y   N   E   I   F   L   D   S   P   K     210
NUC  586   GTC AGG ACA CAA GGC TAC AAC GAA ATT TTC CTG GAC TCC CCG AAG   630

AA   211   R   K   K   S   N   Y   N   C   L   Y   S   222
NUC  631   AGG AAG AAG AGC AAC TAC AAT TGC TTA TAC AGC   663
```

Figure 16. **Sequence data on the ART2.2 recombinant construct.** ART2.2 was

subcloned into a modified pMALc2x vector and the nucleotide sequence of the clone was

confirmed by the CFAR nucleic acid facility at UMASS Medical Center. The nucleotide

sequence and deduced amino acid sequence of the clone are illustrated and aligned by

codon.

overnight, and then the sample was centrifuged at 100,000 x g at 4° C for 60 minutes.

Supernatants were applied to a Ni $^{++}$ column (Iminodiacetic acid agarose, Sigma) equili-

brated with resolubilization buffer. A linear gradient was applied to the column to equili-

brate it in lysis buffer, and the 6HISMBPART2.2 fusion protein was eluted with an imi-

dazole (Sigma) gradient. The peak was collected and purified over a Q sepharose (Amer-

sham) column. Samples that contained NAD glycohydrolase activity were pooled, and

the 6HISMBP fusion partner was removed by a digestion with factor Xa (NEB) and a

wash through amylose resin (NEB).

Protein Assay

Protein was quantified by an assay based on the Bradford Method (163) using

Protein Dye Reagent Concentrate (BioRad) and BSA (BioRad) as a standard.

SDS-PAGE, Westerns, and Sequencing Gels

Proteins were solubilized in Laemmli sample buffer and separated by SDS-PAGE

chromatography. Gels were 1.0 mm thickness and 20 cm in length. Briefly, stacking gels

were made up from 4X stacking gel buffer (0.5M Tris·Cl, 0.4% SDS, pH 6.8) and 30%

(37.5:1, Biorad) acrylamide mixture to a 5% final concentration of acrylamide. Resolv-

ing gels were made up of a 4X resolving gel buffer (1.5 M Tris·Cl, 0.4% SDS, pH 8.9) to

a final acrylamide concentration of 12%. Gels were run in 25 mM Tris, 192 mM Glycine,

0.1% SDS, pH 8.3, at 150 volts for 45 minutes through the stack and 300 volts for 180

minutes through the resolving gel until the bromophenol blue dye front was approxi-

mately 2 cm. from the bottom of the gel. Protein gels were fixed and stained in a

Coomassie blue solution (50% methanol, 10% acetic acid and 0.2% R250 dye) at room temperature for 45 minutes. Destaining was carried out in a 50% methanol/10% acetic acid solution overnight.

Western blots were carried out by the SDS-PAGE protocol above, but the gels were not fixed and stained after completion of the run. Instead, proteins were transferred using a Biorad Transblot apparatus onto nitrocellulose membranes (0.45μm, Biorad) in a transfer buffer (25 mM Tris, 192 mM Glycine, pH 8.3, 20% methanol). The transfer was carried out at 100 volts for 90 minutes. Transfer was confirmed with 1 minute of Ponseau S staining (Sigma). The stain was completely removed by several washes of TBS (50 mM Tris·Cl, 150 mM NaCl, pH 7.5). The membrane was then submerged in blocking buffer (7% nonfat dry milk (Biorad) in TBS) overnight at 4° C. After blocking, the membrane was washed twice for 10 minutes at room temperature in TBS-T (TBS with 0.05% Tween detergent (Biorad). The remaining steps were carried out at room temperature with rigorous shaking. The membrane was then submerged in primary antibody solution (1° diluted into blocking buffer) for 60 minutes. For ART2 blots, sera containing the rabbit polyclonal antibody 1126 developed at the Diabetes Division of UMASS Medical school to the ART2 peptide, TGPLMLDTAPNAFD, was used at 1:1000 dilutions in blocking buffer. For polyADPR, the anti-polyADPR (BIOMOL) rabbit polyclonal antibody, which recognizes polymers of 8 or more in length, was used at concentrations of 1:1000. Following the incubation with primary antibody, the membrane was again washed twice with TBS-T for 10 minutes each wash. Secondary antibody (goat-

anti-rabbit conjugated to horseradish peroxidase from Santa Cruz) at a dilution of 1:5000 in blocking buffer was applied to the membrane and incubated for 30 minutes. The membrane was then washed twice with TBS-T for 10 minutes and once with TBS for 5 minutes. The blot was developed with ECL chemiluminescence reagent from Amersham on Kodak X-OMAT AR2 film. If the blots contained ^{32}P-labeled samples, then after chemiluminescent development, the blots were washed vigorously with TBS 3 times for 30 minutes each. The blots were exposed to film for up to 30 minutes to confirm the loss of the chemiluminescence signal, and then were exposed to film with the aid of an intensifying screen and placed in the -70° C freezer for autoradiography development.

Sequencing gels were based on the method developed by the Alvarez-Gonzalez and Jacobson (144). Briefly, samples were solubilized in sample buffers containing 25 mM NaCl; 4mM EDTA, pH 7.5; 0.02% xylene cyanol; 0.02% bromophenol blue; and 40% urea. Gels were poured at a 20% final concentration containing acrylamide and bis(acrylamide) in a ratio of 19:1; 89 mM Tris Borate, pH 8.3; 2 mM EDTA; 4.4 mM ammonium persulphate; and 3.4 mM TEMED. The gel dimensions were 20 x 20 x 0.15 cm. The electrode buffer was 45 mM Tris-borate, pH 8.3, and electrophoresis was carried out at 400 V until the bromophenol blue dye front had migrated 2/3 of the way from the origin to the end of the gel. At this point, electrophoresis was stopped and the gels were exposed to film at -70° C overnight with the aid of an intensifying screen.

DHBB Chromatography

Because of its affinity for cis-hydroxyl groups, dihydroxylboronyl Bio-Rex (DHBB) affinity resin was utilized to purify reaction products ADP-ribose and poly-ADP-ribose. DHBB affinity was prepared according to the protocols set up by Shah *et al.* (145). Briefly, 25 g of Bio-Rex resin (200-400 mesh, sodium form, BioRad) was soaked for 30 minutes in 0.25 M ammonium acetate (pH 5.0), washed with 1 liter of water, and suspended in 100 ml of water. All reactions were then carried out maintaining a pH of 5.0 with hydrochloric acid and stirring at room temperature. First, 2.5 g of 1-ethyl-3-(3-dimethylaminopropyl)carbodiimide was added to the resin and stirred for 15 minutes. Then 2.5 g of *m*-aminophenylboric acid was dissolved in 15 ml of water and added to slurry and incubated in the dark overnight at room temperature. Following the overnight incubation, the resin was washed with 1 liter of water; 1liter of 0.1M ammonium acetate, pH 4.5; 1 liter of 0.1M ammonium bicarbonate and 1M ammonium chloride, pH 9.0; and lastly with 500 ml of water. The resin was then suspended in 50 ml of storage buffer, 6 M guanidine hydrochloride, 50 mM 3-[*N*-morpholino]propanesulfonic acid, 10 mM EDTA, pH 6.0, for storage at 4° C in the dark. Resin capacity is confirmed with NAD before use in experiments.

Enzyme Assays

NADase

NADase assays were carried out as previously described (164). Briefly assays (total volume of 0.3 ml), containing 50 mM potassium phosphate (pH 7.5); 100 µM β-NAD;

and 55,000 cpm carbonyl-^{14}C NAD, were incubated for 5 min at 30° C.   Samples (0.2 ml) of reaction mix were passed through BioRad AG1-X2 (chloride form) mini-columns (1.5ml each and equilibrated in milliQ water), and the wash-through, containing nicotinamide, was quantified in a scintillation counter.

Auto-ADP-ribosyl transferase

NAD concentration curve assays for studying auto-ADP-ribosylation of ART2 were carried out in a total volume of 0.15 ml, containing 1.25 μg purified ART2.2, 100 mM potassium phosphate (pH 7.5); a range of nine different NAD concentrations from 0.1 to 10 mM β-NAD and a ratio of 1.5 μCi ^{32}P-labeled NAD to 0.1 mM NAD, were incubated for 6 min at 30° C and were analyzed by Western blot and autoradiography. Time-course assays (total volume of 0.8 ml), containing 100 mM potassium phosphate (pH 7.5); 20 mM β-NAD; 1 mCi ^{32}P-labeled NAD, were incubated for several time-points at 30° C and were analyzed by Western blot and autoradiography.

To analyze whether ADP-ribose polymers were forming, ART2 and PARP were incubated in 10 ml samples containing 100 μg enzyme, 100 mM potassium phosphate (pH 7.7), 25 mM NAD, and 0.5 mCi ^{32}P-labeled NAD for 10 hours at 30° C. The samples were precipitated in 25% TCA and incubated at -70° C for 30 minutes. The samples were thawed to 4 °C and centrifuged in the microcentrifuge for 30 minutes. Supernatants were removed and pellets were washed twice with cold 25% TCA and then twice with cold ethanol-acetone (50:50 v/v). After the final wash, the pellets were dried for 3 minutes in the speed vacuum to remove any trace ethanol-acetone. Pellets were then resolu-

bilized with the aid of sonication in a solution of 2 M hydroxylamine (pH 7.0 with ammonium hydroxide). Hydroxylamine cleaves the ADPR-protein bond of ART2(56). The freed ADP-ribose was then purified using DHBB chromatography, and after elution, samples were dried down in the speed vacuum and brought up in sequencing gel sample buffer for analysis.

Enzymatic Digestion

To discover the site of auto-ADP-ribosyl transferase activity on ART2, ART2 was subjected to a limited modification with NAD. Modification reactions (10 ml) were carried out with 200 μg purified ART2 protein, 0.1 M potassium phosphate pH 7.5, and 1 mM NAD, and were incubated for 30 min at 30° C. To detect polymers, the level of modification was increased by preparing the samples with 20 mM NAD and incubating for 60 minutes. Protein was precipitated with 25% TCA as described above. After the pellets were washed with ethanol-acetone, they were dried and digested with protease (chymotrypsin, trypsin, glu-c). Digestions were carried out in 0.1 M ammonium bicarbonate buffer, pH 7.8, containing 0.1% (w/v) RapiGest SF detergent (Waters). Samples were digested for 1 hour at 37° C and dried down by speed vacuum for analysis by mass spectrometry.

HPLC

High Performance Liquid Chromatography (HPLC) was run using a Waters 600 pump and Waters dual absorbency (2487) detector with a Waters 600 controller. The product ID column was a SynChropak Q (Eichrom) 250 x 4.6 mm ID with a 50mm guard

column. Samples of DHBB-purified polyADPR were digested with snake venom phosphodiesterase I (Worthington) according to manufacturer's recommended protocols and Shah *et a*. (145). The digest was carried out in 0.2 ml of digestion buffer (25 mM Tris·Cl, pH 7.5, 100 mM NaCl, and 5 mM MgCl). The reaction mixture was injected into the HPLC and applied to the column in Buffer A (20 mM Tris·Cl, pH 4.6). The flow rate over the column was 0.5 ml/min with an average pressure of 300 psi. The column protocol was 100% Buffer A for 20 minutes, a linear gradient from Buffer A to Buffer B (20 mM Tris·Cl, pH 4.6, 1 M NaCl), and 100% Buffer B for 30 minutes. Elutions were followed by monitoring ultraviolet absorption at 260 nm.

Mass Spectrometry

Samples for electrospray-ionization-mass spectrometry (ESI-MS) were desalted using DEAE sepharose (Amersham) in ammonium formate buffer (pH 5.0). Briefly, samples were applied in 10 mM ammonium formate, pH 5.0, and after several washes were eluted in 1 M ammonium formate. After drying down the samples by speed vacuuming, they were brought up in 50% methanol at a final concentration of 100 μg/ml and infused at a rate of 5 μl/min into the ESI ion source. Negative ion ESI-mass spectra were acquired using a ThermoFinnigan LCQ quadropole ion trap mass spectrometer. Full spectra were acquired from m/z 150-1500 and the major ions were subsequently trapped and MS^n was performed to obtain structural information.

MALDI-TOF (matrix-assisted laser desorption ionization time-of-flight) and Q-TOF (quadropole-time-of-flight) mass spectrometry were carried out by the Evans' Mass

Spectrometry Core Facility at UMASS Medical Center. MALDI-TOF analysis of digested peptides were carried out on a Waters M@LDI-L/R mass spectrometer. Sinnapinic acid was used as the matrix. Peptides were identified from MALDI-TOF spectra by comparison to theoretical digests of ART2. QTOF nanoscale HPLC-MS (MS/MS) analysis was carried out on a Waters Model QTOF API-US mass spectrometer. Peptides were separated on a PorousR2 (Applied Biosciences), 10cm x 75μm internal diameter, C18 reverse phase HPLC column and directly introduced into the nanoelectrospray ion source of the QTOF. Peptide sequence determination was carried out by collisional activation decomposition analysis in the QTOF of peptides previously identified in the MALDI-TOF spectra.

Structural Comparisons

Structural comparisons were carried out by downloading various ART structures from the Protein Data Bank (PDB). PDB files that were used in the comparisons include: 1A26.pdb, PARP complexed with carba-NAD; 4PAX.pdb, PARP complexed with 8-hydroxy-2-methyl-3-hydro-quinazolin-4-one; 3PAX.pdb, PARP complexed with 3-methoxybenzamide; 2PAX.pdb, PARP complexed with 4-amino-1,8-naphthalimide; 2PAW.pdb, PARP; 1PAX.pdb, PARP complexed with 3,4-dihydro-5-methyl-isoquinolinone; 1AER.pdb, Domain III of *Pseudomonas Aeruginosa* exotoxin A complexed with TAD; 1HE9.pdb, *Pseudo. a.* exotoxin S; 1BPC.pdb, pertussis toxin and ATP; 1PRT.pdb, pertussis toxin; 1GXY.pdb, ART2.2 crystal form A; 1GXZ.pdb, ART2.2 crystal form B; 1GYO.pdb, ART2.2 crystal form C; 1LTS.pdb, heat-labile enterotoxin

(*E.coli*); 1SGK.pdb, diphtheria toxin; 1TOX.pdb, diphtheria toxin with NAD; 1XTC.pdb, cholera toxin; 1GZF.pdb, C3 Toxin; 1QS2.pdb, VIP Toxin; 1LBE.pdb, *Aplysia* ADPR cyclase. Various ART structures were aligned using the program O. Figures were generated from the aligned structures with PyMol, an open source molecular modeling program.

Chapter 5 Results

Chapter Introduction

Chapter 5 will serve to illustrate the experimental results of the dissertation work. To address the major hypothesis, several approaches were taken. Structural modeling analyzed the similarities of the various ART groups and, in particular, compared the similarities and differences of PARP and ART2. Several studies of the recombinant construct were carried out to introduce it as a system for the study of ART2 auto-ADP-ribosylation. A combination of electrophoresis, HPLC, and mass spectrometry were used to specifically address whether the recombinant construct had PARP-like activity and to gather any structural information on the polymer. Lastly, a combination of enzymatic digestion, HPLC, and mass spectrometry were used to identify any sites of auto-ADP-ribosylation of ART2.

Structural Alignments and Similarities

Recent resolution of the crystal structure of ART2.2 provided the data with which to perform a multiple structural alignment of ART2.2, several mono-ART toxins, PARP, and ADP-ribosyl cyclase to compare their catalytic regions (165). Figure 17 illustrates the aligned peptide backbones of the regions of structural similarity of several crystallized ARTs. The regions center on the NAD-binding cleft. NAD from the NAD-bound diphtheria toxin structure (1XTC.pdb) is illustrated to show how NAD sits in the cleft.

Figure 17

A

Region I   Region II   Region III

B

Region II   Region III
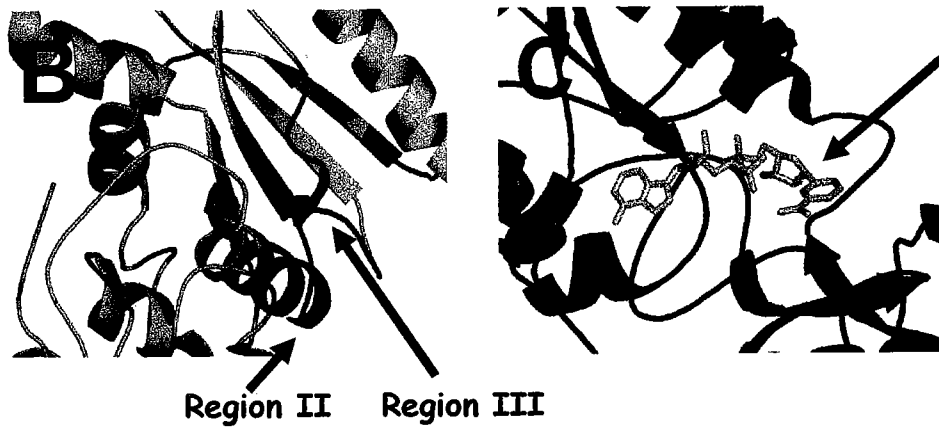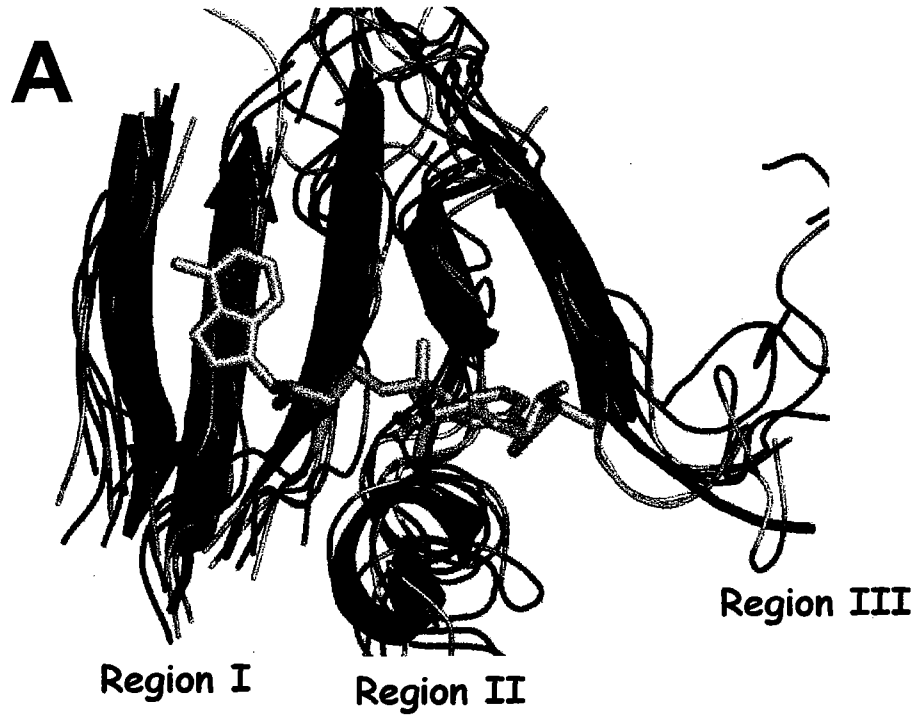
Figure 17. Structural insights to the ART family of proteins. A. Structural Alignment. The peptide backbones of the crystal structure models of several ARTs were aligned to analyze secondary and tertiary structural similarities on which to base a primary sequence alignment. The catalytic sites of several ARTs aligned well with three regions of similarity. Region I contained a β-sheet composed of three short β-strands. Region II contained an α-helix down to β-strand up, U-shaped, pocket that appears to hold the nicotinamide moiety. Region III contained a coil to β-strand loop. DT is used to model the ribbon cartoon and NAD from the DT structure is positioned in the catalytic cleft. DT, blue; PARP, red; ETA, cyan; PT, green; ART2, yellow; CT, orange; C3, salmon; VIP, violet; NAD, gray. **B.** Aplysia ADP-ribosyl cyclase. ADP-ribosyl cyclase does not appear to contain a Region I, but does contain a Region II and a variant version of Region III as an α-helix. **C.** SIR2 with NAD. Though SIR2 does not contain any regions of similarity with the catalytic clefts of the other ARTs, SIR2 does appear to hold NAD in a similar conformation as indicated by the arrow.

Alignment revealed that all ARTs contained some level of structural similarity except the SIR2, which had no appreciable similarity to the structures of the other ARTs. SIR2, however, did share share similarity with the way NAD was positioned in its cleft, which will be discussed later. As previously determined by primary sequence analysis, the catalytic site can be broken down into three regions; however, some additional data about each region were generated by this structural approach.

Region I was made up of three, largely nonpolar, anti-parallel β-strands forming a small β-sheet. This β-sheet was present in all the ARTs crystallized thus far with the exception of the *Aplysia* ADP-ribosyl cyclase, which was the most divergent ART superfamily member by secondary and tertiary structure. The first two β-strands of Region I bound adenosine and were each 6-7 amino acids in length. The third β-strand of Region I contained the highly conserved arginine or histidine that is typically followed by a glycine and appears to be crucial for NAD binding. This innermost β-strand was adjacent to Region II. Interestingly, the β-strands do not form from hairpin turns of primary sequence typically associated with β-sheets but come from three different stretches of primary sequence: the outer most β-strand is a stretch of amino acids that is C-terminal of Region III according to primary sequence; the second β-strand contains a stretch of amino acids that is N-terminal to Region III but C terminal to Region II; and the third and inner most β-strand that is adjacent to Region II by tertiary structure is 20-30 amino acids N-terminal of Region II by primary sequence.

Region II appears to be present in all ARTs, including the ADP-ribosyl cyclase, and was the most highly conserved by secondary structure. Region II could be generalized as having a $Y/SXS-X_{10}-Y/F$ motif regardless of the ART subgroup. The first Y/S and/or final Y of the Region II motif appeared to form a hydrogen-bond with the catalytic glutamate in many of the structures. Region II, by its U-shaped nature, appears to a critical pocket for the nicotinamide mononucleotide. The nicotinamide appears to be held in a very rigid conformation.

Region III, which was known as a β-sheet, was also present in all ARTs, but was expanded to include a conserved coil upstream of the catalytic glutamate which has been referred to as the ARTT motif. Though the coil had some flexibility of structure depending on the ART, it appeared to be an important and conserved part of the catalytic region. The Region III of ADP-ribosyl cyclase diverged from the other family members by secondary structure, containing a large α-helix instead of a coil to β-sheet motif, but Region III still contained the crucial catalytic glutamate.

Primary sequence alignments and a generalized model of the three regions (Fig 18) were derived from the structural alignments. This is the first structurally derived primary sequence alignment to contain representatives from all three ART subgroups; the monoARTs, PARPs, and ADP-ribosyl cyclases. Of interest, K903 and M890, which are important to the polymerase activity of PARP, appear unique to PARP, according to the structurally derived primary sequence alignments.

Figure 18

REGION I

DT	160	SVELEI	165	78	GGVVKVT	84	15	ENFSSYHGTK	24	
ETA	565	VVIPSA	570	496	GALLRVY	502	434	YVFVGYHGTF	443	
PARP	998	NLKYLL	1003	917	GLILLGE	923	856	NRQLLWHGSR	865	
ART2.2	213	DLFIEN	208	166	GTLFIIK	172	121	DCHSVYRGTK	130	
CT	123	QIYGWY	128	83	YYIYVIA	89	1	NDDKLYRADS	10	
PT	140	NIRRVT	145	86	GYIYEVR	92	3	PPATVYRYDS	12	
VIP	458	TADVVY	453	402	IILRLQV	408	343	ENITVYRWCG	352	
C3	242	TATIII	237	188	IITKFKV	194	122	ENIMFLRGDD	131	
								**		

REGION II

DT	52	GFYSTDNKYDAAG--Y	65
ETA	468	GFYIAGDPALAYG--Y	481
PARP	894	GIYFADMVSKSAN--Y	907
ART2.2	146	FTSSSLSKKVAQSQEF	161
CT	59	YVSTSISLRSAHLVGQ	74
PT	50	FVSTSSSRRYTEV--Y	63
VIP	384	YMSTSLSSERLAA--F	397
C3	172	YISTSLMVSQFAG--R	185
ADPRC	142	MASSSYAHSAEGEVTY	157
		* *	

REGION III

DT	139	PFAEGSSSVEYINNWE	154
ETA	544	GPEEEGGRLETILGWP	559
PARP	979	INDTCLLYNEYIVYDV	994
ART2.2	181	EFSFRPDQEEVLIPGY	196
CT	103	AYSPHPDEQEVSALGG	118
PT	120	AGALATYQSEYLAHRR	135
VIP	419	AIGGFASEKEILLDKD	433
C3	205	PISAFAGQLEMLLPRH	220
ADPRC	170	RPDSFFGKYELPNLTN	185
ARTT R		φ--E-E	
ARTT N		φ--Q-E	
		*	

REGION I

REGION II
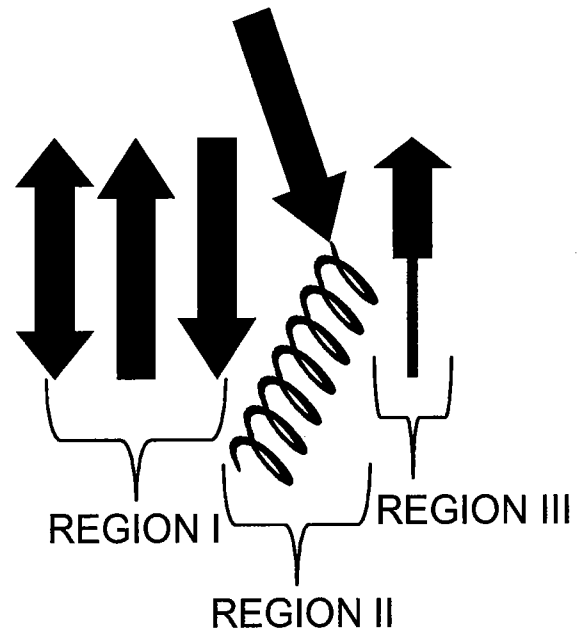
REGION III

Figure 18. Primary Sequence Alignment Based on Structures. The three regions of structural similarity reveal novel insights into the primary sequence alignment of the ARTs. All ARTs but the cyclase have a three β-strand Region I with the last strand containing the conserved arginine or histidine. Region II now aligns the "PARP-like" ARTs with the rest by the generalized motif Y/SXS-$X_{8/10}$-Y/F motif. Region III contains a catalytic glutamate in the same position in all ARTs. The insert presents a generalized cartoon model of the typical ART catalytic cleft.

To analyze the similarities and differences between ART2.2 and PARP more closely, a structural alignment between ART2.2 and PARP was performed. Figure 19 illustrates the structures and sequence alignments of ART2 and PARP. Carba-NAD was situated in the ADPR acceptor site according to the PARP crystal model (1A26.pbd) and NAD (from the diphtheria toxin model) was situated in the primary NAD-binding site. Both proteins had the three regions of structure and sequence similarity shared by most ARTs and demonstrated by the peptide backbone alignment. In Region I, however, ART2 contained a parallel outer β-strand whereas PARP contained the typical anti-parallel β-strand. Region II of PARP was composed of the Y-X10-Y motif, but Region II of ART2 was composed of the SXS-X10-F motif.

K903, which appears to be important to polymerization activity of PARP, can be found on the α-helix of Region II with the amide group of the lysine extending down toward the catalytic glutamate. Instead of a lysine at the equivalent location on ART2, there is a valine (V155) that appears up and away from the catalytic glutamate; however, the T2 (ARTT motif) glutamine (Q188) of ART2 does provide an amide to the same spatial region as K903 of PARP. M890 provides a hydrophobic cushion for the acceptor site adenine in the PARP model. Though there is no equivalent of M890 near the potential acceptor site of ART2, F184, with a hydrophobic side chain, appears in a similar spatial region as M890.

Despite the similarities of tertiary structure and the substitution of similar side chains to spatial locations important to the PARP activity, there is a major difference be-

Figure 19

A
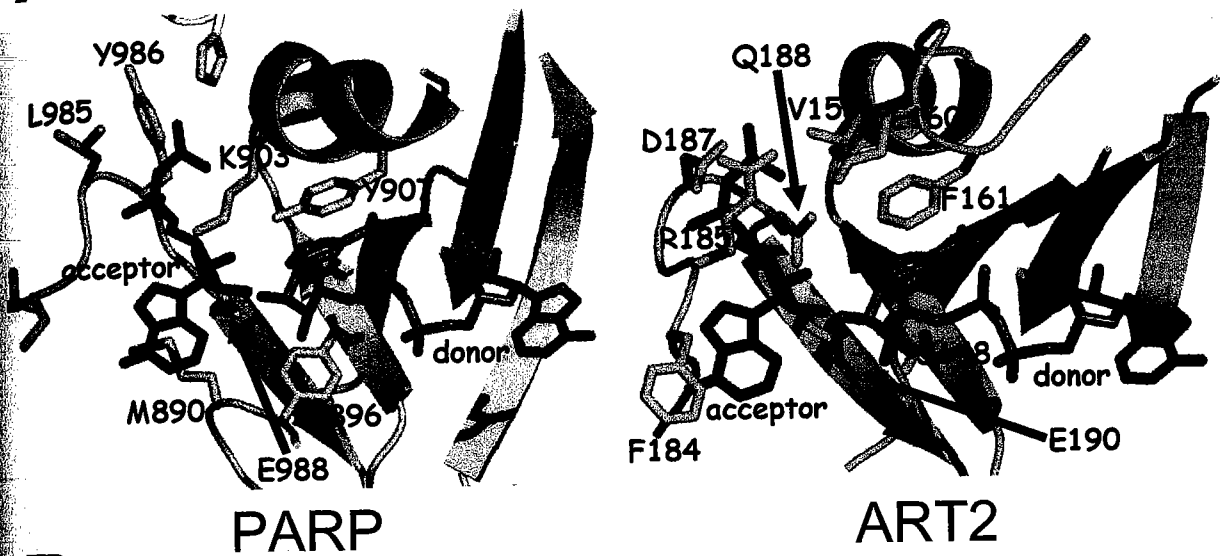
PARP

ART2

B

REGION I

```
PARP     998  NLKYLL 1003    917  GLILLGE 923    856  NRQLLWHGSR 865
ART2.2   213  DLFIEN  208    166  GTLFIIK 172    121  DCHSVYRGTK 130
```

REGION II

```
PARP     894  GIYFADMVSKSAN--Y 907
ART2.2   146  FTSSSLSKKVAQSQEF 161
```

REGION III

```
PARP     979  INDTCLLYNEYIVYDV 994
ART2.2   181  EFSFRPDQEEVLIPGY 196
```


REGION I   REGION III

REGION II
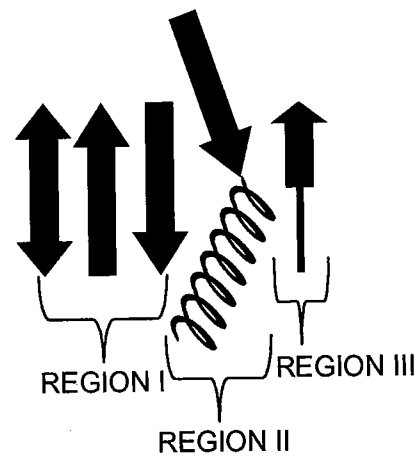
Figure 19. PARP and ART2 alignment. A. Backbone alignment of PARP and ART2 depicted as a ribbon diagram. NAD from the DT structure is aligned to the catalytic cleft and signified by the label "donor." Carba-NAD from the PARP structure is aligned to the "acceptor" site of polymer elongation. There appears to be room for an "acceptor" site in ART2, but access to it appears to be blocked by a salt bridge between R185, E160, and D187. **B.** Primary sequence alignment based on structural data. Both molecules share the three regions of similarity, but have very different primary amino acid sequences associated with each region. Key conserved amino acids appear in bold.

tween ART2.2 and PARP in the ADPR acceptor site that sterically hinders ADPR from entering. In PARP, ARTT coil of Region III was pulled outward allowing for more space for the ADP-ribose moiety of carba-NAD to enter into the site. ART2.2, however, has a constricted ARTT coil due to the formation of a salt bridge between E160, R185, and D187 that encloses the ADPR acceptor site (Fig 19). R185 is unique to ART2 and is the same T1 arginine of the ARTT motif thought to be significant to determine the multimeric nature of ART2 auto-ADP-ribosylation.

Recombinant ART2 Purification

To analyze accurately the reaction products of the auto-ADP-ribosylation of ART2.2 and identify any modified sites, a recombinant construct was designed to purify ART2.2 to a level that had no detectable background levels of auto-ADP-ribosyl transferase, poly(ADP-ribose) polymerase, or NAD glycohydrolase activities. The construct was designed as a fusion protein with maltose-binding protein (MBP) to aid in refolding and purifying the recombinant ART2. The linker region between MBP and ART2 has a factor Xa protease signal sequence to cleave and remove the MBP-fusion partner. Because ART2 contains an N-terminal endoplasmic reticulum signal sequence and a C-terminal GPI-anchor signal sequence (59), the subclone was designed to exclude the initial 25 amino acids and the last 29 amino acids of the ART2 propeptide that would be posttranslationally processed. The final purified construct contains most of what would be the core of the soluble ART2 molecule, with a short linker sequence (ISEFGS) from the factor Xa cleavage site (Fig 20).

Figure 20

```
WT            1 MPSNICKFFL TWWLIQQVTG LTGPLMLDTA PNAFDDQYEG 40
Construct     1                        I SEFGSMLDTA PNAFDDQYEG 21


WT           41 CVNKMEEKAP LLLQEDFNMN AKLKVAWEEA KKRWNNIKPS 80
Construct    22 CVNKMEEKAP LLLQEDFNMN AKLKVAWEEA KKRWNNIKPS 61


WT           81 RSYPKGFNDF HGTALVAYTG SIAVDFNRAV RGFKENPGQF 120
Construct    62 RSYPKGFNDF HGTALVAYTG SIAVDFNRAV RGFKENPGQF 101


WT          121 HYKAFHYYLT RALQLLSNGD CHSVYRGTKT RFHYTGAGSV 160
Construct   102 HYKAFHYYLT RALQLLSNGD CHSVYRGTKT RFHYTGAGSV 141


WT          161 RFGQFTSSSL SKKVAQSQEF FSDHGTLFII KTCLGVYIKE 200
Construct   142 RFGQFTSSSL SKKVAQSQEF FSDHGTLFII KTCLGVYIKE 181


WT          201 FSFRPDQEEV LIPGYEVYQK VRTQGYNEIF LDSPKRKKSN 240
Construct   182 FSFRPDQEEV LIPGYEVYQK VRTQGYNEIF LDSPKRKKSN 221


WT          241 YNCLYSSAGA RESCVSLFLV VLPSLLVQLL CLAEP 275
Construct   222 YNCLYS 227
```

Figure 20. Amino acid alignment of the deduced amino acid sequence of the ART2 construct with that of the full length ART2 propeptide. The construct was designed to contain a core region of the ART2 molecule that would reflect a soluble non-GPI-linked version of the molecule. The six amino acids from the linker sequence of the fusion partner are in red. WT, wild-type ART2.2 of the WF strain of rat; Construct, recombinant construct of ART2.2 subcloned from the wild-type.

Guanidine resolubilization of inclusion bodies and refolding on a nickel column appeared to provide a good yield of enzymatically active and relatively pure material. After the subsequent chromatographic steps, the specific activity was increased another 20 fold. Data from a typical purification are summarized in Fig 21, and the final specific activity of the purified ART2.2 was 2.3 μmol/min·mg. Assays contained 50 mM potassium phosphate (pH 7.5), 100μM β-NAD, and 55,000 cpm carbonyl-^{14}C NAD (total volume = 0.3 ml), and were incubated for 5 min at 30° C. No detectable background levels of NADase activity were found as measured by the vector minus insert control. Interestingly, the fusion protein did not appear to interfere with the ability of ART2 to catalyze the NAD glycohydrolase activity.

Upon refolding and elution from the nickel column, the recombinant protein was detected as a major band by Coomassie blue staining after SDS-PAGE. After several steps of purification and proteolytic processing, the final recombinant form of ART2.2 ran as a 28 kD band by SDS-PAGE and was the major band detected by Coomassie blue staining (Fig 22).

To confirm that the purified band was ART2.2, the band was excised from the gel and sent to the DERC proteomics core facility at UMASS Medical Center. There it was digested with either Lys-C or Trypsin and subjected to MALDI-TOF mass spectral analysis in a matrix of α-cyano-4-hydroxycinnaminic acid. The mass spectrum yielded a peptide map that confirmed the identity of the Coomassie stained band as ART2. Figure 23

Figure 21

Sample	Protein (mg)	Units (μmol/min)	Specific Activity (μmol/min·mg)	Yield %	Fold Purification
1	170	*ND*	--	--	--
2	120	14	0.12	100%	1
3	5.5	4.6	0.84	33	7
4	5.7	5.4	0.95	39	8
5	2.6	5.9	2.3	42	20

ND: not detectable

Figure 21. **Purification Table.** Assays containing 50 mM potassium phosphate (pH 7.5), 100 μM β-NAD, and 55,000 cpm carbonyl-^{14}C (total volume = 0.3 ml) were incubated for 5 min at 30° C. Details of purification are given in the chapter on Materials and Methods. Samples include: 1. guanidine-nickel eluate vector minus insert (negative control); 2. guanidine-nickel eluate vector plus ART2.2 insert; 3. Q eluate; 4. Xa digest; 5. amylose wash. Data are from one experiment representative of 6.

Figure 22

kD					
200 →					
116 →					
97 →					
66 →					6HISMBPART2.2
					6HISMBP(-)
45 →					6HISMBP
31 →					ART2.2
22 →					
14 →					

1   2   3   4   5
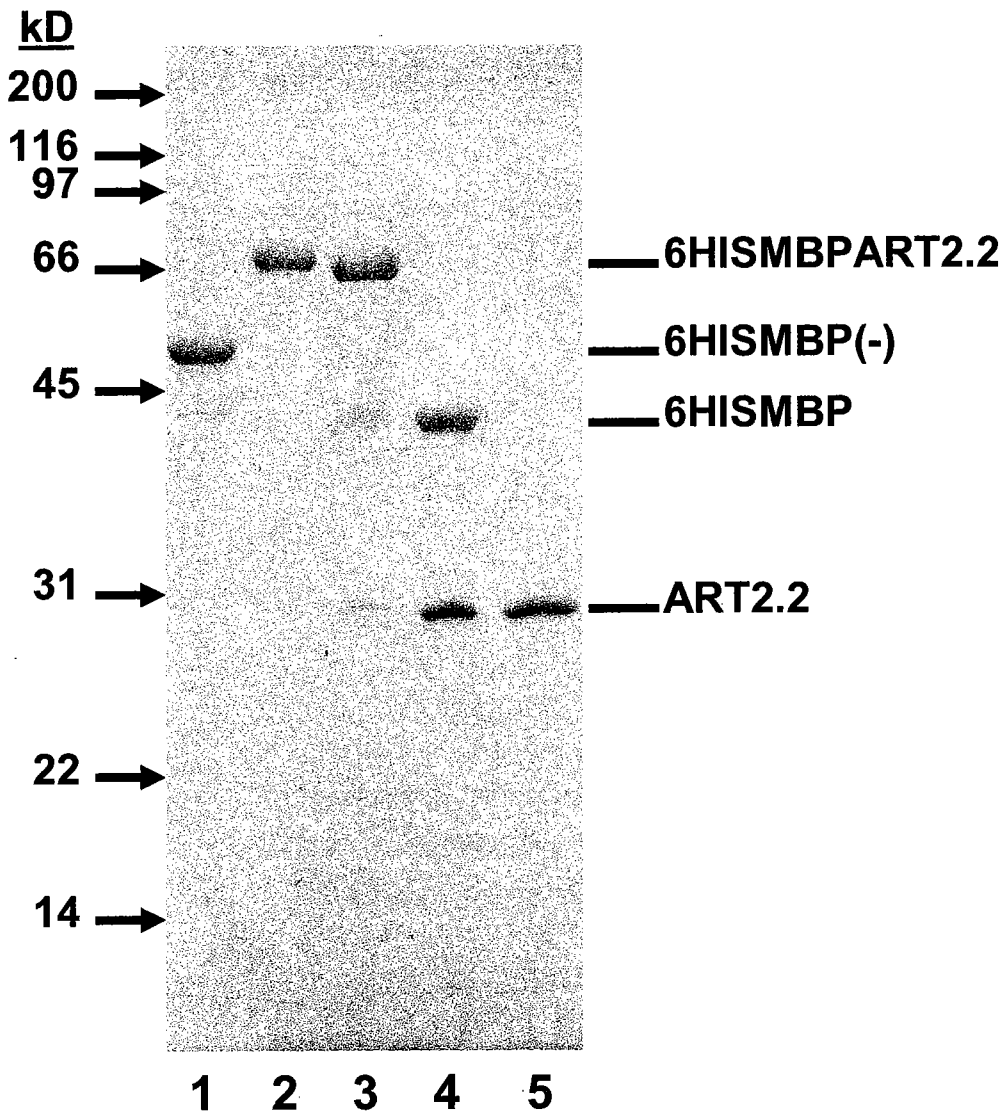
Figure 22. **Coomasie blue stained Purification Gel.** At each point in the purification, aliquots were set aside for SDS-PAGE analysis of purity. Samples include: 1. guanidine-nickel eluate vector minus insert (negative control); 2. guanidine-nickel eluate vector plus ART2.2 insert; 3. Q eluate; 4. Xa digest; 5. amylose wash.

Figure 23

A

m/z	Peptide Sequence	Modification
960.58	VAWEEAKK	
1119.6	ENPGQFHYK	
1604.01	APLLLQEDFNMNAK	
1619.96	APLLLQEDFNMNAK	Met-ox
1767.08	VRTQGYNEIFLDSPK	
2521.41	TRFHYTGAGSVRFGQFTSSSLSK	
2573.35	EFSFRPDQEEEVLIPGYEVYQK	

B

m/z	Peptide Sequence	Modification
1014.64	WNNIKPSR	
1070.64	AFHYYLTR	
1094.62	FHYTGAGSVR	
1188.70	FGQFTSSSLSK	
1511.89	TQGYNEIFLDSPK	
1603.90	APLLLQEDFNMNAK	
1619.93	APLLLQEDFNMNAK	Met-ox
1667.95	TQGYNEIFLDSPKR	
1767.05	VRTQGYNEIFLDSPK	
1923.12	VRTQGYNEIFLDSPKR	
2067.15	VAQSQEFFSDHGTLFIIK	
2121.07	MEEKAPLLLQEDFNMNAK	
2472.18	GFNDFHGTALVAYTGSIAVDFNR	
2573.23	EFSFRPDQEEEVLIPGYEVYQK	

Figure 23. **Table of Peptides from In Gel Digest.** The observed m/z values and their deduced amino acid sequences are presented to confirm that the purified band in lane 5 of figure 22 is ART2. **A.** Peptides from Lys-C digestion. **B.** Peptides from trypsin digestion.

summarizes the data as a table of observed mass peaks and their corresponding theoretical amino acid sequences. Post source decay was used to confirm sequences of identified peptides.

Recombinant ART2 Auto-ADP-ribosyl transferase activity

To confirm that the recombinant construct had auto-ADP-ribosyl transferse activity, the purified sample was incubated with [^{32}P] NAD and analyzed by SDS-PAGE. The gel samples were transferred to a nitrocellulose membrane and exposed to film (Fig 24). ART2.2 had auto-ADP-ribosyl transferase activity at all stages of the purification as detected by SDS-PAGE in conjunction with autoradiography. In the vector minus insert control, there was no detectable background ^{32}P-labeling to suggest contamination of another ART or PARP. A single band occurred in the fusion protein, illustrating that the fusion partner did not appear to interfere with auto-ADP-ribosylation. The radio-label followed the ART2 recombinant protein through the purification and processing steps, where it remained the only labeled band.

To understand the kinetics of the auto-ADP-ribosyl transferase activity of the recombinant ART2, it was incubated with a range of nine different NAD concentrations for 6 min at 30 °C. To analyze the data, the samples were run by SDS-PAGE and transferred to nitrocellulose membrane for Western blot analysis using the ART2-specific antibody, 1126 (Fig 25). The blot revealed an increasing level of modification at each concentration with a leveling off at the maximum of six band shifts by 7.5 mM and 10mM NAD. The samples also contained ^{32}P-labeled NAD for autoradiography. The autoradiography

Figure 24

kD					
116 →					
97 →					
66 →					— 6HISMBPART2.2
45 →					
31 →					— ART2.2
22 →					

1   2   3   4   5
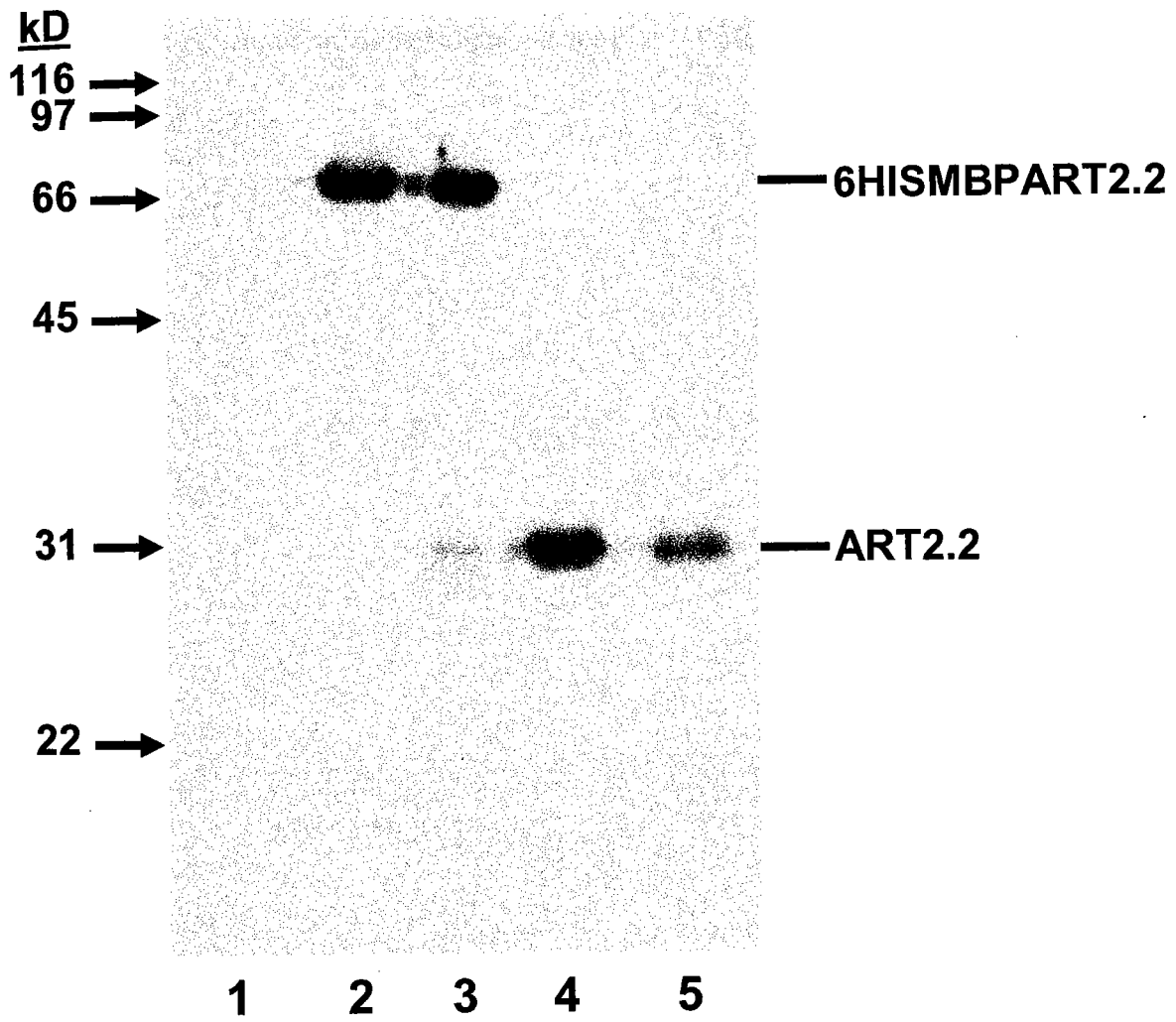
Figure 24. **Autoradiogram of Auto-ADP-ribosylated Recombinant ART2.** The autoradiogram depicts labeling in only ART2 samples and only where ART runs in each sample indicating no background levels of ADP-ribosyltranferase activity from *E. coli* contaminants. Samples include: 1. guanidine nickel eluate vector minus insert (negative control); 2. guanidine, nickel eluate vector plus ART2.2 insert; 3. Q eluate; 4. Xa digest; 5. amylose wash.

Figure 25
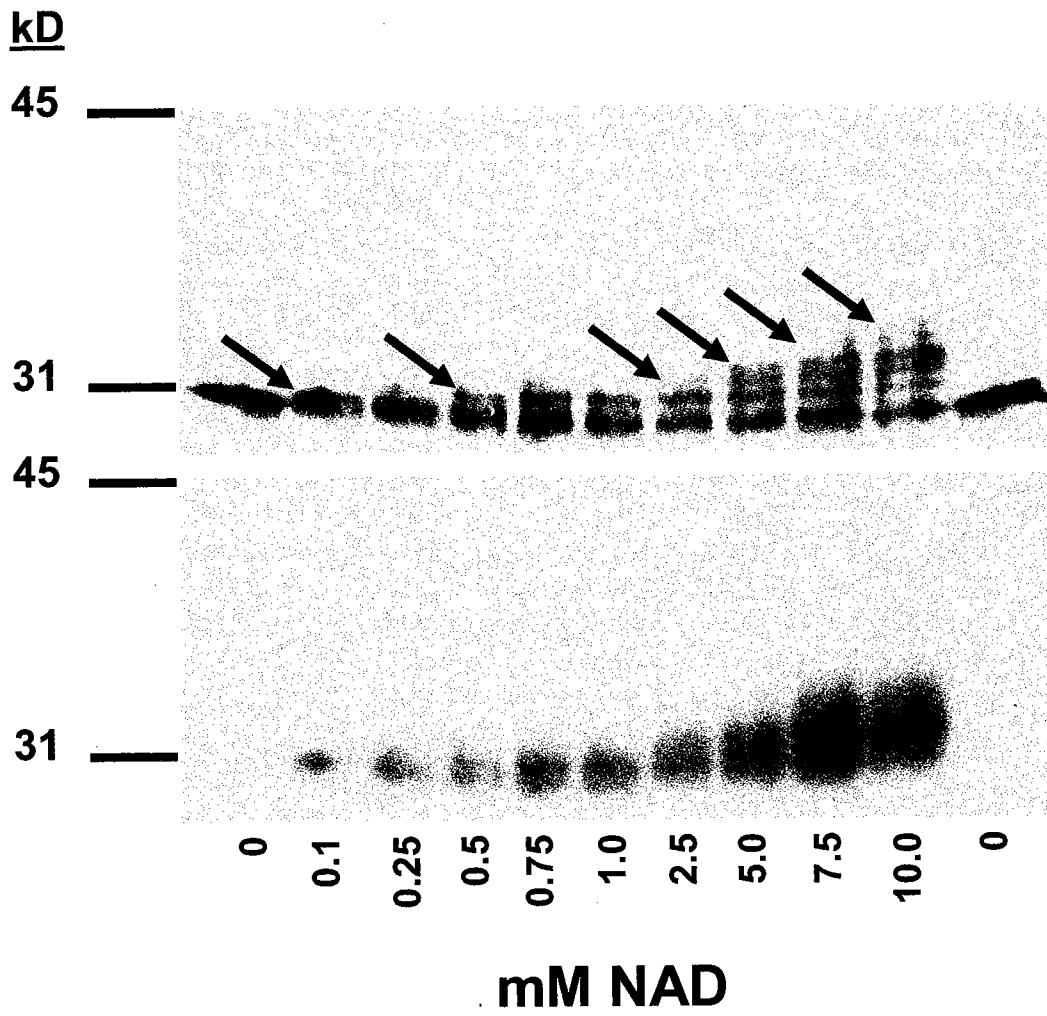
Figure 25. Auto-ADP-ribosylation Concentration Curve. ART2 was incubated with various concentrations of NAD for 6 minutes at 30 °C to illustrate the kinetics of ADP-ribosylation. The upper plate is an immunoblot for ART2 with the 1126 antibody. The lower plate is an autoradiogram. Arrows depicted each band shift in molecular mass.

confirmed the Western results of at least six band shifts, and being more sensitive, the autoradiogram demonstrated traces of a seventh band shift.

To confirm that each band shift corresponded to the molecular weight of ADP-ribose, a limited modification with 250 μM and 500 μM NAD was carried out. Samples were then desalted and purified by C4 HPLC reverse phase chromatography before being analyzed by MALDI-TOF mass spectrometry in a matrix of sinnapinic acid. Analysis of unmodified ART2 revealed a single major band of m/z = 26108 (Fig 26). This corresponds to the theortical molecular mass, 26100 kDa, of the deduced amino acid sequence of the recombinant construct. When ART2 was incubated with 250 μM NAD, a second major peak of m/z = 26647 appeared in the spectra. The difference of 539 corresponds to the theoretical molecular mass of covalently bonded ADP-ribose which is 541 Da. When incubated with 500 μM NAD, fractions that eluted a minute later on the HPLC contained the singly modified ART2 at m/z = 26645 and two more major peaks at m/z's 27182 and 27731. The differences, 537 and 549 respectively, also correspond to the molecular mass of covalently bonded ADP-ribose (541 Da).

To determine the temporal kinetics of auto-ADP-ribosylation, ART2.2 was incubated with 20 mM NAD over a range of nine time points that covered a 10 hour period. Samples were analyzed by Western blot and auto-radiography (Fig 27). The data revealed a sharp rise in bandshifts to a maximum of nine in the first hour that tapered to a gradual rise to 10-16 band shifts by the end of the 10 hours period. At all time points, the level of modification presented itself as a heterogeneous population.

Figure 26

A

m/z = 26108

B

m/z = 26107

m/z = 26647

C

m/z = 26645

m/z = 27182

m/z = 27731
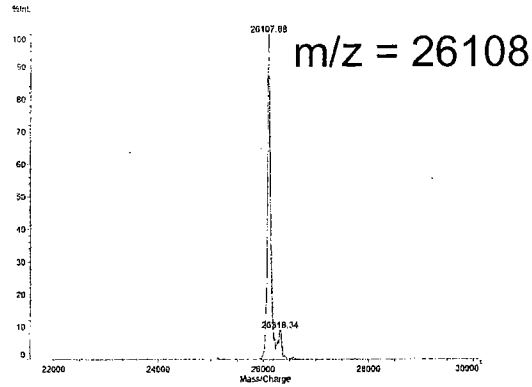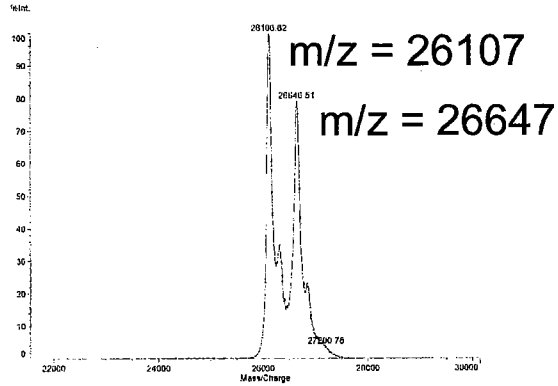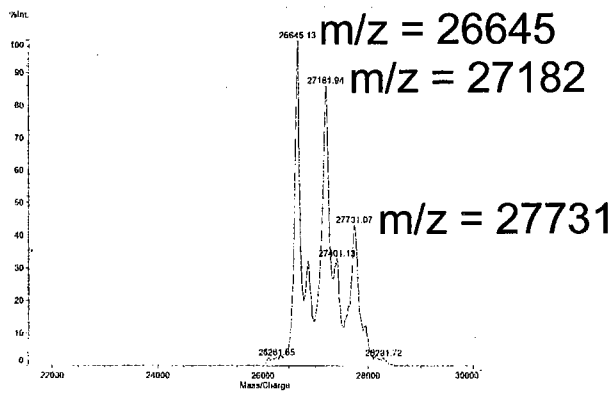
Figure 26. **Mass spectra of Auto-ADP-ribosyaltion.** **A.** Mass spectrum of purified ART2 protein depicting a single ion at *m/z* 26107.88. **B.** Mass spectrum of purifed ART2 incubated with 250 μM NAD for 5 minutes reveals two major ion species, *m/z* 26107 and *m/z* 26647. **C.** Mass spectrum of ART2 incubated with 500 μM NAD for 5 minutes reveals three major ion species; *m/z* 26645, *m/z* 27182, and *m/z* 27731.

Figure 27
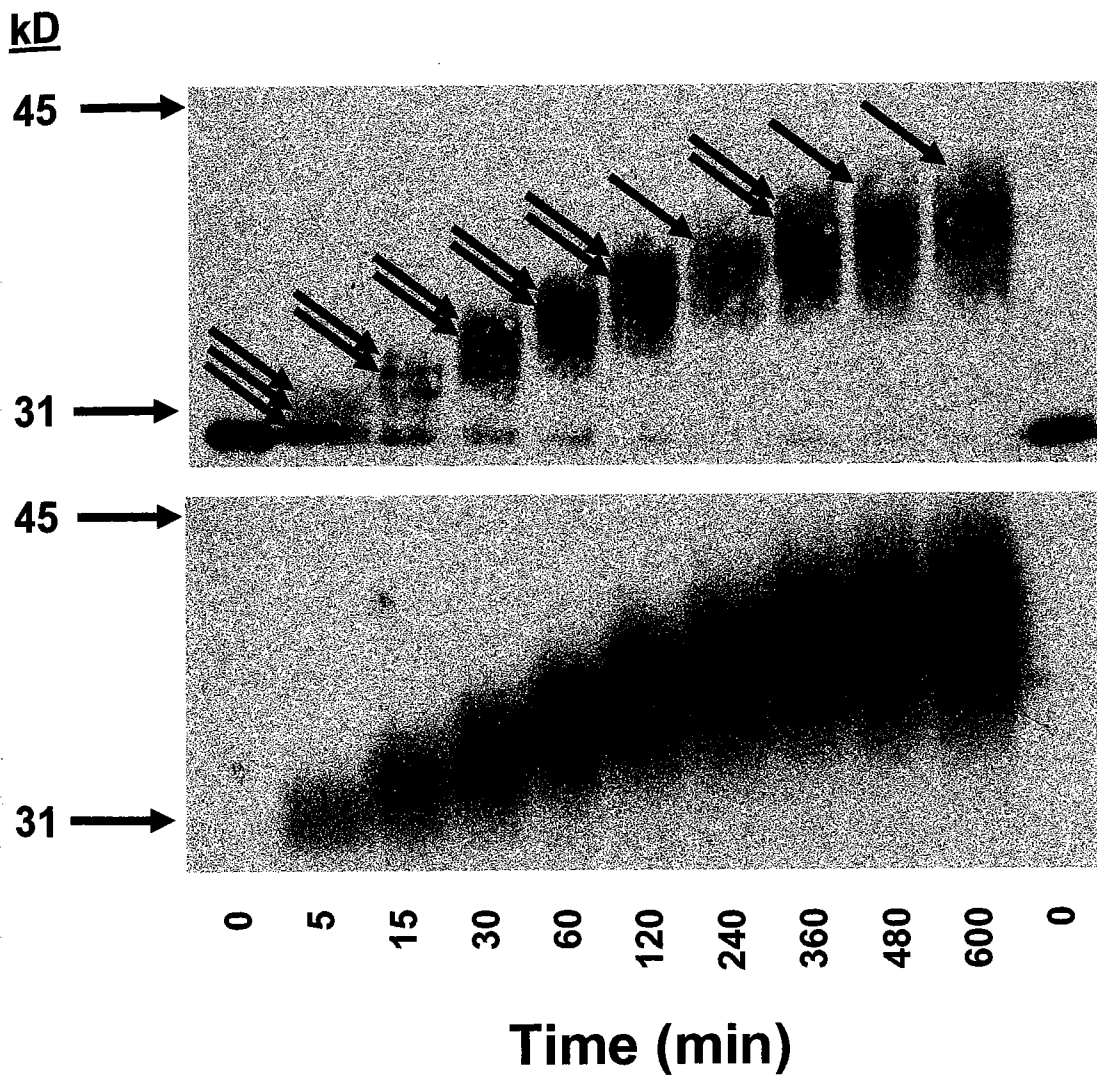
Figure 27. **Time course of Auto-ADP-ribosylation.** ART2 incubated with 20 mM NAD over a time course from 5 to 600 minutes. Samples were analyzed by Western blot (upper plate) and autoradiography (lower plate). Arrows indicate each detected band shift in molecular mass.

Multimeric ADP-ribosylation consists of polymers

To determine if the level of auto-ADP-ribosylation reached in the ten hour time-course consisted of any polymers, recombinant ART2.2 and purified PARP (BIOMOL) were incubated with ^{32}P-labeled NAD at a concentration of 20 mM NAD for ten hours at 30 °C. The ADPR moieties were cleaved with 2 M hydroxylamine, pH 7.0, run on a modified sequencing gel, and analyzed by autoradiography (Fig 28). As established in the literature (144;145), free ^{32}P-labeled ADPR was used as a marker for the monomers, bromophenol blue was used as a marker for 8-mers, and xylene cyanol was used as a marker for 20-mers. The modified sequencing gel revealed that both the PARP and ART2 samples contained a heterogeneous population of polymers. The PARP sample contained populations far greater than 20 in length, but the ART2 sample contained populations that barely reached 20 in length.

Digestion of the ADP-ribose polymers (pADPR) generated by PARP with snake venom phosphodiesterase results in a polymer specific product, 2'-O-α-D-ribosyladenosine 5', 5"-bisphosphate (PR-AMP) that can be resolved by analytical, ion-exchange HPLC and often has retention times similar to that of ADP. To confirm whether the ADPR polymers generated by ART2.2 had a similar structural composition to those of PARP, the hydroxylamine cleaved polymers were digested with snake venom phosphodiesterase and subjected to HPLC analysis. The reaction products were followed by absorption at 260 nm for adenine (Fig 29). HPLC spectra showed a snake venom

Figure 28

ADP-ribose
20-mer →

ADP-ribose
8-mer →

ADP-ribose
monomer →

1   2
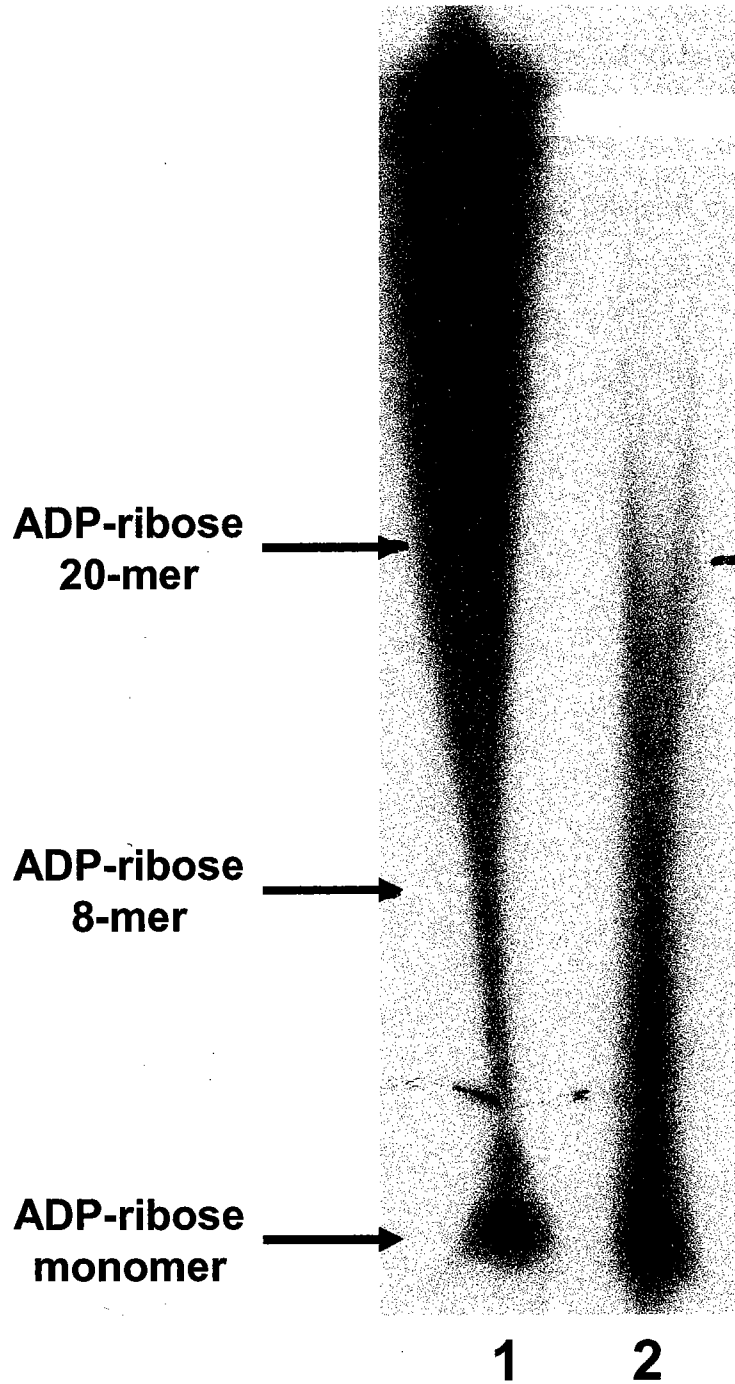
Figure 28. Modified Sequencing Gel. ADP-ribose moieties isolated from hydroxyl-amine cleavage of auto-ADP-ribosylated PARP (Lane 1) and ART2 (Lane 2) were run on a modified sequencing gel and analyzed by autoradiography. ADPR from the NADase activity of ART2 was isolated by HPLC and used as a control for monomer. Bromophenol blue is a marker for 8 mers and xylene cyanol is marker for 20-mers.

Figure 29
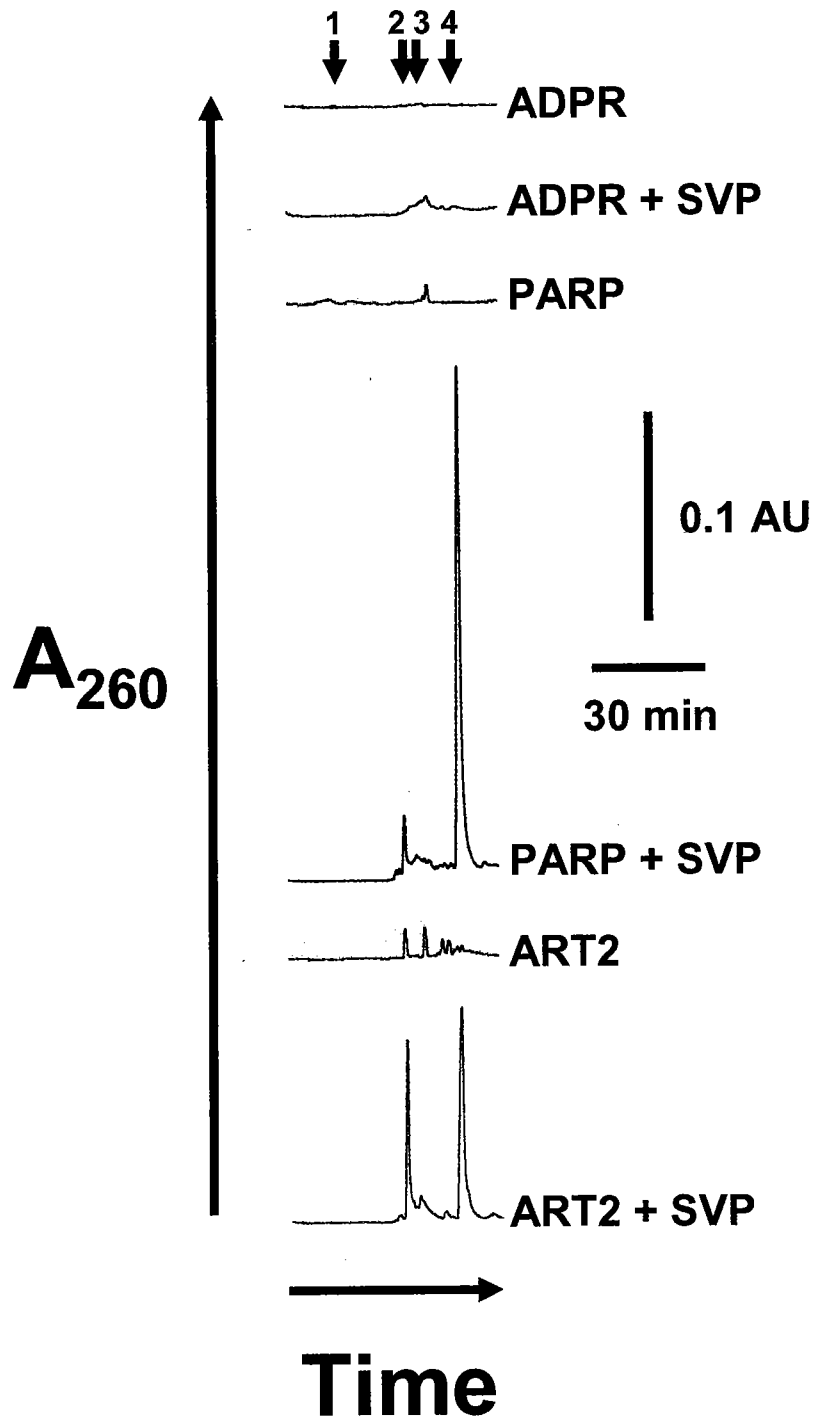
Figure 29. HPLC analysis of reaction products generated from phosphodiesterase treated polymers. PARP and ART2 were incubated with NAD for 600 minutes along with ADP-ribose as a negative control. The proteins were precipitated and their auto-modification polymers were cleaved with hydroxylamine. After isolation with DH-BB chromatography, the polymers were either treated with (+SV) snake venom phosphodiesterase or left untreated. The products were analyzed on the HPLC using anion exchange chromatography. Standards elute as indicated and include: 1. NAD, 2. AMP, 3. ADP-ribose, and 4. ADP.

phosphodiesterase-specific peak with a retention time later than the control sample, ADP, both in the PARP and ART2 samples. The ratios of the snake venom phosphodiesterase-specific peak to AMP were different between the PARP and ART2 samples. Also, to control for any non-enzymatic product formation due to highly reactive free ADP-ribose (a product of ART2's NAD glycohydrolase activity), free ADPR, at the same concentrations of NAD in the the enzyme assay, was subjected to the same incubations and analysis and did not produce any detectable levels of AMP or the phosphodiesterase-specific peak.

To confirm the phosphodiesterase-specific peaks from both PARP and ART2 were PR-AMP, fractions corresponding to the peaks were collected and analyzed by negative ion ESI-MS^n (Fig 30). A single major ion species occurred at m/z 558, which corresponds to the [M-H]$^-$ of PR-AMP, M_r 559. Since ADPR and PR-AMP are isomers, they have the same mass, but differ structurally, and though ADPR has a different retention time on the HPLC column, it is a major component of the in vitro reaction mix. Therefore, the phosphodiesterase-specific peaks and ADPR, as a negative control, were subjected to MS^n using the mass spectrometer to determine structural composition. MS2 on m/z 558 [M-H]$^-$ from ADPR revealed a major product ion species at m/z 346 corresponding to AMP (M_r 347), a fragment of ADPR. MS2 on the phosphodiesterase-specific peaks from PARP and ART2 revealed a major product ion at m/z 460, which corresponded to the loss of phosphoric acid (M_r 98). Because ADPR does no contain a 1° phosphate, it cannot lose a phosphoric acid in a single cleavage event without some sort of molecular re-arrangement; however PR-AMP can lose a phosphate in a single cleavage resulting in ribosyl-AMP, M_r 461.

Figure 30
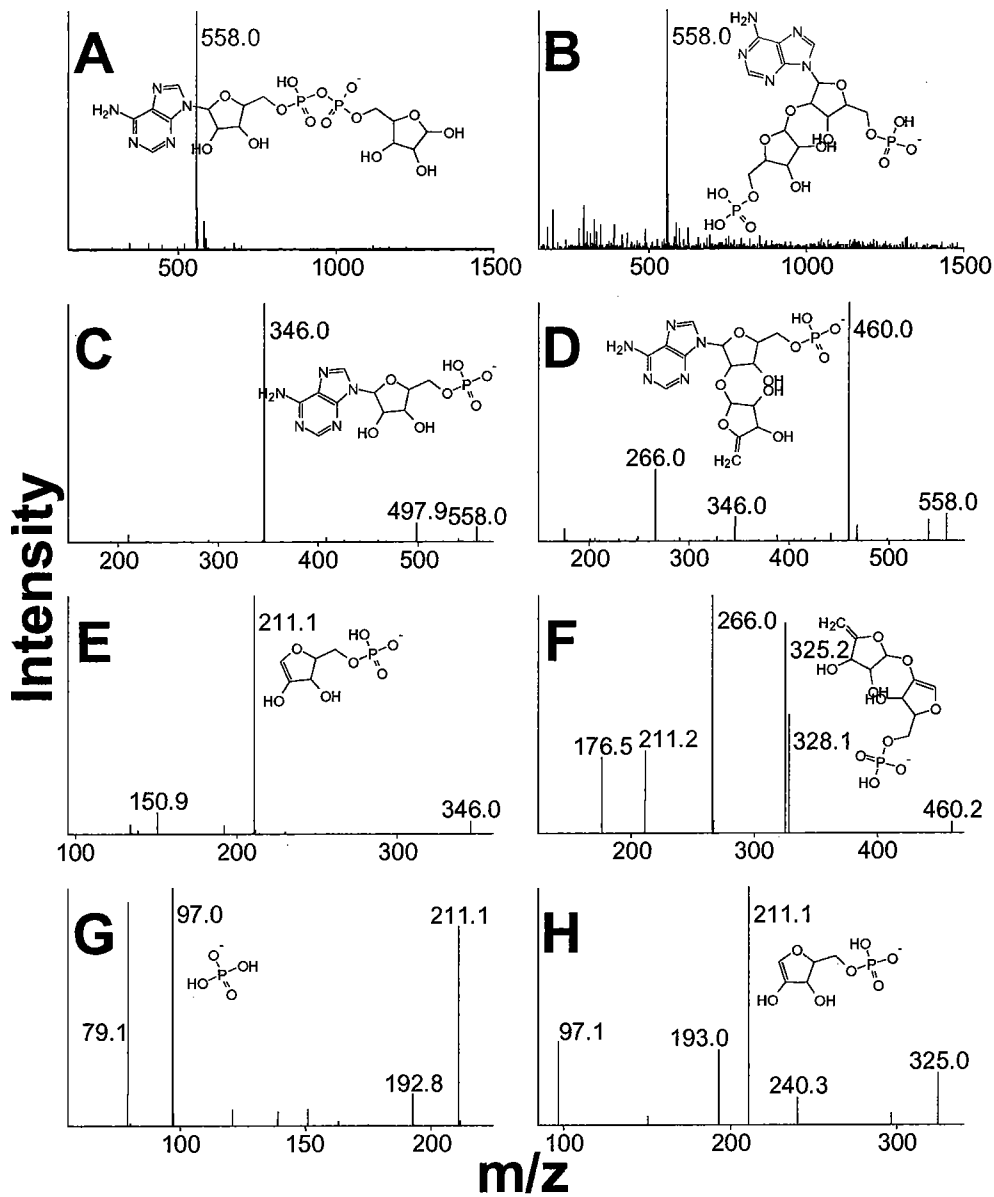
Figure 30. Negative mode ESI-MS of ADP-ribose versus phosphodiesterase specific product. **A.** Full spectrum of ADP-ribose. **B.** Full spectrum of ART2 generated phosphodiesterase-specific product. **C.** CAD of isolated m/z 558.0 from A. **D.** CAD of isolated m/z 558.0 from B. **E.** CAD of isolated 346.0 from C. **F.** CAD of isolated m/z 460.0 from D. **G.** CAD of isolated m/z 211.2 from E. **H.** CAD of isolated 325.2 from F. Inserts represent deduced structures of major product ions. CAD; collisional activation decomposition analysis.

MS3 of AMP revealed a major product ion at m/z 211, corresponding to 5'phospho-ribose, M_r 212. MS3 of the m/z 460 produced a major product ion at m/z 325 that corresponds to ribosyl-(5'phospho-ribose), M_r 326. CAD MS4 of the m/z 211 species of ADP-ribose revealed a major product ion at m/z 97, which corresponds to phosphoric acid, M_r 98. Lastly, CAD MS4 of the m/z 325 ion revealed a major product ion at m/z 211, which corresponds to 5'phospho-ribose, M_r 212.

Poly(ADP-ribose) structural data

Previous work on PARP has determined that the average polymer length and the average branching frequency of pADPR can be calculated by the ratios PR-AMP to AMP(145). Compared to the PARP generated pADPR, ART2 generated pADPR had lower ratios of PR-AMP to AMP when digested with phosphodiesterase. This suggests a different structure to the polymer molecule. To better understand the structure of ART2 generated pADPR, the polymer was purified by DHBB chromatography, digested with snake venom phosphodiesterase, and the reaction mix was subsequently analyzed by MALDI-TOF mass spectrometry using sinnapinic acid as a matrix. The spectrum revealed the presence of an ion species ladder with repeating intervals of m/z 211 (Fig 31). The spectrum was consistent with a hetergeneous population of phosphor-ribose polymers that began with a dimer and ended with a 10-mer. This polymer of phospho-ribose is consistent with ADP-ribosylation of the initial ADP-ribose moiety at the 2C of the ribose from the NMN. The ribose is the same ribose that has a 1C linkage to an amino acid on ART2.

Figure 31

TOF LD+
1.32e4

x20

%

211x3
+ H⁺

211x3
+ Na⁺

211x4
+ H⁺

211x4
+ Na⁺

211x5
+ Na⁺

211x6
+ Na⁺

211x7
+ Na⁺

211x8
+ Na⁺

211x9
+ Na⁺

m/z

550.4
633.9
655.9
656.9
657.9
677.9
845.2
867.1
868.1
1078.1
1223.7
1245.7
1289.1
1290.1
1291.1
1305.0
1321.7
1493.8
1500.1
1501.0
1502.1
1503.1
1701.5
1711.1
1713.2
1923.1
1924.0
2151.6
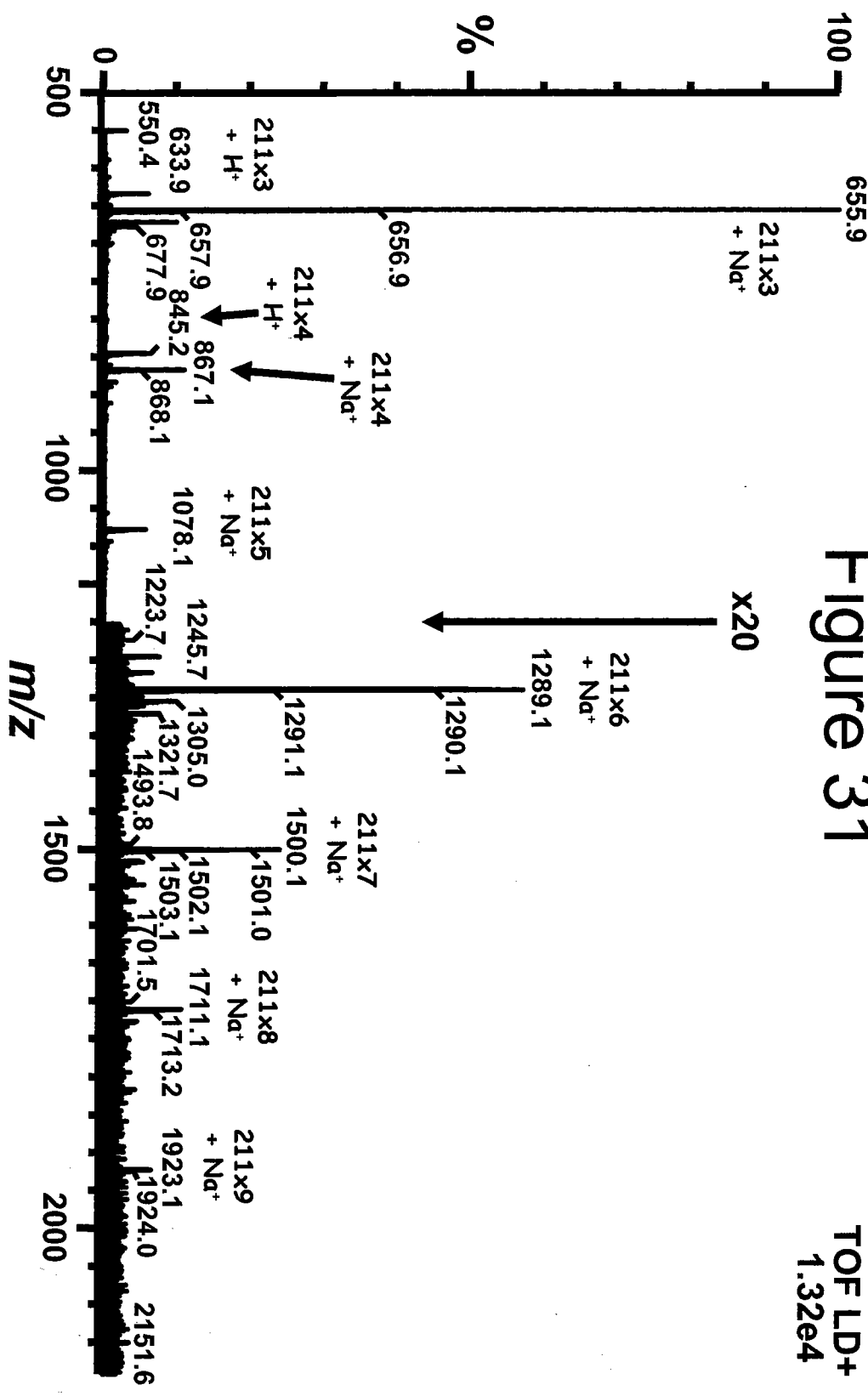
Figure 31. **Mass spectra of phosphoribose polymers.** Products from the snake venom phosphodiesterase-treated ART2 generated polymer were analyzed by MALDI-TOF mass spectrometry. Iions in multiples of m/z 211 were generated. The Y-axis above m/z 1200 was magnified by a factor of 20.

Identification of Site of Polymer

In order to identify the site of polymer linkage on the recombinant form of ART2, an initial study of limited modification was carried out to identify a site of mono-ADP-ribosylation. Identification of any mono-ADP-ribosylated peptides would be a foundation for looking for any poly-ADP-ribosylated peptides that exist. ART2 was incubated with 1 mM NAD for 30 minutes at 30 °C, and after TCA precipitation, the sample was digested with chymotrypsin. The chymotrypsin digests were analyzed by MALDI-TOF mass spectrometry using sinnapinic acid as a matrix (Fig 32). The unmodified ART2 contained a major ion species at m/z 2041 in the region of the spectra between m/z 1,000 to 5,000. In addition to the corresponding peak of m/z 2041 in the modified ART2 sample, there was a peak at m/z 2582 that was not detectable in the unmodified sample. The difference corresponded to the the molecular mass of ADP-ribose, 541 Da. The observed ion species m/z 2041 and 2041 corresponded to a theoretical chymotrypsin-generated ART2 fragment whose m/z is 2041. This fragment has the deduced amino acid sequence, SFRPDQEEVLIPGYEVY, and corresponds to amino acids, 183-199, located in Region III of the catalytic cleft (Fig 18-20). A closer inspection of the mass spectrum between m/z 2500 and 3250 revealed a weaker ion species at m/z 3123. This ion species represented a mass difference of 541 from the ion species, m/z 2582, and corresponds to a second ADP-ribose moiety attached to the identified peptide.

Figure 32
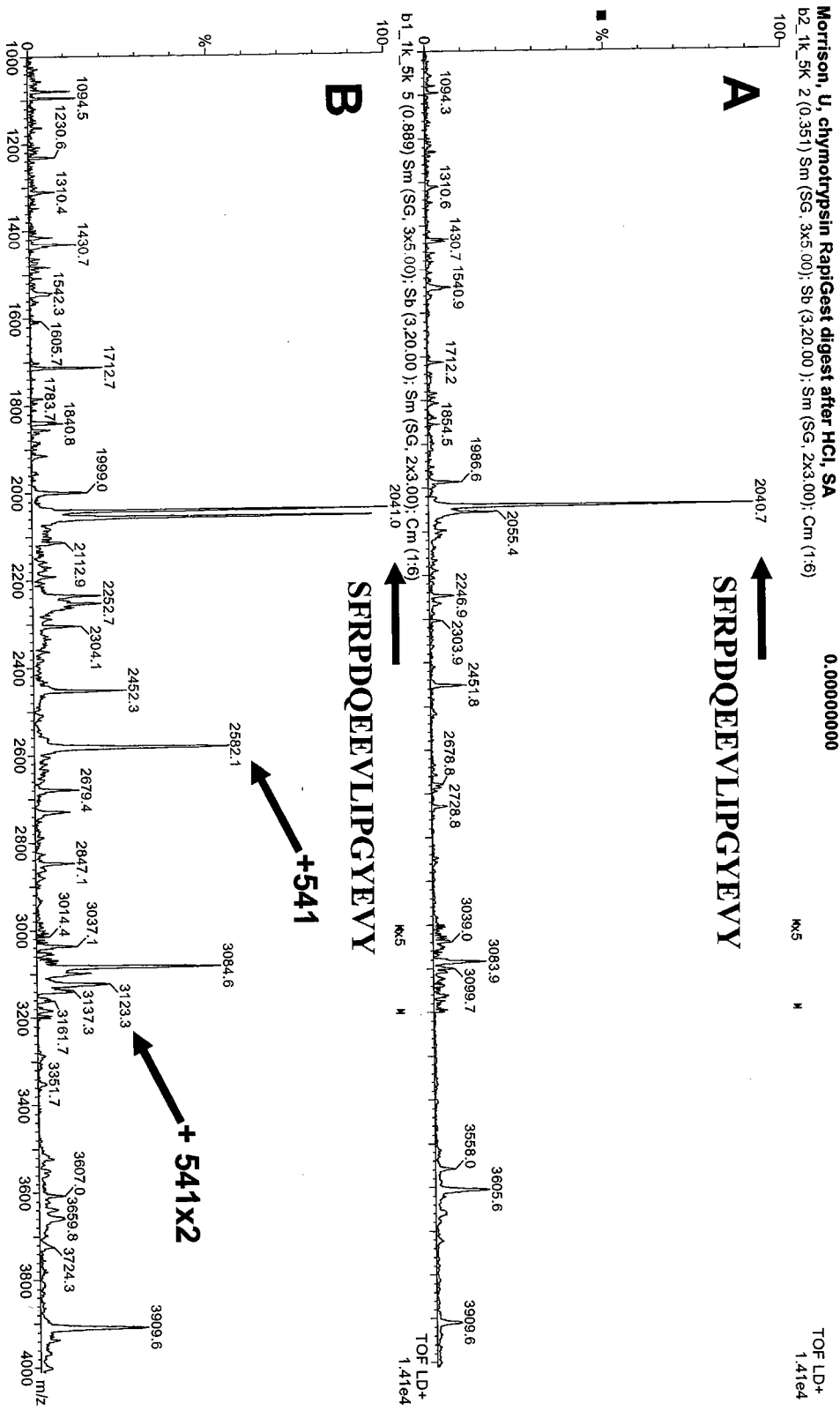
Figure 32. **Mass Spectra of unmodified versus modified ART2.** ART2 was modified with limiting amounts of NAD, digested with chymotrypsin, and analyzed by MALDI-TOF mass spectrometry. A major peak at m/z 2041 occurred in both samples. Two additional peaks were observed in the modified sample but not the unmodified at *m/z* 2582 and *m/z* 3123 (+541 and + 2x541, respectively).

Figure 33

A set of three mass-spectrometry / chromatography traces labeled A, B, and C.

A — 1: QTOF LC-MS ES+
BPI
1.19e3

Labeled m/z peaks: 649.8, 547.7, 449.6, 488.9, 649.8, 604.3, 923.4, 809.4, 718.3, 833.5, 462.2, 722.7, 1292.0, 818.1, 910.8, 1104.6, 1028.5, 1021.4

B — MS ES+
m/z 1021.4
2.30e4

Labeled peaks: 1021.4, 1310.7

C — MS ES+
m/z 1292
1.74e4

Labeled peak: 1292.0

X-axis: Time (min), values 20.00, 25.00, 30.00, 35.00, 40.00, 45.00, 50.00, 55.00, 60.00, 65.00, 70.00

Y-axis: % (0 to 100) for each trace.

Figure 33. Isolation of unmodified and modified peaks using C18 reverse phase

HPLC-MS. A. A base peak mass spectral chromatogram indicating the major ion species that eluted over the course of the reverse phase gradient. **B.** Ion plot for *m/z* 1021.4.
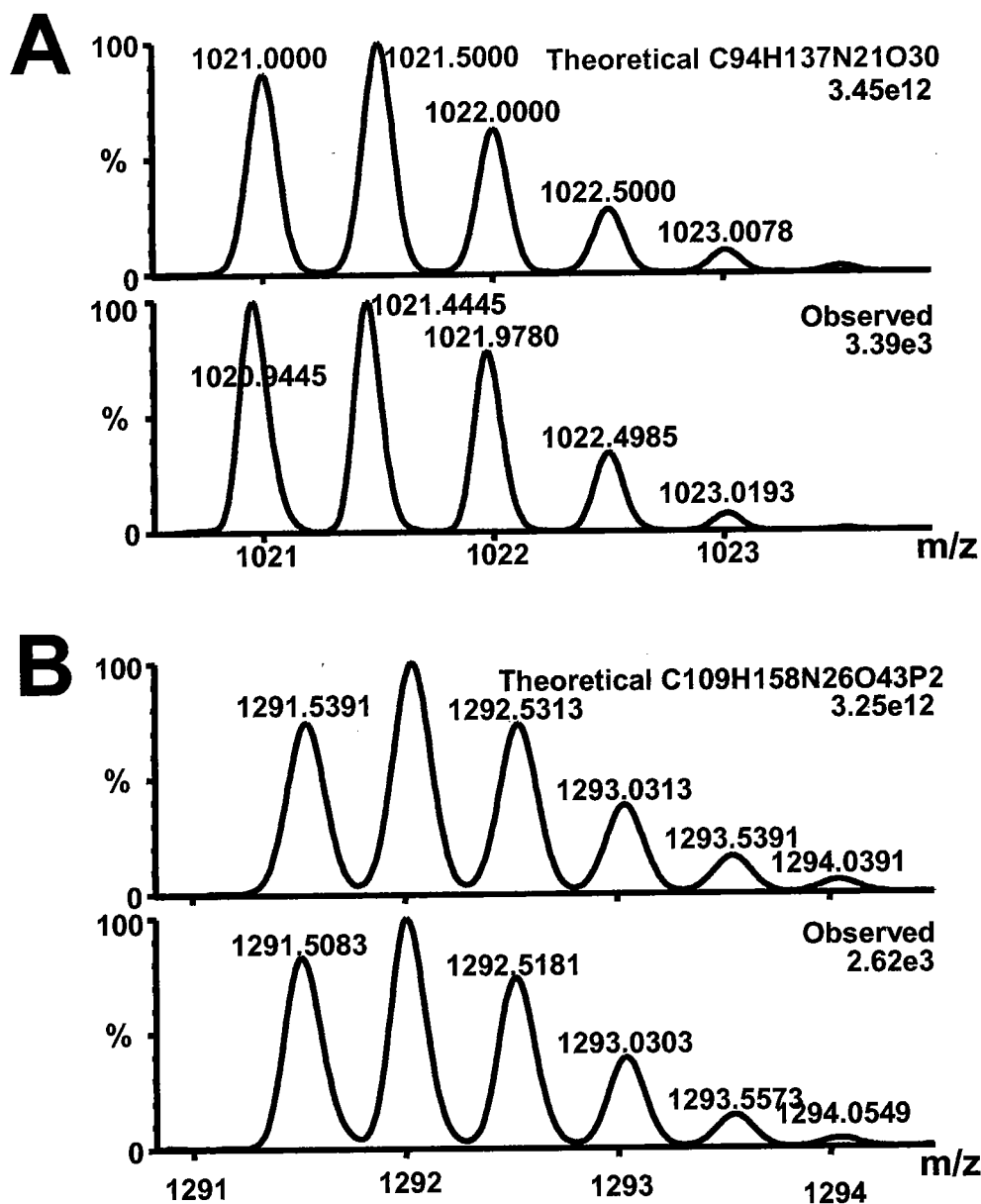
C. Ion plot for *m/z* 1292.0.

To confirm the identity of the peptide, SFRPDQEEVLIPGYEVY, the chymotryptic digest of modified ART2 was analyzed by nanoscale HPLC-MS using a C18 column (10cm x 75μm id) with a gradient of 2-70% acetonitrile in 0.1% formic acid (2-17% in 15 min, 17-40% in 35 min, and 40-70% in 15 min). The elution profile was subject to real-time QTOF mass spectrometry. Collision induced decomposition spectra were carried out in realtime to gather structural information about the peptides as they eluted from the column. Figure 33A shows a base peak chromatogram of the ions that eluted from the column over the period of the gradient. The peak, m/z 1021.46 eluted from 53-54.5 minutes and corresponded to a doubly charged ion of M_r 2042.8. Another major peak (m/z 1291.51) eluted from 50-52 minutes and corresponds to a doubly charged species of a M_r 2582.1. Figure 34 shows the full mass spectra for the unmodified and modified peptides. Relative isotope profiles obtained corresponded to theoretical amounts calculated for elemental composition of both the proposed unmodified and modified peptides (Fig 35). The observed monoisotopic mass of the unmodified peptide was 1020.9445 Da, and the theoretical based on elemental composition was 1021.0000 Da yielding a difference of 0.056 mass units. The observed monoisotopic mass of the modified peptide was 1291.5083 Da, and the theoretical based on elemental composition was 1291.5391 Da yielding a difference of 0.031 mass units. The observed mass difference of m/z 270.564 (541.138 Da) for ADP-ribose, whose theoretical mass calculated from its elemental composition is 541.078. The difference beween observed and the theoretical mass for ADP-ribose is 0.06 Da. The precision of the QTOF is 50 mDa in the mode used for the above analysis.

Figure 34
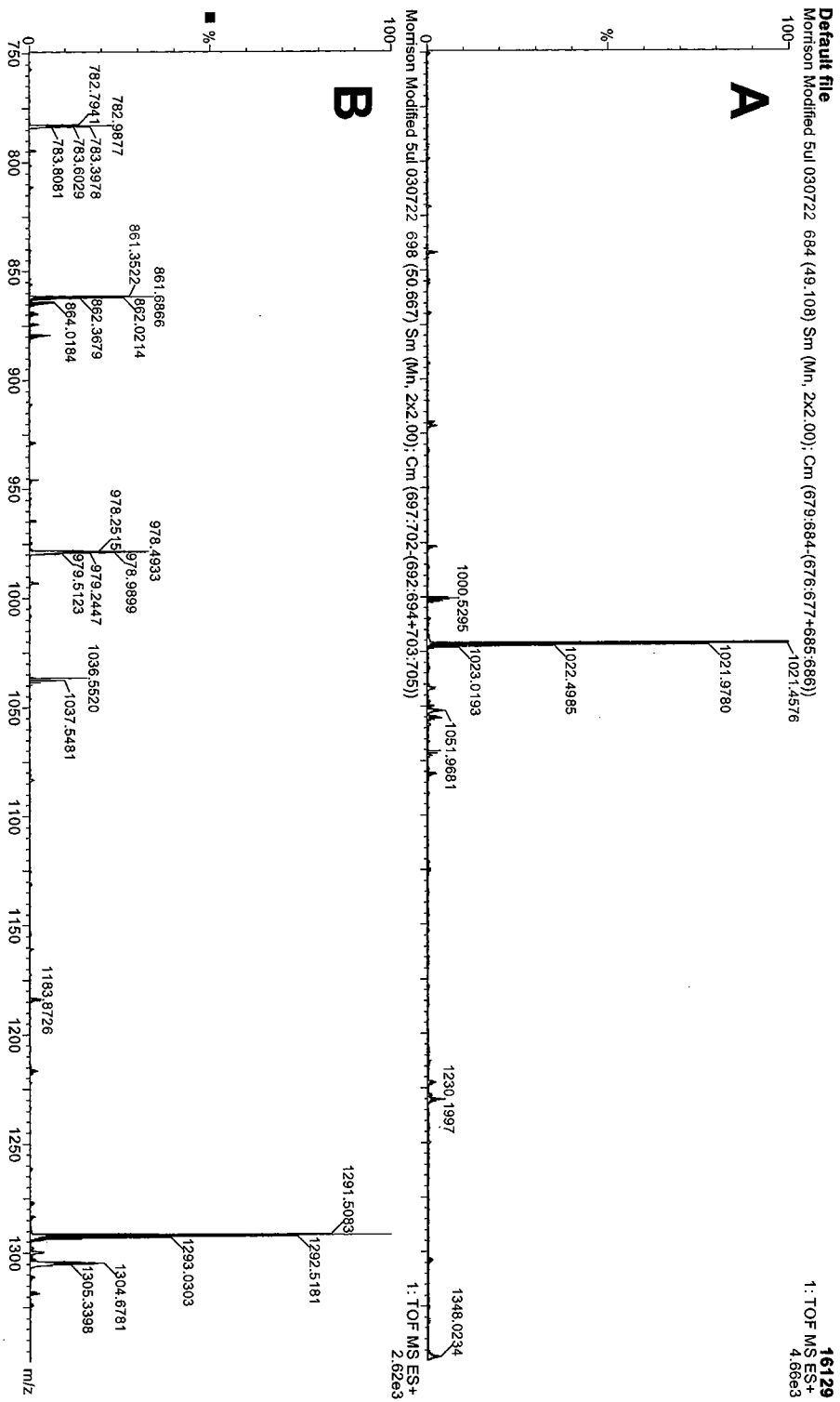
Figure 34. Full mass spectra of elution regions containing the modified and un-

modified peptides. **A.** Full spectrum for the compound eluting at 53.5 min. *m/z* 1021.4

is a doubly charged ion. **B.** Full spectrum for the compund eluting at 51.0 min. *m/z*

1291.5 is a doubly charge ion. *m/z* 861.7, another major peak in the spectrum is the triply

charged version of the same peptide as *m/z* 1291.5.

Figure 35

A

100 — 1021.0000   1021.5000   Theoretical C94H137N21O30
                                          3.45e12
%   1022.0000
                    1022.5000
                              1023.0078
0 —

100 —   1021.4445   Observed
                1021.9780   3.39e3
%   1020.9445
                    1022.4985
                              1023.0193
0 —
   1021   1022   1023   m/z

B

100 —   Theoretical C109H158N26O43P2
   1291.5391   1292.5313   3.25e12
%   1293.0313
                    1293.5391
                              1294.0391
0 —

100 —   1291.5083   Observed
                1292.5181   2.62e3
%
                    1293.0303
                              1293.5573
                                    1294.0549
0 —
   1291   1292   1293   1294   m/z

Figure 35. **Elemental Composition spectra.** **A.** Theoretical vs. observed isotope profiles for m/z 1020.9445, a doubly charged ion. It closely matches the theoretical profile of the peptide SFRPDQEEVLIPGYEVY and is 0.056 Da lower than the theoretical monoisotopic mass value of m/z 1021.0000. **B.** Theoretical vs. observed isotope profiles for m/z 1291.5083, a doubly charged species. The experimental closely matches the theoretical profile of the peptide SFRPDQEEVLIPGYEVY plus the modification of ADP-ribose and is 0.031 Da lower than the theoretical monoisotopic value of m/z 1291.5391.

Both these doubly charged ions were subjected to collision activation decomposition (CAD) analysis to obtain a complete MS^2 product ion spectra containing peptide sequence information (Fig 36, 37). Fragmentation of the unmodified peptide resulted in y, a, and b fragment ion series as well as several internal fragments that confirmed the deduced sequence of the peptide as SFRPDQEEVLIPGYEVY. Though much of the y series could be found in the modified peptide fragmentation spectra, the a and b series were not as prominant as in the unmodified peptide. In addition, there are several prominant internal fragment ions in both modified and unmodified peptides. Several fragment ions were identified in the modified sample spectrum but were not seen in that from the unmodified spectrum. When the molecular mass of ADP-ribose (541 Da) was subtracted from these ions, the resulting ion m/z ratio matched those of theoretical internal fragment ions. Deduced modified fragmentation sequences included; RPDQEEVL, RPDQEEV, SFRPDQ, RPDQ, SFR, and R. The amino acid that all of the modified fragments had in common is arginine. This corresponds to R185 of Region III.

To confirm the location of modification by an alternative digestion protocol and to identify whether the site identified for mono-ADP-ribosylation can be a site of poly-ADP-ribosylation, ART2 was modified by 20 mM NAD for 60 minutes at 30° C in addition to the monomer ADP-ribosylation of 1 mM NAD for 30 minutes. The modified protein was subjected to digestion with Glu-c endopeptidase and analyzed by MALDI-TOF mass spectrometry (Fig 38). In the unmodified digest, the spectra between m/z 1000 to m/z 5000 revealed a major ion species at m/z 1926 which corresponded to the theoretical monoisotopic ion m/z 1925.93, which has the deduced amino acid sequence,

Figure 36

Figure 36: Product Ion Table I

Observed m/z	% Base Intensity	Theoretical m/z	Δ m/z	Ion type: Sequence
70.07	0.4	70.07	0.0	Amino acid: R/P
86.10	2.0	86.10	0.0	Amino acid: I/L
102.07	0.5	102.06	0.01	Amino acid: E
112.09	0.7	112.09	0.0	Amino acid: R
120.08	0.8	120.08	0.0	Amino acid: F
127.09	0.8	127.09	0.0	Internal: PG
136.08	20	136.08	0.0	Amino acid: Y
155.08	25	155.08	0.0	Internal: PG
182.09	20	182.11	0.02	y_1: Y
193.10	5.0	193.10	0.0	Internal: GY-28
201.13	4.0	201.12	0.01	Internal: EV-28
211.12	1.8	211.11/ 211.14	0.01/ 0.02	Internal: EV-H_2O/IP
221.10	7.5	221.09	0.01	Internal: GY
229.13	7	229.12	0.01	Internal: EV
235.13	0.6	235.11	0.02	b_2: SF
265.12	2.0	265.12	0.0	Internal: YE-28
281.16	20	281.15	0.01	y_2: VY
290.15	20	290.15	0.0	Internal: PGY-28
293.12	20	293.11	0.01	Internal: YE
318.16	40	318.15	0.01	Internal: PGY
350.15	7.5	350.14	0.01	Internal: GYE
374.19	1.3	374.17/ 374.18	0.02/ 0.01	Internal: YEV- H_2O/ b_3-NH3: SFR
391.22	8.5	391.21	0.01	b_3: SFR
401.20	25	401.23	0.03	Internal: FRP
410.20	1.6	410.19	0.01	y_3: EVY
419.21	18	419.19	0.02	Internal: PGYE-28
429.19	18	429.18	0.01	Internal: PGYE-H_2O
447.20	100	447.19	0.01	Internal: PGYE
470.21	1.0	470.19/ 470.25	0.02/ 0.04	Internal: PDQEE/ B_4-H_2O: SFRP
495.22	1.0	495.22	0.0	b_8^{+2}: SFRPDQEE

518.27	20	518.26	0.01	Internal: PGYEV-28
528.26	5.0	528.25	0.01	Internal: PGYEV-H_2O
546.26	75	546.26	0.0	Internal: PGYEV
560.29	3.0	560.27	0.02	Internal: IPGYE
573.27	1.2	573.25/ 573.26	0.02/ 0.01	Internal: DQEEV-28/ y_4: YEVY
599.24	1.2	599.23/ 599.30	0.01/ 0.06	Internal: PDQEE/ QEEVL
601.31	4.0	601.30	0.01	B_{10}^{+2}: SFRPDQEEVL
603.31	20	603.29	0.02	b_5: SFRPD
631.35	1.5	631.35	0.0	Internal: IPGYEV-28
659.36	3.0	659.34	0.02	Internal: IPGYEV
681.31	1.3	681.27/681.38	0.04/ 0.07	Internal: PDQEEV-NH_3/ EEVLIP
698.31	1.0	698.30	0.01	Internal: PDQEEV
709.34	4.0	709.32	0.02	y_6-H_2O: PGYEVY
727.34	85	727.33/727.34	0.01/ 0.0	y_6: PGYEVY/ Internal: RPDQEE-28
772.44	0.6	772.72	0.02	Internal: EVLIPGY/ VLIPGYE/ LIPGYEV
794.40	0.3	794.36	0.04	Internal: PDQEEVL-NH_3
811.40	1.2	811.38	0.02	Internal: PDQEEVL
840.43	8.0	840.41	0.02	Y_7: IPGYEVY
860.42	3.0	860.39	0.03	b_7: SFRPDQE
902.46	0.2	902.40	0.06	Internal: FRPDQEE
924.50	0.4	924.47	0.03	Internal: PDQEEVLI/ DQEEVLIP
961.46	1.0	961.44	0.02	a_8: SFRPDQEE
989.45	8.0	989.43	0.02	b_8: SFRPDQEE
1060.53	1.6	1060.51/ 1060.53	0.02/ 0.0	a_9: SFRPDQEEV/ Internal: PDQEEVLIPG-H_2O
1088.51	8.0	1088.50	0.01	b_9: SFRPDQEEV
1173.61	6.0	1173.59	0.02	a_{10}: SFRPDQEEVL
1201.61	30	1201.59	0.02	b_{10}: SFRPDQEEVL
1286.70	20	1286.67	0.03	A_{11}: SFRPDQEEVLI
1314.68	60	1314.67	0.01	B_{11}: SFRPDQEEVLI
1468.78	0.6	1468.74	0.04	b_{13}: SFRPDQEEVLIPG

Figure 36. **Product Ion Table I.** The data generated from collisional activation decomposition MS^2 analysis of isolated peptide m/z 1021.46 by quadrapole time of flight (QTOF) mass spectrometry. Eighty-five percent of the ions that appeared in the spectra are identified and presented in the above table. The spectra were calculated to have a dynamic range of about 5000; and the lowest percent base ion intensity used was 0.2%, which was 10 fold over baseline. The largest Δ m/z was 0.07 with an average of 0.02.

Figure 37

Figure 37: Product Ion Table II

Observed m/z	% Base Intensity	-541.3: new value	Theoretical m/z	Δ m/z	Ion type: Sequence
70.08	0.1	N	70.07	0.01	Amino acid: R/P
86.10	0.24	N	86.10	0.0	Amino acid: I/L
102.07	0.6	N	102.06	0.01	Amino acid: E
120.08	0.6	N	120.08	0.0	Amino acid: F
127.09	0.3	N	127.09	0.0	Internal: PG-28
136.07	30	N	136.08	0.01	Amino acid: Y
155.08	6.5	N	155.08	0.0	Internal: PG
182.09	3.5	N	182.11	0.02	y_1: Y
193.10	1.2	N	193.10	0.0	Internal: GY-28
201.12	0.8	N	201.12	0.0	Internal: EV-28
211.11	0.6	N	211.11/ 211.14	0.0/ 0.03	Internal: EV-H_2O/ IP
216.05	0.2	N	216.10	0.05	Internal: DQ-28
221.10	2.0	N	221.09	0.01	Internal: GY
229.13	2	N	229.12	0.01	Internal: EV
232.08	0.4	N	232.2	0.12	Modification: Adenosine-2H_2O
235.13	0.6	N	235.12	0.02	b_2: SF
250.10	25	N	250.2	0.10	Modification: Adenosine-H_2O
265.12	0.4	N	265.12	0.0	Internal: YE-28
281.16	3.0	N	281.15	0.01	y_2: VY
290.17	4.0	N	290.15	0.02	Internal: PGY-28
293.13	0.5	N	293.11	0.02	Internal: YE
318.16	20	N	318.15	0.01	Internal: PGY
348.08	30	N	348.2	0.12	Modification: 5'AMP
392.19	6.0	N	392.08	0.11	Y_3-H_2O: EVY/ Internal: YEV
401.20	10	N	401.23	0.03	Internal: FRP
410.22	1.4	N	410.19	0.03	y_3: EVY
419.22	1.4	N	419.19	0.02	Internal: PGYE-28

428.06	10	N	428.2	0.14	Modification: ADP
447.20	50	N	447.19	0.01	Internal: PGYE
470.20	1.7	N	470.19/ 470.25	0.01/ 0.05	Internal: PDQE/ b_4-H_2O: SFRP
518.28	12	N	518.26	0.02	Internal: PGYEV-28
528.24	2.0	N	528.25	0.01	Internal: PGYEV-H_2O
546.27	50	N	546.26	0.01	Internal: PGYEV
560.30	1.5	N	560.27	0.03	Internal: IPGYE
573.28	1.2	N	573.25/ 573.26	0.03/ 0.02	Internal: DQEEV-28/ y_4: YEVY
584.09	1.0	N	584.22/ 584.33	0.13/ 0.24	Internal: DQEEV-NH_3/ EEVLI
599.27	0.8	N	599.23/ 599.30	0.04/ 0.03	Internal: PDQEE/ QEEVL
603.26	0.6	N	603.29	0.03	b_5: SFRPD
631.35	0.6	N	631.35	0.0	Internal: IPGYEV-28
641.36	0.2	Y: 100.06	100.09	0.03	Amino acid: R
653.22	0.2	N	653.39	0.17	Internal: EEVLIP-28
659.37	1.0	N	659.34	0.03	Internal: IPGYEV
670.36	0.2	N	670.30	0.06	Internal: PDQEEV-28
680.31	0.8	N	680.29	0.02	Internal: PDQEEV-H2O
681.31	1.3	N	681.27/ 681.38	0.04/ 0.07	Internal: PDQEEV-NH3/ EEVLIP
698.31	1.0	N	698.30	0.01	Internal: PDQEEV
709.35	1.9	N	709.32	0.03	y_6-H_2O: PGYEVY
727.35	1.9	N	727.33/ 727.34	0.02/ 0.01	y_6: PGYEVY/ Internal: RPDQEE-28
772.44	0.6	N	772.42	0.02	Internal: EVLIPGY/ VLIPGYE/ LIPGYEV
779.22	0.8	Y: 237.92	237.14	0.78	Internal: RP-NH_3
794.36	1.8	N	794.36	0.0	Internal: PDQEEVL-NH_3
811.40	1.5	N	811.38	0.02	Internal: PDQEEVL
840.43	8.5	N	840.41	0.02	y_7: IPGYEVY
871.85	0.9	N	871.92	0.07	B_{15}-H_2O^{+2}: SFRPDQEEVLIPGYE
914.30	0.8	Y: 373.0	373.14/ 373.20	0.14/ 0.20	Internal: DQE/ b_3-H_2O: SFR

924.46	1.2	N	924.47	0.01	Internal: PDQEEVLI/ DQEEVLIP
932.33	0.8	Y: 391.03	391.21	0.18	b_3: SFR
953.51	0.4	N	953.49/ 953.50	0.02/ 0.01	Internal: DQEEVLIPG-28/ y_8: LIPGYEVY
1011.41	0.2	N	1011.52	0.11	Internal: QEEVLIPGY-H_2O
1038.56	0.7	Y: 497.26	497.25	0.01	Internal: RPDQ
1144.33	0.65	Y: 603.03	603.29	0.26	b_5: SFRPD
1159.60	0.8	N	1159.61	0.01	Internal: RPDQEEVLIP-H_2O
1167.50	0.4	Y: 626.20	626.29/ 626.30	0.09/ 0.1	Internal: RPDQE/ FRPDQ-H_2O
1183.42	0.5	N	1183.57	0.15	b_{10}-H_2O: SFRPDQEEVL
1201.53	0.4	N	1201.59	0.06	b_{10}: SFRPDQEEVL
1244.65	0.4	Y: 703.35	703.35	0.0	a_6: SFRPDQ
1254.68	0.8	Y: 713.38	713.34	0.04	b_6-H_2O: SFRPDQ
1272.69	4.0	Y: 731.39	731.37	0.02	b_6: SFRPDQ
1314.72	0.3	N	1314.67	0.05	b_{11}: SFRPDQEEVLI
1377.55	0.6	Y: 836.26	836.37	0.12	Internal: RPDQEEV-H_2O
1393.67	0.6	N	1393.71	0.04	b_{12}-H2O: SFRPDQEEVLIP
1395.68	1.0	Y: 854.38	854.40	0.02	Internal: RPDQEEV
1450.65	0.4	N	1450.73	0.08	b_{13}-H2O: SFRPDQEEVLIPG
1480.74	1.0	Y: 939.44	939.49	0.05	Internal: RPDQEEVL-28
1490.75	0.6	Y: 949.45	949.47	0.02	Internal: RPDQEEVL-H_2O
1491.71	1.0	Y: 950.41	950.46	0.05	Internal: RPDQEEVL-NH_3

Figure 37. **Product Ion Table II.** The data generated from collisional activation decomposition MS^2 analysis of isolated peptide *m/z* 1291.51 by quadrapole time of flight (QTOF) mass spectrometry. Seventy-five percent of the ions that appeared in the spectra are identified and presented in the above table. The spectra were calculated to have a dynamic range of 5000; and the lowest percent base ion intensity used was 0.2%, which was 10 fold over baseline. The largest Δ *m/z* was 0.07 with an average of 0.02. Ions that were unique to these spectra compared with Fig 37 and did not match theoretical fragmentation data were subjected to subtraction of 541.3, the average mass of ADP-ribose. If the resulting *m/z*'s matched theoretical data, they were placed in the table. Modified peptide data are highlighted.

Figure 38
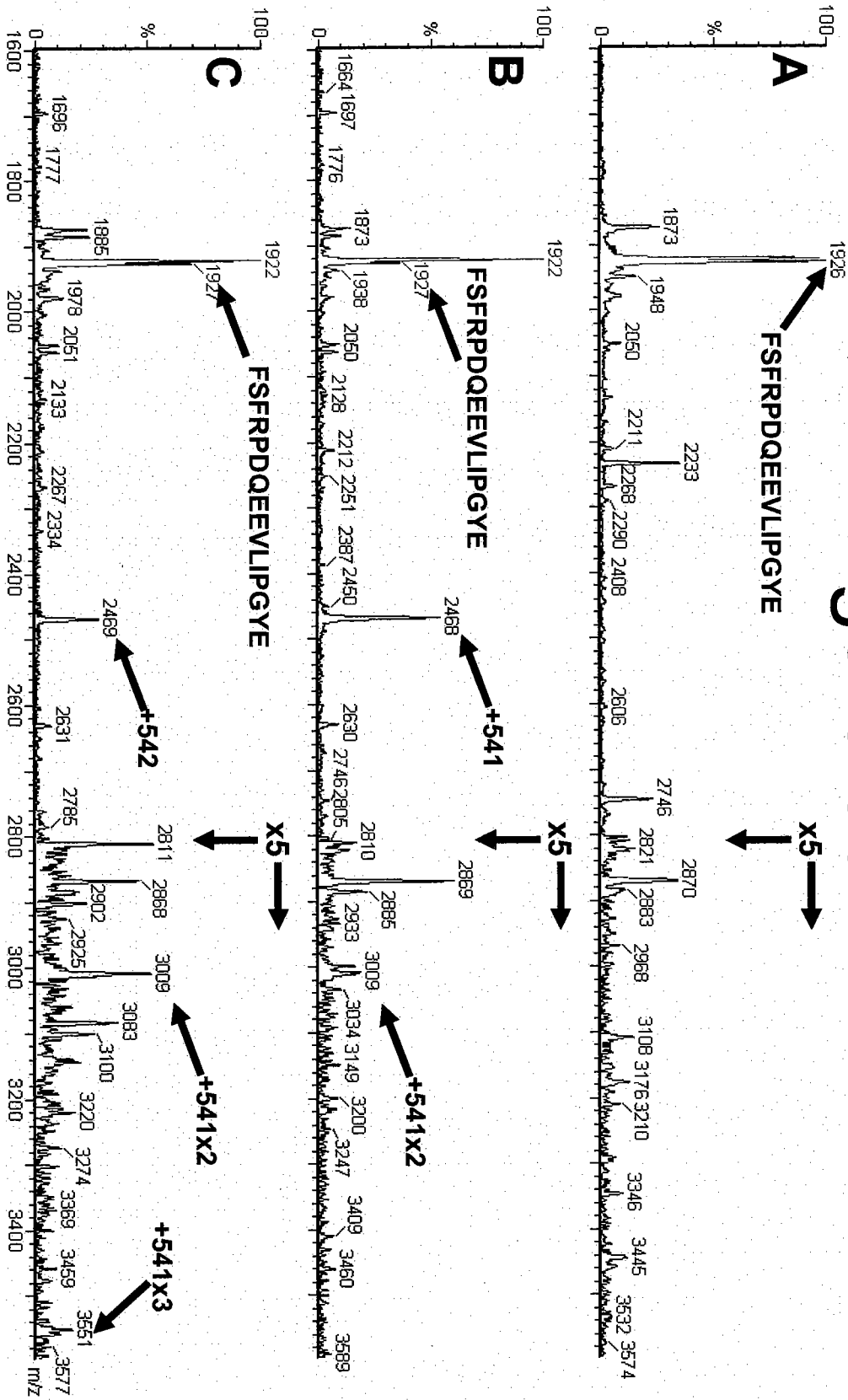
Figure 38. **MALDI-TOF mass spectra of a multiply modified peptide from a Glu-C digestion of ART2.** ART2 was incubated with a two different concentrations of NAD and subjected to digestion with the glu-c endopeptidase. **A.** Unmodified ART2 glu-c digest sample with major ions at *m/z* 1926. **B.** Modified ART2 glu-c digest sample with ions at *m/z* 1927, *m/z* 2468 (+541), and *m/z* 3009 (+2x541). C. Slightly more modified ART2 with ions at *m/z* 1927, *m/z* 2469 (+542), *m/z* 3009 (+2x541), and *m/z* 3551 (+3x 541). Regions from *m/z* 2800 to end of the spectra were magnified 5 fold. A theoretical digest of glu-c yields a *m/z* 1927 of sequence FSFRPDQEEVLIPGYE.

FSFRPDQEEVLIPGYE. The limited modification revealed a new ion at *m/z* 2468, which corresponds to the addition of ADP-ribose. The sample which was modified further with 20 mM NAD spectra show three ions, *m/z* 2469, *m/z* 3009, and *m/z* 3551 which correspond to the addition of one, two, and three ADP-riboses.

Chapter Conclusions

All ARTs share some common secondary and tertiary structures within the NAD-binding catalytic cleft. MonoARTs and PARPs share three regions of structural homology with each other. ADP-ribosyl cyclases share two regions of homology with the monoARTs and PARPs. SIR2 does not appear to share any obvious structural similarities with the rest of the ARTs, but it does appear to hold NAD in the same configuration as the other ARTs indicating a possible shared nucleophilic substitution mechanism for the cleaving of the N-glycosidic bond of NAD. A closer inspection of ART2 and PARP suggest structural similarities in the catalytic cleft that may indicate the potential for ART2 to contain an ADP-ribose acceptor site for polymer elongation; however, R185 appears to block this site by forming a salt bridge with E160 and D187 (Fig 19, 41).

A recombinant construct of ART2 was designed to generate relatively high yields of relatively pure ART2 enzyme. The purified recombinant protein had NAD glycohydrolase and auto-ADP-ribosyl transferase activity and was confirmed to be ART2 by sequence analysis. The kinetics of auto-ADP-ribosylation revealed multimeric heterogeneous forms of product. When isolated from the protein and purified, the product ran as polymers on a modified sequencing gel. When the polymer was digested with snake

venom phosphodiesterase, a poly(ADP-ribose) specific product, PR-AMP, was generated and the structure of PR-AMP was confirmed by ESI-MS. Another product, poly(phospho-ribose) appeared to be generated by the phosphodiesterase treatment.

A site of ADP-ribosylation was identified to be R185. This was confirmed by sequence data generated by CAD MS/MS of a mono-ADP-ribosylated ART2 peptide generated by chymotrypsin digestion. Further modification of the peptide revealed a second and third modification on the same peptide region. R185 is the same arginine that appears to sit over the potential ADP-ribose acceptor site by crystallography modeling.

Chapter 6 Discussion

Structural Insights

Structural alignment revealed novel insights into the similarities among the various ART family members. It is clear that mono-ADP-ribosyltransferases and poly(ADP-ribose) polymerases (PARPs) share three regions of structural similarity within the catalytic cleft. Region I has been expanded from previous reports to include a β-sheet composed of three hydrophobic β-strands. By primary sequence the new outer β-strand contains an amino acid string that is downstream of the Region III catalytic glutamate. The middle new β-strand is also a highly hydrophobic string that contains a string of amino acids found in between Region II and III by primary sequence. It appears that these two strands aid in the formation of a hydrophobic pocket for the adenine ring of NAD. The inner most β-strand is composed of the conserved histidine or arginine and is the original Region I previously reported (59). Interestingly the Aplysia ADP-ribosyl cyclase did not contain a Region I that was like the monoARTs and PARPs, but that would make sense in that ADP-ribosyl cyclases would not need a pocket to hold the adenine ring since it takes part in the formation of the cyclic bond. In theory, the way cyclases would hold adenine should be different.

Region II has the most highly conserved secondary structure among all the ARTs. Region II is composed of U-shaped, β-strand downward and α-helix upward, pocket that holds the nicotinamide mononucleotide in a unique conformation. The motif that can be

used to generalize Region II is Y/SXS-X$_{10}$-Y/F. It has been postulated that this conformation may provide the steric strain necessary to catalyze the breaking of the nicotinamide bond and the formation of a carbocation that would be stabilized by the oxygen of ribose forming a oxycarbonium ion (153). The conserved glutamate, by its positioning relative to the oxycarbonium ion, is hypothesized to stabilize the oxycarbonium ion for nucleophilic-like attack. This structural alignment of Region II allowed for the first reported primary sequence alignment of members from all three ART subgroups; monoARTs, PARPs, and ADP-ribosyl cyclases, providing further evidence of how closely they are related.

Region III of all ARTs contained the highly conserved glutamate that has been published in prior reports but was expanded to include the pre-β-strand coil that appears to be conserved as a structure throughout the monoARTs and PARPs. The significance of this coil is supported by data suggesting its amino acid composition might influence amino acid specificity by the ARTT motif (160). The T1 and T2 positions of the ARTT motif can be found in the pre-β-strand coil that has been included as part of Region III. Also, evidence that this coil is significant to the polymerization activity of PARP has recently been generated through crystal structure analysis of the ADP-ribose acceptor site which appears to be encompassed by the coil (154). Though the ADP-ribosyl cyclases contained a different secondary structure, α-helix, to Region III than PARP and the monoARTs, it still contained the catalytic glutamate along with some other similarities such as a T1 phenylalanine (T1 amino acids are often Y or F).

Though Sir2 contained no obvious similarity to the catalytic clefts of the other ARTs, it did appear to hold NAD in a similar conformation suggesting it might cleave NAD by a mechanism similar to the other ARTs. In fact, Sir2 has been reported to act via nucleophilic-like mechanisms generating α-anomers from βNAD (166). It is possible that Sir2 is distantly related to the ARTs.

A closer look at an alignment of ART2 and PARP revealed structural similarities and differences. Both ART2 and PARP contain Region I of the catalytic cleft, but PARP contains a histidine in the conserved position whereas ART2 contains an arginine. In Region II, they again share similarities of structure, but differ markedly by amino acid sequence; PARP contains the $Y-X_{10}-Y$ motif and ART2 contains the $SXS-X_{10}-F$ motif. In Region II, PARP contains K903, which has been demonstrated to be crucial to the polymer elongation reaction by previous mutational work (154), but ART2 contains a valine at position 155 which aligns with K903. However, in the structural model, Q188 (T2 of ARTT) appears to provide an amine to the same spatial location as K903 in PARP. Could this be a form of semi-conservative substitution? In Region III, both PARP and ART2 appear to have room to position ADP-ribose as an acceptor, but the ART2 acceptor site appears blocked by a salt bridge between R185, E160, and D187. Interestingly, R185 is the same arginine that was determined by mutational work to be important for multimerization of auto-ADP-ribosylation. The potential role that R185 may play will be discussed later.

Recombinant Protein Insights

The ART2 construct contained the soluble core of the ART2 molecule. Its specific activity after purification averages 2.5 μmol/min·mg which is 5 to 10 fold higher than previously reported for ART2 constructs (56;109;161;165). The average yield of purified ART2 was 2-3mg. The generation of a construct with this combination of high specific activity and relatively high protein yield was the rate-limiting step of this project and was crucial to characterizing the auto-PARP activity of ART2.

There were no detectable levels of background NAD glycohydrolase activity or ADP-ribosyltransferase as determined by the vector-minus-insert, *E. coli* controls. This supports the notion that essentially all the catalytic activity detected was generated by the ART2 construct. The construct had auto-ADP-ribosyltransferase activity as previous studies have demonstrated (56;109). More importantly the construct presented increasing levels of heterogeneous, multiple ADP-ribosylated forms when incubated with NAD for 5 minutes. The rate appeared to level off to a maximum of five to six band shifts by 10 mM NAD. Mass spectrometry confirmed the band shift molecular mass difference to be close to 541 Da, the molecular mass of covalently bonded ADP-ribose. This also confirms that there is ADP-ribosylation taking place and not an unusual artifact like NAD-binding complexes in the gels. When ART2 was incubated with 20 mM NAD for a time-course of up to ten hours, the band shifting occurred rapidly in the first hour and then tapered to a slow climb over the course of the next several hours. The band shift assays are all consistent with previous data published on PARP (145). PARP auto-ADP-ribosylates

in a multiple, heterogeneous band shift pattern by immunoblot and autoradiograhy, though to a much greater extent than ART2 with polymers >100. Also, PARP's auto-ADP-ribosylation does slow down further auto-ADP-ribosylation.

Polymer Data

To determine whether the multimers were indeed polymers, the hydroxylamine cleaved and DHBB purified ADP-ribose moieties from both auto-ADP-ribosylated ART and auto-ADP-ribosylated PARP were run and compared on a modified sequencing gel. Both samples produced a heterogeneous mixture of polymers on the gel. Though ART2 did not generate polymer lengths as large as those of PARP, it was evident that polymers up to twenty in length were being generated.

The gold standard method for determining if the ADP-ribose structure is poly-meric is to treat the polymer with snake venom phosphodiesterase. The phosphodi-esterase cleaves the polymer at the pyrophosphate bond generating a series of PR-AMP monomers that are isomers of ADP-ribose. If the multimers were only monomers at mul-tiple sites, the only reaction product from phosphodiesterase treatment would be 5'AMP. Upon digestion of the isolated ADP-ribosyl moieties of ART2 and PARP and product analysis by anion exchange HPLC, there appeared a phosphodiesterase-specific peak that did not appear in the controls. The peak eluted at a retention time close to the ADP stan-dard consistent with previously published reports of PR-AMP (146). To confirm that the product was PR-AMP, it was subjected to ESI-MS. The product peak consisted of one major ion, m/z 588.0. This was consistent with PR-AMP as it is an isomer of ADP-

ribose. To further confirm that the ion represented PR-AMP, the ion species and ADP-ribose, as a negative control, were subjected to CAD MS^n. The major product ion produced by MS^2 of m/z 558 was m/z 460.0, reflecting a neutral loss of 98 Da, indicative of a terminal phosphate. ADP-ribose cannot lose a phosphate via a single cleavage event without an unlikely molecular rearrangement taking place. The loss of a single phosphate is, however, consistent with the structure of PR-AMP. To further support the evidence, MS^3 of m/z 460.0 produced as the major product ion m/z 325.2 which reflects the neutral loss of adenine (135 Da). This suggested that the resulting fragment ion was composed of two riboses and a phosphate. MS4 of the m/z 325 ion confirmed this producing only phospho-ribose (m/z 211) and ionized phosphoric acid (m/z 97) as product ions.

Ratios of PR-AMP to AMP are indicative of the relative length and branching frequencies of PARP generated ADP-ribose polymer. PARP tends to have large ratios of around 20:1 PR-AMP to AMP because the average branchpoint frequency of the PARP-generated polymer averages about 20 ADP-riboses and the average chain length tends to be over 100. ART2 had a PR-AMP to AMP ratio of just over 1:1. This suggests two possibilities. First, that in addition to any polymer, there still may be a few mono-ADP-ribosylated sites and/or multiple short chains at multiple sites. The second possibility is that the polymer may have a different branching pattern than the polymer of PARP, making the ART2 polymer-structures fundamentally different, and possibly unique to ART2.

Phospho-ribose polymers and polymer modeling

A common product of the branching in the PARP polymers is the phosphodi-esterase-specific product PR_2-AMP, which occurs as a result of cleavage of branch points. HPLC analysis did not appear to have sufficient dynamic range to pick up the small amounts of PR_2-AMP generated in either the PARP or ART2 sample. To analyze for the presence of a low occurence product, the phosphodiesterase digested polymers of ART2 were subjected to MALDI-TOF analysis. The mass spectra revealed the presence of a hetergeneous group of ions with a consistent mass difference of 211 Da. These increments are consistent with a polymer whose structure consists of the monomer phospho-ribose. Figure 39 depicts the polymer chain structure typically thought to be generated by PARP. Cutting at the pyrophosphate bonds of this structure does not appear to produce ribose phosphate polymers. Figure 40 depicts a proposed structure of ART2 generated polymers. Because ART2 polymers produce PR-AMP as a product, there is some degree of longitudinal branching that occurs like PARP. However, because the ratio of PR-AMP to AMP is low, the size of the polymer is small, and there appear to be phospho-ribose polymers, an alternative branching may occur which has not been demonstrated to occur with PARPs. The branching appears to take place at the base ADP-ribose which is covalentaly linked to an amino acid. The C2 of the NMN ribose could act as an acceptor to branch out laterally from the base. This would allow for the formation of a "bush-like" structure rather than the classical "tree-like" pattern associated with PARPs. This structure would also explain the low ratios of PR-AMP to AMP as well as the

Figure 39
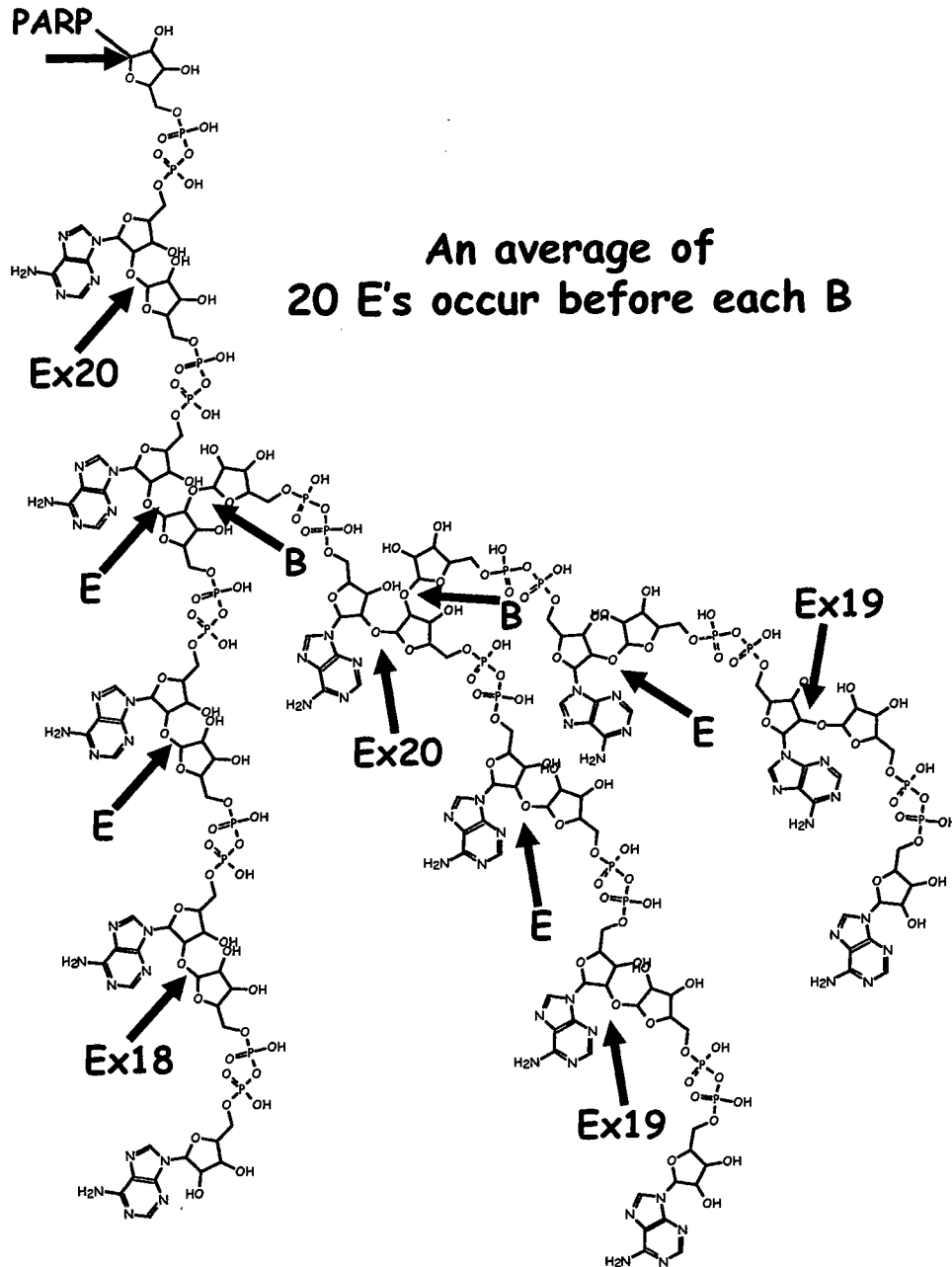
An average of
20 E's occur before each B

PARP

Ex20

E

B

Ex20

B

Ex19

E

E

E

Ex18

Ex19

Figure 39. **Tree-like Structural Model of PARP poly(ADP-ribose).** This figure illustrates the structure of PARP polymers. Elongation bonds (E) occur at an average of 20 before the formation of branch bonds (B).

Figure 40

E:B ratio averages 1.5:1
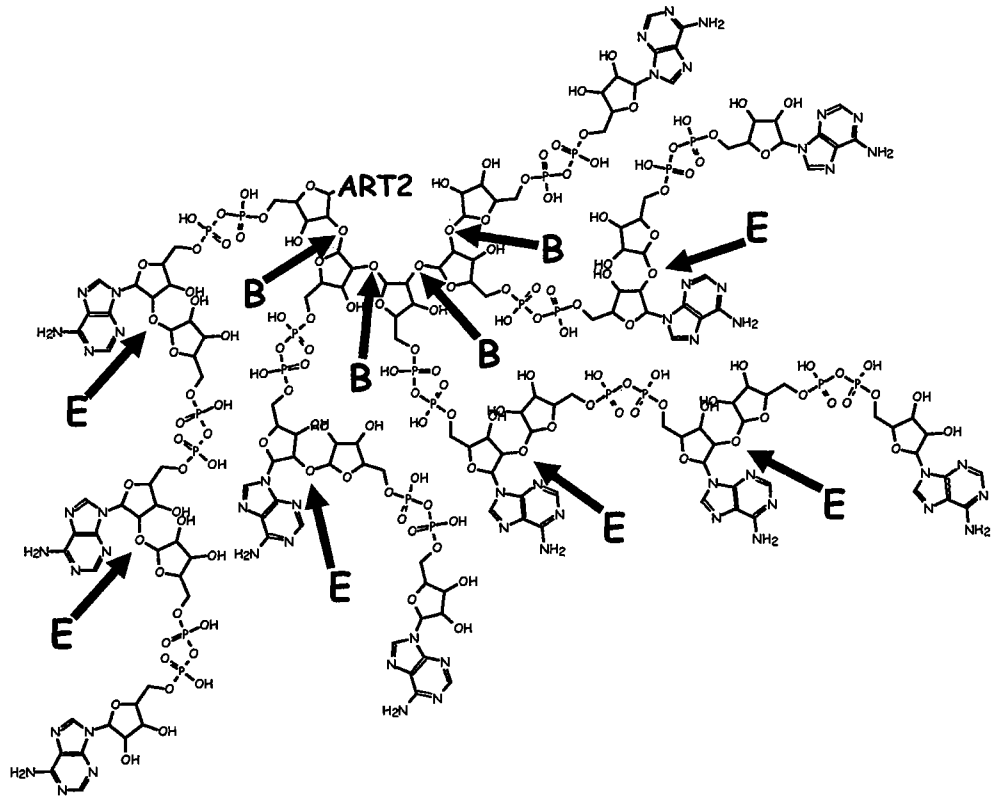
Figure 40. **Bush-like Structural Model of ART2 poly(ADP-ribose).** Unlike the "tree-like" PARP polymers, ART2 polymers appear to be forming a broad, "bush-like" structure. Phosphodiesterase digestion produces phospho-ribose polymers, indicating that branching bonds (B) occur at the base ribose that is attached to ART2. The presence of PR-AMP in phosphodiesterase-treated samples is consistent with a similar elongation bond (E) as PARP. The low ratios of PR:AMP to AMP suggest multiple short chains attached to the branch points.

presence of ribose phosphate polymers. One concern of the phospho-ribose polymers might be that they are monomers that are oligomerizing in the mass spectometer. Un-bonded clusters of monomers, however, would produce MALDI-TOF ion series with multiples of 230 Da not 211 Da, indicating phospho-ribose monomer cluster ions are unlikely.

R185

The sequencing data present both an answer to the location of the polymer as well as a role for R185 in the process of auto-poly(ADP-ribose) polymerase activity. Two modified peptides have been generated from digests with two different enzymes; chymo-typsin and glu-c. Their MH^+ ions were detected at m/z 2041 and 1926, respectively, and based on theoretical digests, they matched peptides whose sequences were SFRPDQEEVLIPGYEVY and FSFRPDQEEVLIPGYE. Both peptides were found to be modified with the addition of 541 Da (bonded ADP-ribose) specific to the modified frac-tions. The chymotrypsin peptide's sequence was confirmed by nanoscale HPLC-MS(MS^2) analysis on the mass spectrometer. Of the several modified peptide-fragment ions that were generated by CAD MS^2 analysis, there was one amino acid shared by all the fragment ions, R185. R185 is the same amino acid that sits over the catalytic site in a salt bridge with E160 and D187. R185 is also the same amino acid thought to be crucial to the multimeric band shift pattern by mutational analysis (56). The mass spectra of the two peptides that were identified to contain the modification also demonstrated evidence

of a attachment of a second ADP-ribose. The glu-c peptide contained evidence of a third ADP-ribose. It is likely that R185 is the site of polymerization. Though the data are highly suggestive at this point, CAD MS^2 analysis must be performed on the multiply modified peptides to absolutely confirm that R185 is the site of polymerization.

Interestingly, if R185 is the site of polymerization, crystallographic models suggest a mechanism for how modification at R185 can take place. Figure 41 illustrates a mechanism whereby R185 receives the intial ADP-ribosylation and opens up the catalytic site for auto-PARP activity to take place. Like PARP, the auto-PARP activity of ART2 can elongate in a longitudinal fashion, but unique to ART2 this dissertation proposes that in an intra-molecular ADP-ribosylation event, the base ADP-ribose attached to R185 can fold back into the catalytic site to branch out laterally forming the bush-like structure proposed in Figure 40.

Significance of this Dissertation

The major find of this work is the observation that ART2.2 has auto-poly(ADP-ribose)polymerase activity. This observation is the first demonstration of the potential for hybrids between monoARTs and PARPs. ART2 is the first identified PARP-like enzyme to exist outside the nucleus, although evidence of PARP activity outside the nucleus has recently emerged in the literature. The PARP knockout mice still generate ADP-ribose polymers (167) sparking the search and identification of other nuclear PARPs like PARP-2 and the Tankyrase, previously mentioned. Recent studies have identified poly-ADP-ribosylated proteins in the mitochondria of mice, though the enzyme responsible for this

Figure 41
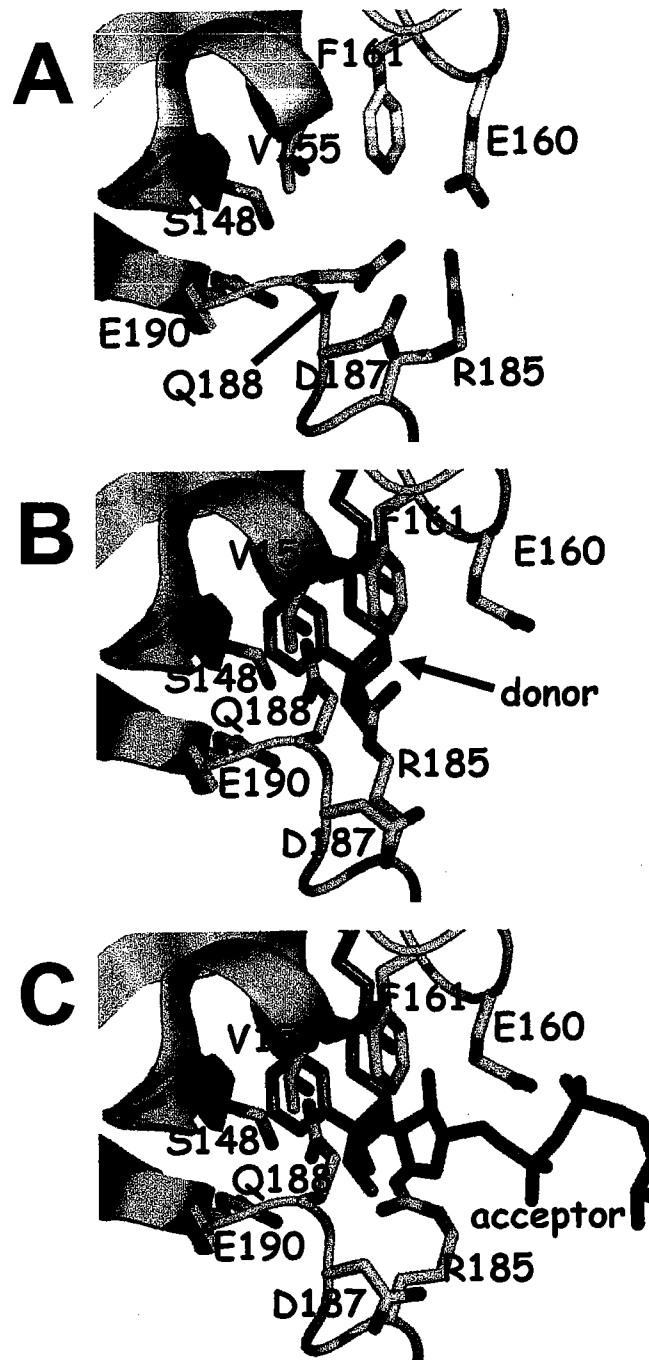
Figure 41. **R185 ADP-ribosylation Model.** **A.** A lateral view of the NAD-binding cleft of ART2. The "acceptor" site for polymer elongation is blocked by a salt bridge between R185, E160, and D187. **B.** NAD bound to the catalytic cleft may induce a conformational shift that breaks the salt bridge and allows R185 to enter the "acceptor" site for ADP-ribosylation. **C.** After ADP-ribosylation of R185, the bridge remains open for polymer elongation or branching to occur. In this illustration, ADP-ribosylated R185 returns to the "acceptor" site for the "bush-like" branching bond formation to occur. This "bush-like" branching is unique to ART2 polymers. NAD bound to the "donor" site is colored orange; NAD bound to the "acceptor" site is colored red.

activity has not beem identified (168). Because the polymer appears to differ structurally with the classical PARP polymer model, questions about alternative modes of signalling and altenative receptors that might recognize the differences in structure arise. A major question remains with respect to ART2; does it generate the polymers outside the cell or is it internalized to make use of intracellular NAD stores?

The finding that R185 serves as the acceptor arginine for at least one ADP-ribose and possibly the entire polymer is also significant. The model of R185 serving as a draw-bridge opening up ART2 to PARP-like activity upon its modification is a novel form of enzymatic regulation. Since R185 is the T1 position of Region III in the catalytic cleft, it further lends support to the notion that the ARTT motif is important in modulating sub-strate specificity. One *caveat* remains, however; though the peptides that contain R185 have been modified with multiple ADP-riboses, this does not rule out multiple sites of modification of the peptides. It could be that there is no polymer on R185, but merely a monomer. To confirm that R185 is the site of polymer chain, it must be identified through the previous sequencing methods to have a polymer on it. This will be part of the future directions of this work.

Future Directions

Polymer site

There are several future directions this work will take. The *caveat* regarding R185 has already been discussed above. Whether or not a single polymer takes place at that residue needs to be determined. Samples of ART2 should be modified to a higher

extent, and after digestion, the modified peptides can be subjected to the same QTOF

MS^2 analysis that revealed the sequence of the mono-ADP-ribosylated peptide. Now that

a specific modified peptide has been identified, it can be tracked in the mass spectra al-

lowing for any polymer identification.

Polymer Structure

Though the ratios of PR-AMP to AMP in the ART2 phosphodiesterase treated

samples are low, suggesting an alternative branching pattern for the ART2 polymer, an

alternative explanation for this is that there are multiple monomer or short oligomer sites

as part of the multimeric auto-ADP-ribosylation. The presence of phosphoribose poly-

mers supports the hypothesis that there is alternative branching, but there are caveats to

the data as well. At this point, it has been difficult to analyze the nature of the phosphori-

bose polymers by fragmentation work, such as CAD MS^n, which would lend structural

support to their identification. Though other monomer or short oligomer sites may not be

ruled out, the best way to characterize the structure of the ADP-ribose polymer is to iso-

late a homogeneous population and analyze the sample by NMR (nuclear magnetic reso-

nance). An alternative way to characterize the polymer structure would be to map the hy-

droxyl groups. As demonstrated by figures 39 and 40, there would be a different pattern

of ribose cis-hydroxyl groups depending on whether the polymer was a "tree-like" or

"bush-like" structure.

Though the mass spectrometry data concerning the snake venom posphodiesterase

products confirms the presence of PR-AMP, follow-up studies that confirm the structure

of the bonds between the riboses should be conducted to confirm their α anomeric link-ages. This can be done by using the present ART2 system to generate larger amounts of PR-AMP for NMR analysis. A thorough desalting would be necessary for NMR analysis and could be carried out by ion exchange with a volatile buffering system.

NAD analogues

The location of R185 in relation to the NAD-binding site is highly suggestive of mechanism for the "bush-like" polymer formation; figure 41 hypothesizes that R185 could move into the catalytic site to accept the first ADP-ribose. This would open up the catalytic site to further PARP-like activity. The polymer could grow in the longitudinal pattern that produces the classical "tree-like" configuration of PARP polymers. The ki-netics of traditional PARP-longitudinal polymer growth suggest a PARP concentration-dependent inter-molecular ADP-ribosylation; one PARP molecule extends the chain on another PARP molecule. Because of the generation of PR-AMP, ART2 may act in a similar fashion to PARP. However, the suggestion of a "bush-like" configuration has in-dicated there may be branching at the ADP-ribosylarginine base. Figure 41 suggests that an intra-molecular (ART2 concentration-independent) mechanism may be taking place where the ADP-ribosylated arginine could return to the site with the nicotinamide mono-nucleotide ribose serving as an acceptor in a lateral-branching pattern. To better get at the mechanisms of branching and the kinetics of these reactions, experiments with NAD ana-logues with riboses that lack the 2C-hydroxyl moieties would be ideal. Methylated, de-oxy-, or flourinated riboses are just three examples. In these situations, if the analogue

was a good substrate for auto-ADP-ribosylation, the polymer could be shunted into one direction or another. This would allow researchers to dissect the components of longitudinal elongation versus lateral branching.

Mutants

To better understand the role of R185 and auto-poly(ADP-ribose) polymerase activity, several mutants could be generated and analyzed for auto-ADP-ribosylation, mono-ADP-ribosylation, and poly(ADP-ribose) polymerization. A mutation of R185 to lysine has already been generated and exhibited no auto-poly(ADP-ribose) polymerase activity (56). Another mutant from the same study was R185W, which did exhibit a low level of auto-poly(ADP-ribose) polymerase activity. Using the system generated by this dissertation, the polymer site could be identified. Based on the present study, the data are suggestive that the modification is taking place on the tryptophan residue. This would reveal the ADP-ribosylation of a novel amino acid side chain. Because there is some similarity in the structure of adenine and the side chain of tryptophan, the ADP-ribosylation mechanism may be similar to the nucleophilic mechanism of the cyclic bond that is the product of the ADP-ribosyl cyclase activity. This would provide further evidence of the relationship between monoARTs and cyclases.

According to the ART2 crystallography model, R185 appears held over the catalytic site by hydrogen bonds with E160 and D187 (Figs 19 and 41). To determine the significance of E160 and D187 to auto-poly(ADP-ribose) polymerase activity, alanine

mutants of each and both should be generated. In addition to assaying for auto-PARP activity, kinetic studies of these mutants may provide interesting clues to their relevance.

In order to determine if poly(ADP-ribose) polymerase and arginine-specific mono-ADP-ribosyltransferase activity could coexist, a mutant like Q188E, which has already been shown to introduce arginine-specific mono-ADP-ribosyltransferase activity to ART2 (161) should be generated. To do this, however, an alanine null mutant of Q188 should also be generated as a control for the significance of Q188 to the PARP activity. Because Q188 provides an amide to the same spatial region as the PARP amino acid K903, which is crucial to polymerization activity, any mutant of Q188 may exhibit a loss of auto-PARP acitivity. It is important to characterize whether introduction of monoART activity via the Q188E mutant is responsible for any loss of PARP activity or whether it is merely the loss of the glutamine.

Biology

ART2 as a PARP from Human Perspective

One concern of significance of the work with ART2 is the level of relevance that extracellular PARP activity may have to humans and the application to human diseases like diabetes. As mentioned earlier, ART2 is a pseudogene in humans and there is no indication that it is expressed. However, because there are at least four other known monoARTs in the human, there is the opportunity for redundancies to exist. ART1 exhibits monoART activity and ART5 exhibits NAD glycohydrolase activity with a latent level of monoART activity. Little has been studied about ARTs 3 and 4. It is very possi-

ble that any one of these monoARTs could be a sufficient substitute for ART2 in the human, providing similar reaction products with which to generate immune signals. ART 4, for example, has a lysine in the position of Q188 or ART2 and a serine in place of the R185 of ART2. A lysine could serve as a semi-conservative substitution for Q188. It is also possible that the hydroxyl group of the serine serves as a nucleophile replacement for the guanidino group of arginine, especially since hydroxyl groups on the polymer riboses serve the same function. The R185W mutant mentioned above also provides support for the argument that all that is needed is the right nucleophile in the R185 position.

Diabetes

How the significance of this dissertation applies to diabetes is a difficult question to answer at this time. There are, however, some indications that it could be answered in the near future. If the ART2 ADP-ribose polymer is viewed as a novel product generated on the surface of T lymphocytes, then there are likely to be receptors for this product. In fact, it has already been established that myeloid leukemia cells can be induced to differentiate into macrophages and granulocytes with PARP poly(ADP-ribose) (169). Chick cartilage cells and mouse erythroid leukemia cells have also been induced to differentiate with poly(ADP-ribose) (170;171). This suggests that there are receptors for poly(ADP-ribose) that exist on the surface of cells, and ART2 poly(ADP-ribose) could be used to search for such receptors.

In the differentiation studies, poly(ADP-ribose) shared its biological effects with molecules like lipopolysaccharide (LPS) and polyI:C, which are known to be Toll-like

receptor (TLRs) ligands (172). Mammalian TLRs are a phylogenetically conserved family of transmembrane proteins that recognize a number of microbial ligands incuding: LPS, peptidoglycan, lipopeptides, double-stranded RNA, bacterial flagellin, and bacterial DNA (172-176). It is possible that TLRs may serve as a receptor for poly(ADP-ribose), and in fact, purinergic analogues were recently demonstrated to have immunostimulatory activity through TLR7 (172).

Figure 42 provides a speculative model that provides a link between ART2 and diabetes. In situations of inflammation or cell lysis and in situations where fibroblasts may regulate the immune system, NAD can be released into the extracellular matrix. This NAD is available as a substrate for ART2 auto-PARP activity. The polymer chains can then signal through purinergic receptors or receptors like TLRs, setting off signaling cascades that can influence the immune response. In a situation where the immune stimulus is large and there is a paucity of ART2, the signalling cascades set off by ADP-ribose polymer may be nonexistent or not strong enough to override the immune stimulation. In those cases, activation of effector cells can lead to the autoimmune state that culminates in diabetes expression. A model like figure 42 provides a working hypothesis from which can be designed a number of experimental approaches that will help provide an answer to the role of ART2 in the immune system.

Chapter Conclusions

ART2 shares structural homology with a number of ARTs including PARP. A closer characterization of the multimeric auto-ADP-ribosyltransferase activity of ART2

Figure 42

A

tissue

tissue

lymphocytes   lymphocytes

Inflammation
Cell Lysis

Resolving
fibroblasts
with open Cx43
channels

B

ART2

$\uparrow$ [NAD]

Poly(ADP-ribose

ART2+
lymphocytes

C

ARTZ

receptor
recognition

Immune Signalling
And
Modulation
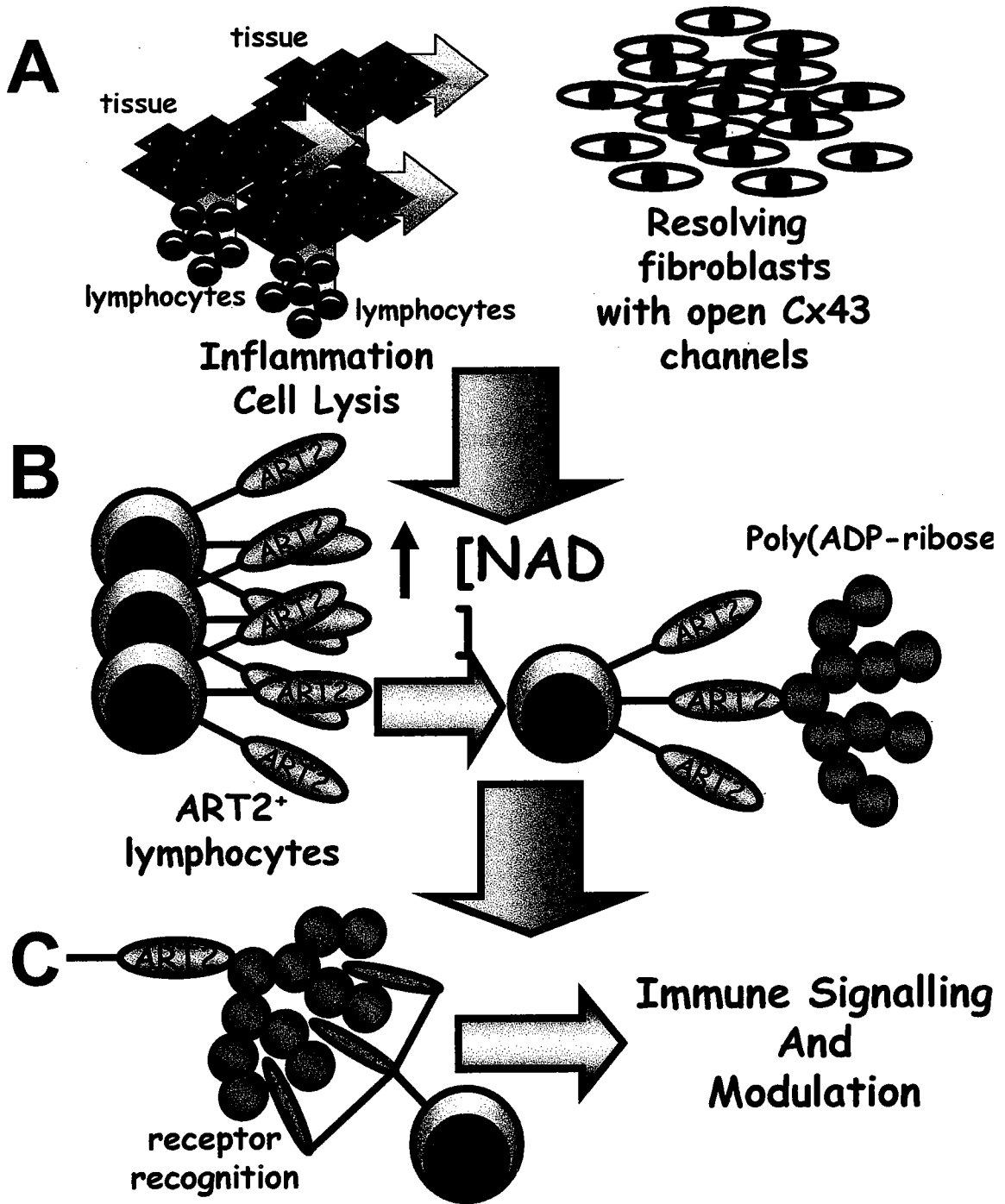
Figure 42. **Proposed Biological Impact of ART2 auto-PARP activity.** **A.** In situations of inflammation and cell lysis or when Connexin 43 hemichannels of fibroblasts are activated, local extracellular concentrations of NAD can increase. **B.** ART2$^+$ lymphocytes make use of the NAD to polymerize ADP-ribose. **C.** ART2 poly(ADP-ribose) is recognized by immune cell receptors (*i.e.* purinergic receptors or possibly TLRs). This recognition causes signalling cascades that may modulate the immune system. In the case of diabetes in the BB rat, genetic and environmental influences may lead to a situation where ART2$^+$ lymphocyte populations are reduced or depleted. The lack of ART2 would lead to a loss of poly(ADP-ribose) and its immunomodulatory signal.

demonstrated that ART2 had auto-poly(ADP-ribose) polymerase activity. The structure of the polymer, however, appears to be different from the structure of PARP polymers; bush-like and not tree-like. A site of auto-ADP-ribosylation is R185, a site previously determined to be important to the levels of auto-ADP-ribosylation. This site also appears to be the site of polymer elongation as multiple ADP-ribose moieties have been found on fragment peptides containing R185. ART2 is the first hybrid between monoARTs and PARPs and is the first extracellular protein discovered to have PARP-like activity.

The data, however, are a work in process and a number of follow-up studies are taking place: sequencing of polymer containing fragment peptides to confirm R185 is the site of polymer elongation and structural mapping of the ribose hydroxyl groups to confirm the bush-like nature of the polymer. Future directions include work with mutants and analogues of NAD to further characterize the mechanism of polymer elongation on ART2. Previous biological data provide indications that there may be receptors like TLRs that may respond to the novel ART2 ADP-ribose polymer product. These data provide insights on how to test the relevance of ADP-ribose polymers to cellular systems, and may ultimately provide the clues that link ART2 to diabetes. In any event, the data provide a rationale to move on two fronts; first, a continued characterization of the polymer phenomenon by biochemical studies, and second, a screening for biological effects and receptors that may signal in response to this novel extracellular product.

Reference List

1. Macfarlane,I.A., Bliss,M., Jackson,J.G.L., and Williams,G. 1997. The history of diabetes mellitus. In Textbook of Diabetes. J.C.Pickup and Willams,G., editors. Blackwell Science, Inc., Cambridge. 1.1-1.21.

2. Veith,I. 1971. Four Thousand Years of Diabetes. *Modern Medicine*118-125.

3. Bryan,C.P. 1990. The Papyrus Ebers. ECA Associates, New York. 1-170 pp.

4. Bliss,M. 1983. The Discovery of Insulin. University of Chicago Press.

5. Crawford,J.M. and Cotran,R.S. 1994. The Pancreas. In Robbins Pathologic Basis of Disease. R.S.Cotran, Kumar,V., Robbins,S.L., and Schoen,F.J., editors. Saunders, Philadelphia. 897-925.

6. Atkinson,M.A. and Maclaren,N.K. 1994. The pathogenesis of insulin-dependent diabetes mellitus. *N.Engl.J.Med.* 331:1428-1436.

7. Barnett,A.H., Eff,C., Leslie,R.D., and Pyke,D.A. 1981. Diabetes in identical twins. A study of 200 pairs. *Diabetologia* 20:87-93.

8. Redondo,M.J., Rewers,M., Yu,L., Garg,S., Pilcher,C.C., Elliott,R.B., and Eisenbarth,G.S. 1999. Genetic determination of islet cell auto-immunity in monozygotic twin, dizygotic twin, and non-twin siblings of patients with type 1 diabetes: prospective twin study. *BMJ* 318:698-702.

9. Kaprio,J., Tuomilehto,J., Koskenvuo,M., Romanov,K., Reunanen,A., Eriksson,J., Stengard,J., and Kesaniemi,Y.A. 1992. Concordance for type 1 (insulin-dependent) and type 2 (non-insulin-dependent) diabetes mellitus in a population-based cohort of twins in Finland. *Diabetologia* 35:1060-1067.

10. Davies,J.L., Kawaguchi,Y., Bennett,S.T., Copeman,J.B., Cordell,H.J., Pritchard,L.E., Reed,P.W., Gough,S.C., Jenkins,S.C., Palmer,S.M. *et al.* 1994. A genome-wide search for human type 1 diabetes susceptibility genes. *Nature* 371:130-136.

11. Dorman,J.S., LaPorte,R.E., Stone,R.A., and Trucco,M. 1990. Worldwide differences in the incidence of type I diabetes are associated with amino acid variation at position 57 of the HLA-DQ beta chain. *Proc.Natl.Acad.Sci.U.S.A* 87:7370-7374.

12. Tisch,R. and McDevitt,H. 1996. Insulin-dependent diabetes mellitus. *Cell* 85:291-297.

13. Tait,B.D. and Harrison,L.C. 1991. Overview: the major histocompatibility complex and insulin dependent diabetes mellitus. *Baillieres Clin.Endocrinol.Metab* 5:211-228.

14. Khalil,I., d'Auriol,L., Gobet,M., Morin,L., Lepage,V., Deschamps,I., Park,M.S., Degos,L., Galibert,F., and Hors,J. 1990. A combination of HLA-DQ beta Asp57-negative and HLA DQ alpha Arg52 confers susceptibility to insulin-dependent diabetes mellitus. *J.Clin.Invest* 85:1315-1319.

15. Kennedy,G.C., German,M.S., and Rutter,W.J. 1995. The minisatellite in the diabetes susceptibility locus IDDM2 regulates insulin transcription. *Nat.Genet.* 9:293-298.

16. Morahan,G., Huang,D., Ymer,S.I., Cancilla,M.R., Stephen,K., Dabadghao,P., Werther,G., Tait,B.D., Harrison,L.C., and Colman,P.G. 2001. Linkage disequilibrium of a type 1 diabetes susceptibility locus with a regulatory IL12B allele. *Nat.Genet.* 27:218-221.

17. Jun,H.S. and Yoon,J.W. 2003. A new look at viruses in type 1 diabetes. *Diabetes Metab Res.Rev.* 19:8-31.

18. Kostraba,J.N., Cruickshanks,K.J., Lawler-Heavner,J., Jobim,L.F., Rewers,M.J., Gay,E.C., Chase,H.P., Klingensmith,G., and Hamman,R.F. 1993. Early exposure to cow's milk and solid foods in infancy, genetic predisposition, and risk of IDDM. *di* 42:288-295.

19. Karjalainen,J., Martin,J.M., Knip,M., Ilonen,J., Robinson,B.H., Savilahti,E., Akerblom,H.K., and Dosch,H.M. 1992. A bovine albumin peptide as a possible trigger of insulin-dependent diabetes mellitus. *N.Engl.J.Med.* 327:302-307.

20. Kaufman,D.L., Erlander,M.G., Clare-Salzler,M., Atkinson,M.A., Maclaren,N.K., and Tobin,A.J. 1992. Autoimmunity to two forms of glutamate decarboxylase in insulin-dependent diabetes mellitus. *J.Clin.Invest* 89:283-292.

21. Atkinson,M.A., Bowman,M.A., Campbell,L., Darrow,B.L., Kaufman,D.L., and Maclaren,N.K. 1994. Cellular immunity to a determinant common to glutamate decarboxylase and coxsackie virus in insulin-dependent diabetes. *J.Clin.Invest* 94:2125-2129.

22. Baker,J.R., Jr. 1997. Autoimmune endocrine disease. *JAMA* 278:1931-1937.

23. Awata,T., Guberski,D.L., and Like,A.A. 1995. Genetics of the BB rat: association of autoimmune disorders (diabetes, insulitis, and thyroiditis) with lymphopenia and major histocompatibility complex class II. *Endocrinology* 136:5731-5735.

24. Herold,K.C. and Rubenstein,A.H. 1988. Immunosuppression for insulin-dependent diabetes. *N.Engl.J.Med.* 318:701-703.

25. Herold,K.C., Hagopian,W., Auger,J.A., Poumian-Ruiz,E., Taylor,L., Donaldson,D., Gitelman,S.E., Harlan,D.M., Xu,D.L., Zivin,R.A. *et al.* 2002. Anti-CD3 monoclonal antibody in new-onset type 1 diabetes mellitus. *N.Engl.J.Med.* 346:1692-1698.

26. Boitard,C. 1992. The differentiation of the immune system towards anti-islet autoimmunity. Clinical prospects. *Diabetologia* 35:1101-1112.

27. Yoon,J.W., Yoon,C.S., Lim,H.W., Huang,Q.Q., Kang,Y., Pyun,K.H., Hirasawa,K., Sherwin,R.S., and Jun,H.S. 1999. Control of autoimmune diabetes in NOD mice by GAD expression or suppression in beta cells. *Science* 284:1183-1187.

28. Baekkeskov,S., Aanstoot,H.J., Christgau,S., Reetz,A., Solimena,M., Cascalho,M., Folli,F., Richter-Olesen,H., De Camilli,P., and Camilli,P.D. 1990. Identification of the 64K autoantigen in insulin-dependent diabetes as the GABA-synthesizing enzyme glutamic acid decarboxylase. *Nature* 347:151-156.

29. Kaufman,D.L., Clare-Salzler,M., Tian,J., Forsthuber,T., Ting,G.S., Robinson,P., Atkinson,M.A., Sercarz,E.E., Tobin,A.J., and Leh-mann,P.V. 1993. Spontaneous loss of T-cell tolerance to glutamic acid decarboxylase in murine insulin-dependent diabetes. *Nature* 366:69-72.

30. Wong,F.S., Karttunen,J., Dumont,C., Wen,L., Visintin,I., Pilip,I.M., Shastri,N., Pamer,E.G., and Janeway,C.A., Jr. 1999. Identification of an MHC class I-restricted autoantigen in type 1 diabetes by screening an organ-specific cDNA library. *Nat.Med.* 5:1026-1031.

31. Alleva,D.G., Crowe,P.D., Jin,L., Kwok,W.W., Ling,N., Gottschalk,M., Conlon,P.J., Gottlieb,P.A., Putnam,A.L., and Gaur,A. 2001. A disease-associated cellular immune response in type 1 diabetics to an immunodominant epitope of insulin. *J.Clin.Invest* 107:173-180.

32. Muir,A., Peck,A., Clare-Salzler,M., Song,Y.H., Cornelius,J., Luchetta,R., Krischer,J., and Maclaren,N. 1995. Insulin immunization of nonobese diabetic mice induces a protective insulitis characterized by diminished intraislet interferon-gamma transcription. *J.Clin.Invest* 95:628-634.

33. Vlahos,W.D., Seemayer,T.A., and Yale,J.F. 1991. Diabetes prevention in BB rats by inhibition of endogenous insulin secretion. *Metabolism* 40:825-829.

34. Izumi,T., Yokota-Hashimoto,H., Zhao,S., Wang,J., Halban,P.A., and Takeuchi,T. 2003. Dominant negative pathogenesis by mutant proinsulin in the Akita diabetic mouse. *di* 52:409-416.

35. Silverstein,J., Maclaren,N., Riley,W., Spillar,R., Radjenovic,D., and Johnson,S. 1988. Immunosuppression with azathioprine and prednisone in recent-onset insulin-dependent diabetes mellitus. *N.Engl.J.Med.* 319:599-604.

36. Bougneres,P.F., Landais,P., Boisson,C., Carel,J.C., Frament,N., Boitard,C., Chaussain,J.L., and Bach,J.F. 1990. Limited duration of remission of insulin dependency in children with recent overt type I diabetes treated with low-dose cyclosporin. *di* 39:1264-1272.

37. Yamada,K., Nonaka,K., Hanafusa,T., Miyazaki,A., Toyoshima,H., and Tarui,S. 1982. Preventive and therapeutic effects of large-dose nicotinamide injections on diabetes associated with insulitis. An observation in nonobese diabetic (NOD) mice. *di* 31:749-753.

38. LeDoux,S.P., Hall,C.R., Forbes,P.M., Patton,N.J., and Wilson,G.L. 1988. Mechanisms of nicotinamide and thymidine protection from alloxan and streptozocin toxicity. *di* 37:1015-1019.

39. Okamoto,H. and Takasawa,S. 2002. Recent advances in the Okamoto model: the CD38-cyclic ADP-ribose signal system and the regenerating gene protein (Reg)-Reg receptor system in beta-cells. *di* 51 Suppl 3:S462-S473.

40. Pozzilli,P., Browne,P.D., and Kolb,H. 1996. Meta-analysis of nicotinamide treatment in patients with recent-onset IDDM. The Nicotinamide Trialists. *Diabetes Care* 19:1357-1363.

41. Greiner,D.L., Rossini,A.A., and Mordes,J.P. 2001. Translating data from animal models into methods for preventing human autoimmune diabetes mellitus: caveat emptor and primum non nocere. *Clin.Immunol.* 100:134-143.

42. Komeda,K., Noda,M., Terao,K., Kuzuya,N., Kanazawa,M., and Kanazawa,Y. 1998. Establishment of two substrains, diabetes-prone and non-diabetic, from Long-Evans Tokushima Lean (LETL) rats. *Endocr.J.* 45:737-744.

43. Yokoi,N., Kanazawa,M., Kitada,K., Tanaka,A., Kanazawa,Y., Suda,S., Ito,H., Serikawa,T., and Komeda,K. 1997. A non-MHC locus essential for autoimmune type I diabetes in the Komeda diabetes-prone rat. *J.Clin.Invest.* 100:2015-2021.

44. Yokoi,N., Komeda,K., Wang,H.Y., Yano,H., Kitada,K., Saitoh,Y., Seino,Y., Yasuda,K., Serikawa,T., and Seino,S. 2002. Cblb is a major

susceptibility gene for rat type 1 diabetes mellitus. *Nat.Genet.* 31:391-394.

45. Chiang,Y.J., Kole,H.K., Brown,K., Naramura,M., Fukuhara,S., Hu,R.J., Jang,I.K., Gutkind,J.S., Shevach,E., and Gu,H. 2000. Cbl-b regulates the CD28 dependence of T-cell activation. *Nature* 403:216-220.

46. Lenzen,S., Tiedge,M., Elsner,M., Lortz,S., Weiss,H., Jorns,A., Kloppel,G., Wedekind,D., Prokop,C.M., and Hedrich,H.J. 2001. The LEW.1AR1/Ztm-iddm rat: a new model of spontaneous insulin-dependent diabetes mellitus. *Diabetologia* 44:1189-1196.

47. Nakhooda,A.F., Like,A.A., Chappel,C.I., Murray,F.T., and Marliss,E.B. 1977. The spontaneously diabetic Wistar rat. Metabolic and morphologic studies. *di* 26:100-112.

48. Mordes,J.P., Bortell,R., Groen,H., Guberski,D.L., Rossini,A.A., and Greiner,D.L. 2001. Autoimmune diabetes mellitus in the BB rat. In Animal models of diabetes: A primer. A.A.F.Sima and Shafrir,E., editors. Harwood Academic Publishers, Amsterdam. 1-41.

49. Mordes,J., Serreze,D.V., Greiner,D., and Rossini,A.A. 2002. Animal Models of Autoimmune Diabetes Mellitus. In Diabetes Mellitus, A Fundamental and Clinical Text. D.LeRoith, Taylor,S.I., and Olefsky,J.M., editors. Lippincott.

50. Sobel,D.O., Ahvazi,B., Jun,H.S., Chung,Y.H., and Yoon,J.W. 2000. Cyclophosphamide inhibits the development of diabetes in the diabetes-prone BB rat. *Diabetologia* 43:986-994.

51. Hornum,L., Rømer,J., and Markholst,H. 2002. The diabetes-prone BB rat carries a frameshift mutation in *Ian4*, a positional candidate of *iddm1*. *di* 51:1972-1979.

52. Pandarpurkar,M., Wilson-Fritch,L., Corvera,S., Markholst,H., Hornum,L., Greiner,D., Mordes,J., Rossini,A., and Bortell,R. 2003. Ian4 is required for mitochondrial integrity and T cell survival. *Proc.Natl.Acad.Sci.U.S.A* 100:10382-10387.

53. Daheron,L., Zenz,T., Siracusa,L.D., Brenner,C., and Calabretta,B. 2001. Molecular cloning of Ian4: a BCR/ABL-induced gene that encodes an outer membrane mitochondrial protein with GTP-binding activity. *Nucleic Acids Res.* 29:1308-1316.

54. Mordes,J.P., Leif,J., Novak,S., DeScipio,C., Greiner,D.L., and Blankenhorn,E.P. 2002. The iddm4 locus segregates with diabetes susceptibility in congenic WF.iddm4 rats. *di* 51:3254-3262.

55. Bortell,R., Kanaitsuka,T., Stevens,L.A., Moss,J., Mordes,J.P., Rossini,A.A., and Greiner,D.L. 1999. The RT6 (Art2) family of ADP-ribosyltransferases in rat and mouse. *Mol.Cell.Biochem.* 193:61-68.

56. Stevens,L.A., Bourgeois,C., Bortell,R., and Moss,J. 2003. Regulatory Role of Arginine 204 in the Catalytic Activity of Rat Alloantigens ART2a and ART2b. *J.Biol.Chem.* 278:19591-19596.

57. Moss,J., Stevens,L.A., Cavanaugh,E., Okazaki,I.J., Bortell,R., Kanaitsuka,T., Mordes,J.P., Greiner,D.L., and Rossini,A.A. 1997. Characterization of mouse Rt6.1 NAD:arginine ADP-ribosyltransferase. *Journal of Biological Chemistry* 272:4342-4346.

58. Haag,F., Koch-Nolte,F., Kuhl,M., Lorenzen,S., and Thiele,H.G. 1994. Premature stop codons inactivate the RT6 genes of the human and chimpanzee species. *J.Mol.Biol.* 243:537-546.

59. Okazaki,I.J. and Moss,J. 1999. Characterization of glycosylphosphatidylinositiol-anchored, secreted, and intracellular vertebrate mono-ADP-ribosyltransferases. *Annu.Rev.Nutr.* 19:485-509.

60. Okazaki,I.J., Kim,H.J., and Moss,J. 1996. Cloning and characterization of a novel membrane-associated lymphocyte NAD:arginine ADP-ribosyltransferase. *J.Biol.Chem.* 271:22052-22057.

61. Bortell,R., Moss,J., McKenna,R.C., Rigby,M.R., Niedzwiecki,D., Stevens,L.A., Patton,W.A., Mordes,J.P., Greiner,D.L., and Rossini,A.A. 2001. Nicotinamide adenine dinucleotide (NAD) and its metabolites inhibit T lymphocyte proliferation: role of cell surface NAD glycohydrolase and pyrophosphatase activities. *J.Immunol.* 167:2049-2059.

62. Prochazka,M., Gaskins,H.R., Leiter,E.H., Koch-Nolte,F., Haag,F., and Thiele,H.G. 1991. Chromosomal localization, DNA polymorphism, and expression of Rt-6, the mouse homologue of rat T-lymphocyte differentiation marker RT6. *Immunogenetics* 33:152-156.

63. Koch-Nolte,F., Klein,J., Hollmann,C., Kuhl,M., Haag,F., Gaskins,H.R., Leiter,E., and Thiele,H.G. 1995. Defects in the structure and expression of the genes for the T cell marker Rt6 in NZW and (NZB x NZW)F1 mice. *Int.Immunol.* 7:883-890.

64. Wang,J., Nemoto,E., Kots,A.Y., Kaslow,H.R., and Dennert,G. 1994. Regulation of cytotoxic T cells by ecto-nicotinamide adenine dinucleotide (NAD) correlates with cell surface GPI-anchored/arginine ADP-ribosyltransferase. *J.Immunol.* 153:4048-4058.

65. Tauxe,R.V. and Blake,P.A. 1992. Epidemic cholera in Latin America. *JAMA* 267:1388-1390.

66. Swerdlow,D.L. and Ries,A.A. 1992. Cholera in the Americas. Guidelines for the clinician. *JAMA* 267:1495-1499.

67. Ramamurthy,T., Garg,S., Sharma,R., Bhattacharya,S.K., Nair,G.B., Shimada,T., Takeda,T., Karasawa,T., Kurazano,H., Pal,A. *et al.* 1993. Emergence of novel strain of Vibrio cholerae with epidemic potential in southern and eastern India. *Lancet* 341:703-704.

68. Swerdlow,D.L. and Ries,A.A. 1993. Vibrio cholerae non-O1--the eighth pandemic? *Lancet* 342:382-383.

69. Swerdlow,D.L., Mintz,E.D., Rodriguez,M., Tejada,E., Ocampo,C., Espejo,L., Greene,K.D., Saldana,W., Seminario,L., Tauxe,R.V. *et al.* 1992. Waterborne transmission of epidemic cholera in Trujillo, Peru: lessons for a continent at risk. *Lancet* 340:28-33.

70. Snow,J. 1849. On the mode of communication of cholera. John Churchill, London.

71. Reidl,J. and Klose,K.E. 2002. Vibrio cholerae and cholera: out of the water and into the host. *FEMS Microbiol.Rev.* 26:125-139.

72. Gill,D.M. 1976. The arrangement of subunits in cholera toxin. *Biochemistry* 15:1242-1248.

73. Moss,J. and Vaughan,M. 1981. Mechanism of action of choleragen and E. coli heat-labile enterotoxin: activation of adenylate cyclase by ADP-ribosylation. *Mol.Cell Biochem.* 37:75-90.

74. Sandvig,K. and van Deurs,B. 2002. Transport of protein toxins into cells: pathways used by ricin, cholera toxin and Shiga toxin. *FEBS Lett.* 529:49-53.

75. Moss,J. and Vaughan,M. 1977. Mechanism of action of choleragen. Evidence for ADP-ribosyltransferase activity with arginine as an acceptor. *J.Biol.Chem.* 252:2455-2457.

76. Wald,A., Gotterer,G.S., Rajendra,G.R., Turjman,N.A., and Hendrix,T.R. 1977. Effect of indomethacin on cholera-induced fluid movement, unidirectional sodium fluxes, and intestinal cAMP. *Gastroenterology* 72:106-110.

77. Speelman,P., Rabbani,G.H., Bukhave,K., and Rask-Madsen,J. 1985. Increased jejunal prostaglandin E2 concentrations in patients with acute cholera. *Gut* 26:188-193.

78. Katada,T. and Ui,M. 1982. Direct modification of the membrane adenylate cyclase system by islet-activating protein due to ADP-ribosylation of a membrane protein. *Proc.Natl.Acad.Sci.U.S.A* 79:3129-3133.

79. Kaslow,H.R., Lim,L.K., Moss,J., and Lesikar,D.D. 1987. Structure-activity analysis of the activation of pertussis toxin. *Biochemistry* 26:123-127.

80. West,R.E., Jr., Moss,J., Vaughan,M., Liu,T., and Liu,T.Y. 1985. Pertussis toxin-catalyzed ADP-ribosylation of transducin. Cysteine 347 is the ADP-ribose acceptor site. *J.Biol.Chem.* 260:14428-14430.

81. Honjo,T., Nishizuka,Y., and Hayaishi,O. 1968. Diphtheria toxin-dependent adenosine diphosphate ribosylation of aminoacyl trans-

ferase II and inhibition of protein synthesis. *J.Biol.Chem.* 243:3553-3555.

82. Bell,C.E. and Eisenberg,D. 1997. Crystal structure of diphtheria toxin bound to nicotinamide adenine dinucleotide. *Adv.Exp.Med.Biol.* 419:35-43.

83. Collier,R.J. and Kandel,J. 1971. Structure and activity of diphtheria toxin. I. Thiol-dependent dissociation of a fraction of toxin into enzymically active and inactive fragments. *J.Biol.Chem.* 246:1496-1503.

84. Gill,D.M. and Dinius,L.L. 1971. Observations on the structure of diphtheria toxin. *J.Biol.Chem.* 246:1485-1491.

85. Oppenheimer,N.J. and Bodley,J.W. 1981. Diphtheria toxin. Site and configuration of ADP-ribosylation of diphthamide in elongation factor 2. *J.Biol.Chem.* 256:8579-8581.

86. Yamaizumi,M., Mekada,E., Uchida,T., and Okada,Y. 1978. One molecule of diphtheria toxin fragment A introduced into a cell can kill the cell. *Cell* 15:245-250.

87. Favero,M.S., Carson,L.A., Bond,W.W., and Petersen,N.J. 1971. Pseudomonas aeruginosa: growth in distilled water from hospitals. *Science* 173:836-838.

88. Silverman,A.R. and Nieland,M.L. 1983. Hot tub dermatitis: a familial outbreak of Pseudomonas folliculitis. *J.Am.Acad.Dermatol.* 8:153-156.

89. Wilson,L.A., Schlitzer,R.L., and Ahearn,D.G. 1981. Pseudomonas corneal ulcers associated with soft contact-lens wear. *Am.J.Ophthalmol.* 92:546-554.

90. Bodey,G.P., Bolivar,R., Fainstein,V., and Jadeja,L. 1983. Infections caused by Pseudomonas aeruginosa. *Rev.Infect.Dis.* 5:279-313.

91. Saiman,L. and Siegel,J. 2003. Infection control recommendations for patients with cystic fibrosis: Microbiology, important pathogens, and

infection control practices to prevent patient-to-patient transmission. *Am.J.Infect.Control* 31:S1-62.

92. Lister,P.D. 2002. Chromosomally-encoded resistance mechanisms of Pseudomonas aeruginosa: therapeutic implications. *Am.J.Pharmacogenomics.* 2:235-243.

93. Cahill,M.M. 1990. Virulence factors in motile Aeromonas species. *J.Appl.Bacteriol.* 69:1-16.

94. Armstrong,S., Yates,S.P., and Merrill,A.R. 2002. Insight into the catalytic mechanism of Pseudomonas aeruginosa exotoxin A. Studies of toxin interaction with eukaryotic elongation factor-2. *J.Biol.Chem.* 277:46669-46675.

95. Coburn,J. and Gill,D.M. 1991. ADP-ribosylation of p21ras and related proteins by Pseudomonas aeruginosa exoenzyme S. *Infect.Immun.* 59:4259-4262.

96. McGuffie,E.M., Frank,D.W., Vincent,T.S., and Olson,J.C. 1998. Modification of Ras in eukaryotic cells by Pseudomonas aeruginosa exoenzyme S. *Infect.Immun.* 66:2607-2613.

97. Ganesan,A.K., Frank,D.W., Misra,R.P., Schmidt,G., and Barbieri,J.T. 1998. Pseudomonas aeruginosa exoenzyme S ADP-ribosylates Ras at multiple sites. *J.Biol.Chem.* 273:7332-7337.

98. Ganesan,A.K., Mende-Mueller,L., Selzer,J., and Barbieri,J.T. 1999. Pseudomonas aeruginosa exoenzyme S, a double ADP-ribosyltransferase, resembles vertebrate mono-ADP-ribosyltransferases. *J.Biol.Chem.* 274:9503-9508.

99. Ganesan,A.K., Vincent,T.S., Olson,J.C., and Barbieri,J.T. 1999. Pseudomonas aeruginosa exoenzyme S disrupts Ras-mediated signal transduction by inhibiting guanine nucleotide exchange factor-catalyzed nucleotide exchange. *J.Biol.Chem.* 274:21823-21829.

100. Aktories,K., Weller,U., and Chhatwal,G.S. 1987. Clostridium botulinum type C produces a novel ADP-ribosyltransferase distinct from botulinum C2 toxin. *FEBS Lett.* 212:109-113.

101. Rosener,S., Chhatwal,G.S., and Aktories,K. 1987. Botulinum ADP-ribosyltransferase C3 but not botulinum neurotoxins C1 and D ADP-ribosylates low molecular mass GTP-binding proteins. *FEBS Lett.* 224:38-42.

102. Aktories,K. 1997. Identification of the catalytic site of clostridial ADP-ribosyltransferases. *Adv.Exp.Med.Biol.* 419:53-60.

103. Sekine,A., Fujiwara,M., and Narumiya,S. 1989. Asparagine residue in the rho gene product is the modification site for botulinum ADP-ribosyltransferase. *J.Biol.Chem.* 264:8602-8605.

104. Yuan,J., Slice,L.W., and Rozengurt,E. 2001. Activation of protein kinase D by signaling through Rho and the alpha subunit of the heterotrimeric G protein G13. *J.Biol.Chem.* 276:38619-38627.

105. Beltman,J., Erickson,J.R., Martin,G.A., Lyons,J.F., and Cook,S.J. 1999. C3 toxin activates the stress signaling pathways, JNK and p38, but antagonizes the activation of AP-1 in rat-1 cells. *J.Biol.Chem.* 274:3772-3780.

106. Zolkiewska,A., Nightingale,M.S., and Moss,J. 1992. Molecular characterization of NAD:arginine ADP-ribosyltransferase from rabbit skeletal muscle. *Proc.Natl.Acad.Sci.U.S.A* 89:11352-11356.

107. Zolkiewska,A. and Moss,J. 1993. Integrin alpha 7 as substrate for a glycosylphosphatidylinositol-anchored ADP-ribosyltransferase on the surface of skeletal muscle cells. *J.Biol.Chem.* 268:25273-25276.

108. Takada,T., Iida,K., and Moss,J. 1994. Expression of NAD glycohydrolase activity by rat mammary adenocarcinoma cells transformed with rat T cell alloantigen RT6.2. *J.Biol.Chem.* 269:9420-9423.

109. Rigby,M.R., Bortell,R., Stevens,L.A., Moss,J., Kanaitsuka,T., Shigeta,H., Mordes,J.P., Greiner,D.L., and Rossini,A.A. 1996. Rat RT6.2 and mouse Rt6 locus 1 are NAD(+): Arginine ADP ribosyltransferases with Auto-ADP ribosylation activity. *J.Immunol.* 156:4259-4265.

110. Adriouch,S., Ohlrogge,W., Haag,F., Koch-Nolte,F., and Seman,M. 2001. Rapid induction of naive T cell apoptosis by ecto-nicotinamide

adenine dinucleotide: requirement for mono(ADP-ribosyl)transferase 2 and a downstream effector. *J.Immunol.* 167:196-203.

111. Ohlrogge,W., Haag,F., Lohler,J., Seman,M., Littman,D.R., Killeen,N., and Koch-Nolte,F. 2002. Generation and characterization of ecto-ADP-ribosyltransferase ART2.1/ART2.2-deficient mice. *Mol.Cell Biol.* 22:7535-7542.

112. Liu,Z.X., Yu,Y., and Dennert,G. 1999. A cell surface ADP-ribosyltransferase modulates T cell receptor association and signaling. *J.Biol.Chem.* 274:17399-17401.

113. Okamoto,S., Azhipa,O., Yu,Y., Russo,E., and Dennert,G. 1998. Expression of ADP-ribosyltransferase on normal T lymphocytes and effects of nicotinamide adenine dinucleotide on their function. *J.Immunol.* 160:4190-4198.

114. Nemoto,E., Yu,Y., and Dennert,G. 1996. Cell surface ADP-ribosyltransferase regulates lymphocyte function-associated molecule-1 (LFA-1) function in T cells. *J.Immunol.* 157:3341-3349.

115. Nemoto,E., Stohlman,S., and Dennert,G. 1996. Release of a glycosyl-phosphatidylinositol-anchored ADP-ribosyltransferase from cytotoxic T cells upon activation. *J.Immunol.* 156:85-92.

116. Kahl,S., Nissen,M., Girisch,R., Duffy,T., Leiter,E.H., Haag,F., and Koch-Nolte,F. 2000. Metalloprotease-mediated shedding of enzymatically active mouse ecto-ADP-ribosyltransferase ART2.2 upon T cell activation. *J.Immunol.* 165:4463-4469.

117. Paone,G., Wada,A., Stevens,L.A., Matin,A., Hirayama,T., Levine,R.L., and Moss,J. 2002. ADP ribosylation of human neutrophil peptide-1 regulates its biological properties. *Proc.Natl.Acad.Sci.USA* 99:8231-8235.

118. Bruzzone,S., Guida,L., Zocchi,E., Franco,L., and De Flora,A. 2001. Connexin 43 hemi channels mediate Ca2+-regulated transmembrane NAD+ fluxes in intact cells. *FASEB J.* 15:10-12.

119. Bruzzone,S., Franco,L., Guida,L., Zocchi,E., Contini,P., Bisso,A., Usai,C., and De Flora,A. 2001. A self-restricted CD38-connexin 43 cross-talk affects NAD+ and cyclic ADP-ribose metabolism and regulates intracellular calcium in 3T3 fibroblasts. *J.Biol.Chem.* 276:48300-48308.

120. Franco,L., Zocchi,E., Usai,C., Guida,L., Bruzzone,S., Costa,A., and De Flora,A. 2001. Paracrine roles of NAD+ and cyclic ADP-ribose in increasing intracellular calcium and enhancing cell proliferation of 3T3 fibroblasts. *J.Biol.Chem.* 276:21642-21648.

121. Yu,S.W., Wang,H., Poitras,M.F., Coombs,C., Bowers,W.J., Federoff,H.J., Poirier,G.G., Dawson,T.M., and Dawson,V.L. 2002. Mediation of poly(ADP-ribose) polymerase-1-dependent cell death by apoptosis-inducing factor. *Science* 297:259-263.

122. Smith,S., Giriat,I., Schmitt,A., and de Lange,T. 1998. Tankyrase, a poly(ADP-ribose) polymerase at human telomeres. *Science* 282:1484-1487.

123. Tulin,A. and Spradling,A. 2003. Chromatin loosening by poly(ADP)-ribose polymerase (PARP) at Drosophila puff loci. *Science* 299:560-562.

124. Okamoto,H. 1981. Regulation of proinsulin synthesis in pancreatic islets and a new aspect to insulin-dependent diabetes. *Mol.Cell Biochem.* 37:43-61.

125. Uchigata,Y., Yamamoto,H., Kawamura,A., and Okamoto,H. 1982. Protection by superoxide dismutase, catalase, and poly(ADP-ribose) synthetase inhibitors against alloxan- and streptozotocin-induced islet DNA strand breaks and against the inhibition of proinsulin synthesis. *J.Biol.Chem.* 257:6084-6088.

126. Uchigata,Y., Yamamoto,H., Nagai,H., and Okamoto,H. 1983. Effect of poly(ADP-ribose) synthetase inhibitor administration to rats before and after injection of alloxan and streptozotocin on islet proinsulin synthesis. *di* 32:316-318.

127. Burkart,V., Wang,Z.Q., Radons,J., Heller,B., Herceg,Z., Stingl,L., Wagner,E.F., and Kolb,H. 1999. Mice lacking the poly(ADP-ribose) polymerase gene are resistant to pancreatic beta-cell destruction

lymerase gene are resistant to pancreatic beta-cell destruction and diabetes development induced by streptozocin. *Nat.Med.* 5:314-319.

128. Masutani,M., Suzuki,H., Kamada,N., Watanabe,M., Ueda,O., Nozaki,T., Jishage,K., Watanabe,T., Sugimoto,T., Nakagama,H. *et al*. 1999. Poly(ADP-ribose) polymerase gene disruption conferred mice resistant to streptozotocin-induced diabetes. *Proc.Natl.Acad.Sci.U.S.A* 96:2301-2304.

129. Pieper,A.A., Brat,D.J., Krug,D.K., Watkins,C.C., Gupta,A., Blackshaw,S., Verma,A., Wang,Z.Q., and Snyder,S.H. 1999. Poly(ADP-ribose) polymerase-deficient mice are protected from streptozotocin-induced diabetes. *Proc.Natl.Acad.Sci.U.S.A* 96:3059-3064.

130. Clapper,D.L., Walseth,T.F., Dargie,P.J., and Lee,H.C. 1987. Pyridine nucleotide metabolites stimulate calcium release from sea urchin egg microsomes desensitized to inositol trisphosphate. *J.Biol.Chem.* 262:9561-9568.

131. Munshi,C., Thiel,D.J., Mathews,I.I., Aarhus,R., Walseth,T.F., and Lee,H.C. 1999. Characterization of the active site of ADP-ribosyl cyclase. *J.Biol.Chem.* 274:30770-30777.

132. Cakir-Kiefer,C., Muller-Steffner,H., and Schuber,F. 2000. Unifying mechanism for Aplysia ADP-ribosyl cyclase and CD38/NAD(+) glycohydrolases. *Biochem.J.* 349:203-210.

133. States,D.J., Walseth,T.F., and Lee,H.C. 1992. Similarities in amino acid sequences of Aplysia ADP-ribosyl cyclase and human lymphocyte antigen CD38. *Trends Biochem.Sci.* 17:495.

134. Howard,M., Grimaldi,J.C., Bazan,J.F., Lund,F.E., Santos-Argumedo,L., Parkhouse,R.M., Walseth,T.F., and Lee,H.C. 1993. Formation and hydrolysis of cyclic ADP-ribose catalyzed by lymphocyte antigen CD38. *Science* 262:1056-1059.

135. Muller-Steffner,H., Muzard,M., Oppenheimer,N., and Schuber,F. 1994. Mechanistic implications of cyclic ADP-ribose hydrolysis and methanolysis catalyzed by calf spleen NAD+glycohydrolase. *Biochem.Biophys.Res.Commun.* 204:1279-1285.

136.   2002. Cyclic ADP-Ribose and NAADP. Kluwer, Norwell.

137.   Frye,R.A. 2000. Phylogenetic classification of prokaryotic and eu-karyotic Sir2-like proteins. *Biochem.Biophys.Res.Commun.* 273:793-798.

138.   Lin,S.J., Defossez,P.A., and Guarente,L. 2000. Requirement of NAD and SIR2 for life-span extension by calorie restriction in Saccharo-myces cerevisiae. *Science* 289:2126-2128.

139.   Tissenbaum,H.A. and Guarente,L. 2001. Increased dosage of a sir-2 gene extends lifespan in Caenorhabditis elegans. *Nature* 410:227-230.

140.   Frye,R.A. 1999. Characterization of five human cDNAs with homology to the yeast SIR2 gene: Sir2-like proteins (sirtuins) metabolize NAD and may have protein ADP-ribosyltransferase activity. *Bio-chem.Biophys.Res.Commun.* 260:273-279.

141.   Tanny,J.C., Dowd,G.J., Huang,J., Hilz,H., and Moazed,D. 1999. An en-zymatic activity in the yeast Sir2 protein that is essential for gene si-lencing. *Cell* 99:735-745.

142.   Tanner,K.G., Landry,J., Sternglanz,R., and Denu,J.M. 2000. Silent in-formation regulator 2 family of NAD- dependent histone/protein deacetylases generates a unique product, 1-O-acetyl-ADP-ribose. *Proc.Natl.Acad.Sci.U.S.A* 97:14178-14182.

143.   Bortell,R., Rigby,M., Stevens,L., Moss,J., Kanaitsuka,T., Mordes,J., Greiner,D., and Rossini,A. 1997. Mouse RT6 locus 1 and rat RT6.2 are NAD+ - Arginine ADP-ribosyltransferases with auto-ADP-ribosylation activity. *Adp-Ribosylation in Animal Tissues* 419:169-173.

144.   Alvarez-Gonzalez,R. and Jacobson,M.K. 1987. Characterization of polymers of adenosine diphosphate ribose generated in vitro and in vivo. *Biochemistry* 26:3218-3224.

145.   Shah,G.M., Poirier,D., Duchaine,C., Brochu,G., Desnoyers,S., Lagueux,J., Verreault,A., Hoflack,J.C., Kirkland,J.B., and Poirier,G.G.

1995. Methods for Biochemical-Study of Poly(Adp-Ribose) Metabolism In-Vitro and In-Vivo. *Analytical Biochemistry* 227:1-13.

146. Sugimura,T. and Miwa,M. 1994. Poly(ADP-ribose): historical perspective. *Mol.Cell Biochem.* 138:5-12.

147. Ogata,N., Ueda,K., and Hayaishi,O. 1980. ADP-ribosylation of histone H2B. Identification of glutamic acid residue 2 as the modification site. *J.Biol.Chem.* 255:7610-7615.

148. Ogata,N., Ueda,K., Kagamiyama,H., and Hayaishi,O. 1980. ADP-ribosylation of histone H1. Identification of glutamic acid residues 2, 14, and the COOH-terminal lysine residue as modification sites. *J.Biol.Chem.* 255:7616-7620.

149. Mendoza-Alvarez,H. and Alvarez-Gonzalez,R. 1999. Biochemical characterization of mono(ADP-ribosyl)ated poly(ADP-ribose) polymerase. *Biochemistry* 38:3948-3953.

150. Kameshita,I., Matsuda,Z., Taniguchi,T., and Shizuta,Y. 1984. Poly (ADP-Ribose) synthetase. Separation and identification of three proteolytic fragments as the substrate-binding domain, the DNA-binding domain, and the automodification domain. *J.Biol.Chem.* 259:4770-4776.

151. Weng,B.Y., Thompson,W.C., Kim,H.J., Levine,R.L., and Moss,J. 1999. Modification of the ADP-ribosyltransferase and NAD glycohydrolase activities of a mammalian transferase (ADP-ribosyltransferase 5) by auto-ADP-ribosylation. *Journal of Biological Chemistry* 274:31797-31803.

152. Zhang,R.G., Scott,D.L., Westbrook,M.L., Nance,S., Spangler,B.D., Shipley,G.G., and Westbrook,E.M. 1995. The three-dimensional crystal structure of cholera toxin. *J.Mol.Biol.* 251:563-573.

153. Bell,C.E. and Eisenberg,D. 1996. Crystal structure of diphtheria toxin bound to nicotinamide adenine dinucleotide. *Biochemistry* 35:1137-1149.

154. Ruf,A., Rolli,V., de Murcia,G., and Schulz,G.E. 1998. The mechanism of the elongation and branching reaction of poly(ADP-ribose) polymerase as derived from crystal structures and mutagenesis. *Journal of Molecular Biology* 278:57-65.

155. Miwa,M., Saito,H., Sakura,H., Saikawa,N., Watanabe,F., Matsushima,T., and Sugimura,T. 1977. A 13C NMR study of poly(adenosine diphosphate ribose) and its monomers: evidence of alpha-(1" leads to 2') ribofuranosy1 ribofuranoside risidue. *Nucleic Acids Res.* 4:3997-4005.

156. Miwa,M., Ishihara,M., Takishima,S., Takasuka,N., Maeda,M., Yamaizumi,Z., Sugimura,T., Yokoyama,S., and Miyazawa,T. 1981. The branching and linear portions of poly(adenosine diphosphate ribose) have the same alpha(1 leads to 2) ribose-ribose linkage. *J.Biol.Chem.* 256:2916-2921.

157. De Flora,A., Guida,L., Franco,L., Zocchi,E., Bruzzone,S., Benatti,U., Damonte,G., and Lee,H.C. 1997. CD38 and ADP-ribosyl cyclase catalyze the synthesis of a dimeric ADP-ribose that potentiates the calcium-mobilizing activity of cyclic ADP-ribose. *J.Biol.Chem.* 272:12945-12951.

158. Okazaki,I.J. and Moss,J. 1998. Glycosylphosphatidylinositol-anchored and secretory isoforms of mono-ADP-ribosyltransferases. *J.Biol.Chem.* 273:23617-23620.

159. Okazaki,I.J. and Moss,J. 1999. Characterization of glycosylphosphatidylinositiol-anchored, secreted, and intracellular vertebrate mono-ADP-ribosyltransferases. *Annu.Rev.Nutr.* 19:485-509.

160. Han,S., Arvai,A.S., Clancy,S.B., and Tainer,J.A. 2001. Crystal structure and novel recognition motif of rho ADP-ribosylating C3 exoenzyme from Clostridium botulinum: structural insights for recognition specificity and catalysis. *J.Mol.Biol.* 305:95-107.

161. Hara,N., Tsuchiya,M., and Shimoyama,M. 1996. Glutamic acid 207 in rodent T-cell RT6 antigens is essential for arginine-specific ADP-ribosylation. *J.Biol.Chem.* 271:29552-29555.

162. Jung,S., Miranda,E.A., Demurcia,J.M., Niedergang,C., Delarue,M., Schulz,G.E., and Demurcia,G.M. 1994. Crystallization and X-Ray Crystallographic Analysis of Recombinant Chicken Poly (Adp-Ribose) Polymerase Catalytic Domain Produced in Sf9 Insect Cells. *Journal of Molecular Biology* 244:114-116.

163. Bradford,M.M. 1976. A rapid and sensitive method for the quantitation of microgram quantities of protein utilizing the principle of protein-dye binding. *Anal.Biochem.* 72:248-254.

164. Moss,J., Manganiello,V.C., and Vaughan,M. 1976. Hydrolysis of nicotinamide adenine dinucleotide by choleragen and its A protomer: possible role in the activation of adenylate cyclase. *Proc.Natl.Acad.Sci.U.S.A* 73:4424-4427.

165. Mueller-Dieckmann,C., Ritter,H., Haag,F., Koch-Nolte,F., and Schulz,G.E. 2002. Structure of the ecto-ADP-ribosyl transferase ART2.2 from rat. *J.Mol.Biol.* 322:687-696.

166. Sauve,A.A., Celic,I., Avalos,J., Deng,H., Boeke,J.D., and Schramm,V.L. 2001. Chemistry of Gene Silencing: The Mechanism of NAD^+-Dependent Deacetylation Reactions. *Biochemistry* 40:15456-15463.

167. Shieh,W.M., Ame,J.C., Wilson,M.V., Wang,Z.Q., Koh,D.W., Jacobson,M.K., and Jacobson,E.L. 1998. Poly(ADP-ribose) polymerase null mouse cells synthesize ADP-ribose polymers. *J.Biol.Chem.* 273:30069-30072.

168. Du,L., Zhang,X., Han,Y.Y., Burke,N.A., Kochanek,P.M., Watkins,S.C., Graham,S.H., Carcillo,J.A., Szabo,C., and Clark,R.S. 2003. Intra-mitochondrial poly(ADP-ribosylation) contributes to NAD+ depletion and cell death induced by oxidative stress. *J.Biol.Chem.* 278:18426-18433.

169. Yamada,M., Shimada,T., Nakayasu,M., Okada,H., and Sugimura,T. 1978. Induction of differentiation of mouse myeloid leukemia cells by poly(ADP-ribose). *Biochem.Biophys.Res.Commun.* 83:1325-1332.

170. Caplan,A.I. and Rosenberg,M.J. 1975. Interrelationship between poly (ADP-Rib) synthesis, intracellular NAD levels, and muscle or carti-

lage differentiation from mesodermal cells of embryonic chick limb. *Proc.Natl.Acad.Sci.U.S.A* 72:1852-1857.

171. Rastl,E. and Swetly,P. 1978. Expression of poly(adenosine diphosphate-ribose) polymerase activity in erythroleukemic mouse cells during cell cycle and erythropoietic differentiation. *J.Biol.Chem.* 253:4333-4340.

172. Lee,J., Chuang,T.H., Redecke,V., She,L., Pitha,P.M., Carson,D.A., Raz,E., and Cottam,H.B. 2003. Molecular basis for the immunostimulatory activity of guanine nucleoside analogs: activation of Toll-like receptor 7. *Proc.Natl.Acad.Sci.U.S.A* 100:6646-6651.

173. Akira,S. and Hemmi,H. 2003. Recognition of pathogen-associated molecular patterns by TLR family. *Immunol.Lett.* 85:85-95.

174. Alexopoulou,L., Holt,A.C., Medzhitov,R., and Flavell,R.A. 2001. Recognition of double-stranded RNA and activation of NF-kappaB by Toll-like receptor 3. *Nature* 413:732-738.

175. Hayashi,F., Smith,K.D., Ozinsky,A., Hawn,T.R., Yi,E.C., Goodlett,D.R., Eng,J.K., Akira,S., Underhill,D.M., and Aderem,A. 2001. The innate immune response to bacterial flagellin is mediated by Toll-like receptor 5. *Nature* 410:1099-1103.

176. Hemmi,H., Takeuchi,O., Kawai,T., Kaisho,T., Sato,S., Sanjo,H., Matsumoto,M., Hoshino,K., Wagner,H., Takeda,K. *et al.* 2000. A Toll-like receptor recognizes bacterial DNA. *Nature* 408:740-745.